ISTANBUL TECHNICAL UNIVERSITY ★ GRADUATE SCHOOL OF SCIENCE ENGINEERING AND TECHNOLOGY

CORROSION PREVENTION OF CARBON STEEL AND ALUMINIUM METALS BY PANI/CeO$_2$ NANOCOMPOSITE COATINGS

M.Sc. THESIS

Hande YOLSAL ACAR

Department of Polymer Science and Technology

Polymer Science and Technology Programme

MAY 2015

CORROSION PREVENTION OF CARBON STEEL AND ALUMINIUM METALS BY PANI/CeO$_2$ NANOCOMPOSITE COATINGS

M.Sc. THESIS

Hande YOLSAL ACAR
(515101011)

Department of Polymer Science and Technology

Polymer Science and Technology Programme

Thesis Advisor: Prof. Dr. Esma SEZER

MAY 2015

İSTANBUL TEKNİK ÜNİVERSİTESİ ★ FEN BİLİMLERİ ENSTİTÜSÜ

PANI/CeO$_2$ NANOKOMPOZİT KAPLAMALAR İLE KARBON ÇELİK VE ALÜMİNYUM METALLERİNİN KOROZYONUNUN ÖNLENMESİ

YÜKSEK LİSANS TEZİ

Hande YOLSAL ACAR
(515101011)

Polimer Bilim ve Teknolojileri Anabilim Dalı

Polimer Bilim ve Teknolojileri Programı

Tez Danışmanı: Prof. Dr. Esma SEZER

MAYIS 2015

Hande Yolsal Acar a **M.Sc.** student of ITU **Institute of Science and Technology** student ID **515101011**, successfully defended the thesis entitled "CORROSION PREVENTION OF CARBON STEEL AND ALUMINIUM METALS BY PANI/CeO$_2$ NANOCOMPOSITE COATINGS" which she prepared after fulfilling the requirements specified in the associated legislations, before the jury whose signatures are below.

Thesis Advisor :   **Prof. Dr. Esma Sezer**   ....
İstanbul Technical University

Jury Members :   **Prof. Dr. Belkıs Ustamehmetoğlu**   ....
İstanbul Technical University

                              Prof. Dr. Yücel Şahin   ....
Yıldız Technical University

Date of Submission : 4 May 2015
Date of Defense :   **25 May 2015**

FOREWORD

I would like to express my greatfulness and thanks to my advisor, Professor Esma SEZER for her encouragement and support through this study.

I would like to thank to my dear friend İpek ÖZTÜRK for her support during all steps of my study.

Finally, I would like to thank to my family for their endless support.

TABLE OF CONTENTS

ABBREVIATIONS

PANI	: Polyaniline
PANI/CeO₂	: Polyaniline Cerium Oxide
SCC	: Stress-corrosion Cracking
E_cell	: Cell Potential
E_corr	: Corrosion Potential
E_oc	: Open Current Potential
I_corr	: Corrosion Current
SVET	: Scanning-Vibrating Electrode Technique
R_p	: Polarization Resistance
EIS	: Electrochemical impedance spectroscopy
β_a	: Anodic Beta Tafel Constant
β_c	: Cathodic Beta Tafel Constant
APS	: Ammonium Peroxidisulfate
ICPs	: Intrinsically Conducting Polymers
PPy	: Polypyrrole
PTh	: Polythiophene
CPs	: Conducting Polymers
OSC	: Oxygen Storage Capacity
DMF	: Dimethyl Formamide
EB	: Emeraldine Base
FTIR	: Fourier Transform Infrared Spectrometry
Al	: Aluminium
CPE_dl	: Charge Transfer Resistance
CR	: Corrosition Rate
CF	: Cyclohexane Formaldehyde
CF-R	: Cyclohexane Formaldehyde Resin

LIST OF TABLES

xiii

LIST OF FIGURES

CORROSION PREVENTION OF CARBON STEEL AND ALUMINIUM METALS BY PANI/CeO$_2$ NANOCOMPOSITE COATINGS

SUMMARY

Carbon steel and aluminium are the most common metals for industrial applications. Corrosion is one of the biggest drawbacks of using these metals in equipments.

Corrosion may be defined as a destructive phenomenon, chemical or electrochemical, which affects the appearance of an object, and in extreme cases may cause structural failure. Economic losses resulting from metallic corrosion costs billions of dollars per year worldwide. In addition to the economic costs, there are times when corrosion is responsible for the even greater costs of human life and safety.

Polymers have already replaced most of the materials we use in our daily life. Innovations on polymeric materials allow them to be used in corrosion inhibition. The use of organic coatings is one of the most common method for minimizing corrosion losses. Conducting polymers have been increasingly investigated for their use in organic coatings. Many studies showed that conducting polymers improve the corrosion inhibition properties of coatings. Polyaniline (PANI) is one of the most widely used conducting polymer because of its superior properties.

Inorganic nanoparticles are a class of new materials having wide variety of applications in many fields. To obtain the materials with synergetic or complementary behavior between polymer and inorganic nanoparticles, various composites of polymer with inorganic nanoparticles have been synthesized in recent years. Among those inorganic nanoparticles, cerium oxide (CeO$_2$) nanoparticles have been intensively studied due to their unique catalytic, electrical, and optic properties, as well as their extensive applications in diverse areas.

The main objective of this study is to investigate the corrosion behaviour of PANI/CeO$_2$ nanocomposite and pure PANI coatings on carbon steel and aluminium metals in corrosive environments such as 0.1 M H$_2$SO$_4$ and 3.5 % sea water.

In the first part of the study, synthesis of PANI and PANI/CeO$_2$ nanocomposite were carried out and they were characterised by Fourier Transform Infrared Spectroscopy, UV-Visible Spectroscopy, conductivity measurements and SEM analysis. It is confirmed by the analysis results that the polymer and nanocomposite were sucsessfully synhesized.

Coatings including pure PANI and PANI/CeO$_2$ nanocomposite were prepared at different concentrations and coated on carbon steel and aluminium electrodes and they were investigated for their corrosion protection properties. In addition to emeraldine salt forms of the polymers, emeraldine base forms of both species were used in order to have more concentrated polymer solutions due to better solubility which increased PANI content of coatings. It is evident from the SEM images of the coatings that PANI/CeO$_2$ nanocomposite formed a more uniform coating which can

lead to a better corrosion protection efficiency; whereas pure PANI polymer formed a rough and curved coating.

Since corrosion occurs via electrochemical reactions, electrochemical techniques are ideal for the study of the corrosion processes. The electrochemical impedance spectroscopy (EIS) is one of the most effective and reliable method to extract information about electrochemical characteristics of the electrochemical system. Electrochemical measurements, including potentiodynamic polarization curves and EIS were performed in a three-electrode cell. EIS data is also analyzed by fitting it to an equivalent electrical circuit model and experimental results were confirmed.

Steady-state current-voltage curves and electrochemical impedance spectroscopy measurements of the coatings in 0.1 M H_2SO_4 for carbon steel and aluminium and in 3.5 % seawater for carbon steel were conducted.

The initial measurements were conducted in 0.1 M H_2SO_4 both for carbon steel and aluminium electrodes after 1 hour immersion to corrosive media. It is evident that both coatings inhibit corrosion of bare electrodes. The increase in polymer concentration effects the corrosion protection efficiency of the coating positively. PANI/CeO_2 polymer coatings showed slightly better corrosion protection efficiency over pure PANI coatings both for carbon steel and aluminium electrodes, which shows the advantage of CeO_2 nanoparticle contrubition in the coating. It is evident from the polarization curves that the coatings retard both anodic and cathodic reactions. In other words, they reduce the anodic dissolution and also retard the hydrogen evolution reaction. PANI/CeO_2 nanocomposite coating with 1,62 % showed the best corrosion protection performance on carbon steel and aluminium electrodes in 0.1 M H_2SO_4.

The corrosion protection efficiencies of the coatings including emeraldine base form of polymers were also measured with increasing exposure time. It was observed that the coating degradetion increased and consequently corrosion currents and corrosion rates increased as the exposure time to corrosive media increased. The differnace in corrosion protection property of the coatings became close to each other by increasing exposure time, which may be due to the effect of corrosion product formation on the electrode surface.

EIS measurements were also supported by equivalent circuit models and it is observed that a reasonable accuracy of the fitting was obtained. Chi-square is in the order of 10^{-3} and 10^{-4} for all the experimental data. Rp values obtained by equivalent circuits and experiments are in agreement with each other.

In order to see the protection performance of coatings in different corrosion media, measurements in 3.5 % seawater for carbon steel electrodes were also carried out. Results suggest that the same concentration of PANI/CeO_2 nanocomposites have better corrosion protection efficiency compared to pure PANI coatings even in emeraldine salt form which has lower concentration owing to the contrubition of CeO_2 nanoparticles in the coating.

PANI/CeO$_2$ NANOKOMPOZİT KAPLAMALAR İLE KARBON ÇELİK VE ALUMİNYUM METALLERİNİN KOROZYONUNUN ÖNLENMESİ

ÖZET

Karbon çelik ve alüminyum, endüstiyel uygulamalarda en sık kullanılan metallerdir. Korozyon, bu metallerin ekipmanlarda kullanımında ortaya çıkan en önemli problemlerden biridir.

En kısa ve genel tanımıyla korozyon, metallerin çevreleriyle etkileşimi sonucu paslanmasıdır. Metaller doğada genellikle oksit ve sülfür bileşikleri olarak kararlı halde bulunur ve serbest enerjileri en düşük durumdadır. Bu bileşikler çeşitli metalurjik proseslerle elementel hallerine dönüştürülür ve amaca uygun bir malzeme haline getirilir. Metaller üretilirken almış oldukları bu enerjiyi geri vererek kendiliğinden doğada bulundukları hale dönme eğilimindedir ve bu eğilim "korozyon" olarak isimlendirilir.

Bir metal, malzeme olarak kullanıldığında onun elementel halde kalması, oksitlenip iyonlarına dönüşmemesi istenir. Ancak metaller hava ve nem ile temasa geldikleri anda kimyasal reaksiyon sonucu kendiliğinden potansiyel üreten galvanik pil oluşur ve metal korozyona uğrar.

Korozyon hem ekonomik hem de sosyal bazı kayıplara sebep olduğu için yaşamı önemli ölçüde etkiler. Korozyon nedeniyle işletmelerdeki sistemlerin tamamen durması, değiştirilmesi ya da yeniden tasarlanması gerekebilir; boyama, metal kaplama veya inhibitör kullanımı gibi ilave masraflar gerekir, ürün kirlenebilir, etkinlik, ısı transfer, ya da değerli ürün kayıpları olur. Bunun yanısıra, ani çatlaklar nedeniyle patlama, yangın, zehirli ürün sızıntısı, sistemin çökerek çevredeki her şeye zarar vermesi, sızıntı dolayısıyla, ya da korozyon ürünleri nedeniyle havanın, doğal kaynakların kirlenmesi gibi güvenlik ve sağlık tehlikesi de olmaktadır.

Polimer malzemeler, günlük hayatta kullandığımız eşyaların birçoğunun yerini almıştır. Polimer teknolojisindeki gelişmeler, bu malzemelerin korozyon önlemede kullanımını da mümkün kılmaktadır.

Organik kaplamalar korozyon önlemede kullanılan en önemli yöntemlerden biridir. Kaplamalar, metal malzemeyi çevresinden ayıran bir bariyer görevi görür. Metal yüzeyi korozif ortamdan koruyabilmesi için kaplamaların pürüzsüz, gözeneksiz ve yüzeye tutunmasının yüksek olması gerekmektedir. İletken polimerlerin organik kaplamalarda kullanımı üzerine yapılan araştırmalar artarak devam etmektedir. İletken polimerlerin, kaplamaların korozyon inhibisyon özelliğini arttırdığı birçok çalışmada ortaya konmuştur.

Polianilin (PANI), ucuz maliyeti, üstün ısı direnci ve kolay eldesi gibi özelliklerinden dolayı en çok kullanılan iletken polimerlerden biridir.

Inorganik nanopartiküller, birçok uygulamada kullanılm alanı bulmuş olan yeni bir malzeme sınıfıdır. Son dönemde polimer ve inorganik nanopartiküllerin avantajlarına sahip olması amacıyla, bu iki maddenin sentezini inceleyen birçok çalışma yapılmaktadır. Bu inorganik nanopartikül çeşitlerinden biri de, benzersiz katalitik, elektriksel ve optik özelliklerinden dolayı bilimsel çalışmalara sıklıkla konu olan seryum oksit (CeO_2) nanpratikülleridir.

Bu çalışmadaki amaç, karbon çelik ve alüminyum metallerine uygulanan PANI/CeO_2 nanokompozit ve PANI içeren kaplamaların korozif ortamlarındaki korozyon davranışlarının incelenmesidir.

Çalışmanın ilk kısmında, PANI ve PANI/CeO_2 nanokompozit kimyasal olarak sentezlenmiştir. Eşzamanlı olarak gerçekleştirilen iki sentez setinden birinde anilin monomeri ile birlikte bir miktar CeO_2 nanopartikül bulunmaktayken, diğer set içinde yalnızca anilin monomeri bulunmaktadır. Kimyasal sentezde anilin monomeri, amonyum peroksidisülfat başlatıcısının etkisi ile HCl ortamında polimerleştirilmiştir.

Elde edilen sentez ürünleri Fourier Transform Infrared Spektroskopi, UV-Visible Spektroskopi, iletkenlik ölçümleri ve SEM analizi ile karakterize edilmiştir. Karakterizasyon sonuçları ile, hedeflendiği şekilde PANI polimeri ve PANI/CeO_2 nanokompoziti elde edildiği tespit edilmiştir. Her iki sentez ürünü de emeraldin tuz formdadır.

Farklı konsantrasyonlarda PANI/CeO_2 nanokompozit ve PANI içeren kaplama çözeltileri hazırlanarak karbon çelik ve alüminyum elektrotlar üzerinde kaplamalar hazırlanmıştır. Kaplamalarda yalnızca sentez ürünleri olan PANI emeraldine tuz formları değil, daha yüksek çözünürlük özelliği sayesinde daha konsantre boya çözeltilerinin eldesine imkan sunan emeraldine baz formları da kullanılmıştır.

Kaplamaların yüzeye tutunmaları için kaplama hazırlanmadan önce metal yüzeyler zımpara kağıdı ve alüminyum pasta ile mekanik olarak temizlenmiştir. Her bir kaplama, belirli miktarda polimer ve reçine içerecek şekilde hazırlanmıştır. Polimer çözücüsü olarak dimetil formamit, reçine çözücüsü olarak ise asteon kullanılmıştır. Boya çözeltisinin elektrot yüzeyine uygulanması sonucu elde edilen kaplamalar kurutulduktan sonra korozyon etkinliği ölçülmüştür.

Metal yüzeyler üzerine uygulanan kaplamaların SEM analiz sonuçlarına göre, PANI/CeO_2 nanokompozit içeren kaplamaların, sadece PANI polimeri içeren kaplamalara kıyasla daha pürüzsüz ve homojen bir yüzeye sahip iken, sadece PANI polimeri içeren kaplama yüzeylerinin daha pürüzlü ve kıvrık bir morfolojide olduğu tespit edilmiştir.

Karbon çelik ve alüminyum üzerinde hazırlanan kaplamaların 0.1 M H_2SO_4 çözeltisi içindeki ve % 3.5 tuzluluk oranına sahip deniz suyu içindeki kararlı durum akım-gerilim eğrileri ve elektrokimyasal impedans ölçümleri yapılarak kaplamaların korozyona karşı etkinlikleri incelenmiştir.

Korozyon olgusu, elektrokimyasal reaksiyonlar ile gerçekleştiği için, korozyon üzerinde yapılan çalışmalarda elektrokiyasal yöntemler kullanılmaktadır. Elektokimyasal empedans spektroskopisi (EIS) elektrokimyasal sistemlere ait süreçleri analiz etmede kullanılan en efektif ve güvenilir ölçüm yöntemidir. Potansiyodinamik polarizasyon eğrilerini de içeren elektrokimyasal ölçümler, 3 elektrotlu hücrelerde gerçekleştirilmiştir. Yardımcı elektrot olarak Pt tel, referans elektrot olarak Ag/AgCl kullanılmıştır.

İlk ölçümler, karbon çelik ve alüminyum metalleri ile, elektrotlar 0.1 M H_2SO_4 çözeltisi içinde 1 saat bekletildikten sonra alınmıştır. Her iki tip kaplamanın da çıplak alüminyum ve karbon çelik elektrotlara kıyasla korozyonu engellediği tespit edilmiştir. Polimer konsantrasyonundaki artış, kaplamanın korozyon inhibisyon etkinliğini pozitif yönde arttırdığı görülmüştür. $PANI/CeO_2$ nanokompozit polimer içeren kaplamalar, hem alüminyum hem karbon çelik metallerinde PANI içeren kaplamalara kıyasla bir miktar daha yüksek korozyon direnci sağlamaktadır, ki bu durum, nanokompozit kaplamaların içerdiği CeO_2 nanopartiküllerin etkisini göstermektedir.

Polarizasyon eğrilerinden elde edilen sonuçlara göre, kaplamalar hem anodik hem katodik reaksiyonları yavaşlatmaktadır. Diğer bir ifade ile, kaplamalar hem anodik çözünmeyi azaltır hem de hidrojen oluşumunu yavaşlatır. % 1,62 konsantrasyondaki $PANI/CeO_2$ nanokompozit kaplamalar karbon çelik ve alüminyum elektrotlar üzerinde en iyi performansı göstermiştir.

Korozif ortama maruz kalma süresinin kaplama etkinlikleri üzerindeki etkisini incelemek amacıyla, emeraldin baz formdaki polimer ve nanokompozit içeren kaplamaların gösterdikleri korozyon dirençleri çözelti içindeki bekleme süreleri arttırılarak ölçülmüştür. Hem alüminyum hem karbon çelik metalleri için yapılan bu deneylerde, her iki tip metal için de, korozif ortama maruz kalma süresi arttıkça, kaplama degredasyonunun arttığı, buna bağlı olarak korozyon akımının ve korozyon hızının arttığı tespit edilmiştir. Kaplamaların korozyon önleme özellikleri arasındaki fark, korozif ortamda bekleme süresi arttıkça azalmaktadır. Bu durumun elektrot yüzeyinde oluşan korozyon ürünlerinin etkisinden kaynaklandığı düşünülmektedir.

EIS dataları eşlenik elektrik devre modelleri oluşturularak da analiz edilmiştir. Tüm eşlenik devre modellerinde chi-square değeri 10^{-3} ve 10^{-4} olarak elde edilmiştir. Tüm eşlenik devrelerden elde edilen Rp değerleri, deney sonuçları ile uyumludur.

Kaplamaların farklı korozif ortamlardaki performanslarının incelenmesi amacıyla, karbon çelik elektrotların % 3.5 tuzluluktaki deniz suyu içinde ölçümleri yapılmıştır. Sonuçlar göstermektedir ki, $PANI/CeO_2$ nanokompozit kaplamalar, aynı konsantrasyondaki PANI kaplamalara göre, daha düşük konsantrasyona sahip emeraldine tuz formlarında bile, daha yüksek korozyon direnci sağlamaktadır. Bu durum, nanokompozit kaplamaların içerdiği CeO_2 nanopartiküllerin kaplama üzerindeki olumlu etkisini göstermektedir.

1. INTRODUCTION

Corrosion is the destructive result of chemical reactions between a metal or metal alloy and its environment. Corrosion impacts many aspects of our lives. Essentially anything made of metal is subject to corrosion and when corrosion is evident, significant economic consequences may follow. This is true for structural items that comprise the infrastructure of society such as pipelines, storage tanks, bridges and airplanes and for the personal items we own such as automobiles, water heaters and metal lawn furniture [1].

Among various materials for anti-corrosion of metals, conductive polymer coatings are one of the most effective, cheapest and also the most environmentally friendly materials. Even though pinholes and/or cracks are formed in the coatings, the anti-corrosion ability is barely lowered because of the features of the anti-corrosion coatings. The coatings are said to serve simply as an in-situ oxidant or anodic protectant. When the coating oxidizes the metal surface to which it is in contact, the coating is reduced. Since the reduced coating is re-oxidized by ambient air, it continues to oxidize the metal surface and the passive state is maintained. Among conductive polymers, it is widely recognized that polyaniline (PANI) has been one of the best candidate of conductive polymers for an anti-corrosion coating since the anti-corrosion ability was found [2].

Inorganic nanoparticles stand for a class of new materials having enormous applications in broad fields. To obtain the materials with synergetic or complementary behavior between polymer and inorganic nanoparticles, various composites of polymer with inorganic nanoparticles have been synthesized in recent years. Among those inorganic nanoparticles, cerium oxide (CeO_2) nanoparticles have been intensively studied due to their unique catalytic, electrical, and optic properties, as well as their extensive applications in diverse areas [3].

Cerium oxide possesses some interesting characteristics which make it suitable for applications in various fields. The antioxidant and thermal barrier properties of nano ceria have been previously reported by Ivanov et al. and Cao et al.. The barrier properties are due to the lower thermal diffusivity and higher thermal expansion coefficient of CeO_2 than those of other oxides (e.g. ZrO2). Other common applications of ceria are in construction of fuel cells, manufacture of sensors, in catalysis, etc. On the other hand, cerium compounds, used either as coatings or as inhibitors are known to hinder the cathodic reactions, thereby inhibiting corrosion. Therefore, cerium oxide particles have been used to obtain composite coatings with various metals such as zinc and nickel. Incorporation of CeO_2 nanoparticles in the metallic matrix can significantly improve material properties, such as wear, corrosion and temperature oxidation resistance, and microhardness [4].

This work was designed to gain further understanding on the effect of polyaniline and polyaniline/cerium oxide (CeO_2) nanocomposite on corrosion prevention of carbon steel and aluminium metals.

Two types of synthesis were conducted by in situ polymerization of aniline:

1. Polyaniline (PANI) polymer

2. PANI/CeO_2 nanocomoposite

The synthesized PANI and PANI/CeO_2 nanocomposite have been characterised by UV, IR and SEM analysis. Paint solutions of different concentrations including PANI polymer and PANI/CeO_2 nanocomposite were prepared. Aluminium and carbon steel electrodes were coated with paint solutions and corrosion resistance of electrodes were analysed in 0.1 M H_2SO_4 and sea water by electrochemical empedance and polarization measurements.

2. CORROSION PROCESSES AND TYPES

2.1 Corrosion Definition

Corrosion is a naturally occuring process, which is defined as the degradation or deterioration of a substance and/or its properties, usually a metal, over a period of time due to environmental exposure. This is an exergonic process as the metal tends toward the lowest possible energy state. Therefore, metals such as aluminum and steel have a natural tendency to return to their lowest energy state when combined with oxygen and water to form hydrated aluminum and iron oxides (corrosion products). These corrosion products are the eventual final state of processed metals which degrade over time when exposed to the elements. Thus the life cycle from mined and processed ores to industrial products and eventually back to their natural state [5].

Corrosion may be defined as a destructive phenomenon, chemical or electrochemical, which affects the aesthetic appeal of an object, and in extreme cases may cause structural failure [6].

Economic losses resulting from metallic corrosion amount to billions of dollars per year worldwide. In addition to the economic costs, there are times when corrosion is responsible for the even greater costs of human life and safety. Several airplane accidents have occurred in which part of the fuselage tore away during flight, killing passengers. Sections of bridges have collapsed, resulting in injury and loss of life. There is a high probability that these mechanical failures occurred as a result of stress corrosion cracking due to atmospheric corrosion. Hence, considerable expense has gone and will continue to go into the development of corrosion prevention techniques and products [1,7].

Since corrosion is an electrochemical process, it is necessary to have an understanding of the electrochemical techniques used to characterize corrosion processes [1].

2.2 Corrosion Types

There are eight forms of wet corrosion: uniform or general; pitting; crevice; galvanic; erosion (including cavitation and fretting corrosion); intergranular (including sensitization and exfoliation); dealloying (including dezincification and graphite); and environmentally assisted cracking (including stress-corrosion cracking (SCC), fatigue and hydrogen damage). Figure 2.1 schematically shows the types of corrosion listed above. In theory, these forms are distinct but in reality, most metals undergo a variety of corrosion processes.
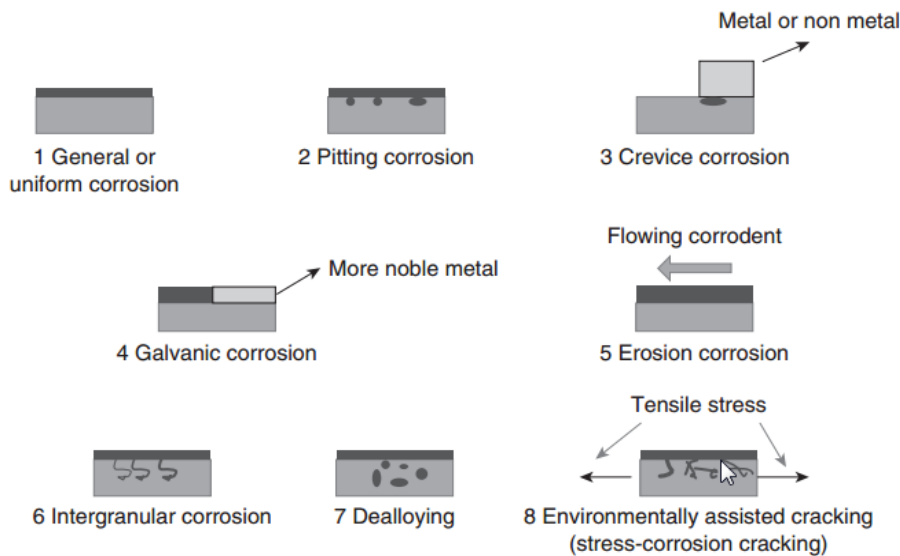
Figure 2.1 : General scheme for various forms of corrosion on metals/alloys [5].

2.3 Corrosion Processes

Water is used for a wide variety of purposes, from supporting life as potable water to performing a multitude of industrial tasks such as heat exchange and waste transport. The impact of water on the integrity of materials is thus an important aspect of system management. Since steels and other iron-based alloys are the metallic materials most commonly exposed to water, aqueous corrosion has been discussed with a special focus on the reactions of iron (Fe) with water.

Metal ions go into solution at anodic areas in an amount chemically equivalent to the reaction at cathodic areas (Figure 2.2). In the cases of iron-based alloys, the following reaction usually takes place at anodic areas:

$$Fe^0 \rightarrow Fe^{2+} + 2e^- \qquad\qquad (2.1)$$
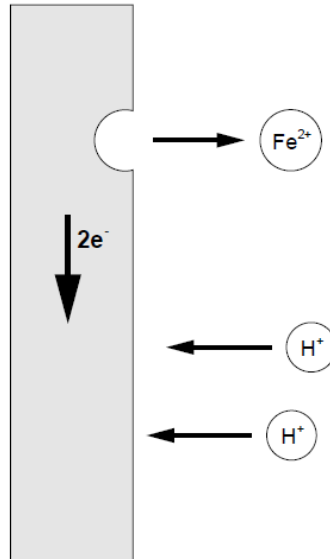
Figure 2.2 : Simple model describing the electrochemical nature of corrosion process [8].

This reaction is rapid in most media, as shown by the lack of pronounced polarization when iron is made an anode employing an external current. When iron corrodes, the rate is usually controlled by the cathodic reaction, which in general is much slower (cathodic control). In deaerated solutions, the cathodic reaction is as follows (Equation 2.2):

$$2H^+ + 2e^- \rightarrow H_2 \tag{2.2}$$

This reaction proceeds rapidly in acids, but only slowly in alkaline or neutral aqueous media. The corrosion rate of iron in deaerated neutral water at room temperature, for example, is less than 5 μm/year. The rate of hydrogen evolution at a specific pH depends on the presence or absence of low-hydrogen overvoltage impurities in the metal. For pure iron, the metal surface itself provides sites for H_2 evolution; hence, high-purity iron continues to corrode in acids, but at a measurably lower rate than does commercial iron.

The cathodic reaction can be accelerated by the reduction of dissolved oxygen in accordance with the following reaction, a process called depolarization (Equation 2.3).

$$4H^+ + O_2 + 4e^- \rightarrow 2H_2O \tag{2.3}$$

Dissolved oxygen reacts with hydrogen atoms adsorbed at random on the iron surface, independent of the presence or absence of impurities in the metal. The oxidation reaction proceeds as rapidly as oxygen reaches the metal surface [8].

The aqueous or, as commonly referred to, the wet corrosion process consists of three important elements which are necessary for the corrosion process to occur: anodic reaction, cathodic reaction and electrolyte solution or conducting liquid. The anodic reaction or oxidation of the metal results in dissolution of the metal, which is transferred to the solution as M^{n+} ions (Equation 2.4). The cathodic reaction or reduction involves oxygen (Equation 2.5). Reduction of oxygen is the dominant cathodic reaction in natural environments (seawater, soil and atmosphere).

$$2Fe \rightarrow 2Fe^{+2} + 4e^- \quad \text{(Anode Reaction)} \qquad \textbf{(2.4)}$$

$$O_2 + 2H_2O + 4e^- \rightarrow 4OH^- \quad \text{(Cathode Reaction)} \qquad \textbf{(2.5)}$$
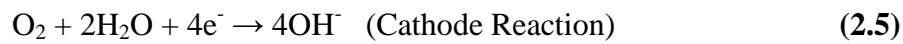
This process forms an electrical circuit without any accumulation of charges. The electrons are released by the anodic process and they are conducted through the metal to the cathode. The electrons released by the anodic process are consumed by the cathodic reaction. This electrochemical process requires an ionically conducting liquid, the 'electrolyte', which must be in contact with the metal. The electrochemical circuit is closed by ion conduction through the electrolyte and all three elements must be present in order for wet corrosion to occur. Typically the metal ions M^{n+} are conducted towards OH^- ions and together they normally produce a metal hydroxide, which is deposited on the surface of the metal. If, for example, the oxidizing metal is zinc and the liquid is water containing oxygen the Zn^{+2} ions and OH^- ions combine to form $Zn(OH)_2$. Iron and copper metals also follow similar corrosion proccesses when the electrolyte is water in the presence of dissolved oxygen (Figure 2.3) [5].
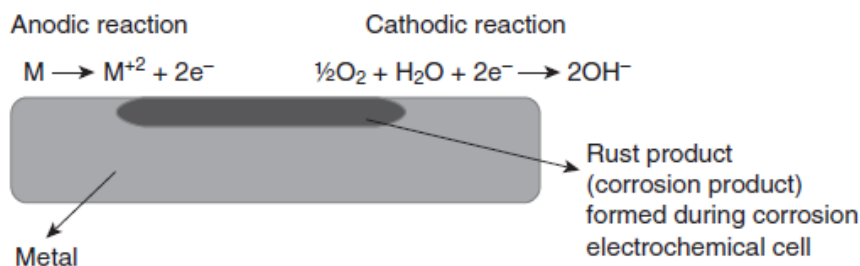
Figure 2.3 : Corrosion process of divalent metal (M) during the electrochemical corrosion cell [5].

For corrosion to occur, the cell potential, E_{cell}, of the overall corrosion reaction must be positive, which corresponds to a decrease in Gibb's Free energy. E_{cell} is the difference in the equilibrium potential of the cathodic half-cell reaction and the anodic half-cell reaction. For example, for the corrosion of a metal in an acidic solution with hydrogen evolution as the cathodic reaction (Equation 2.6), E_{cell} would be calculated as follows:

$$E_{cell} = E_{H^+/H_2} - E_{Fe^{+2}/Fe^0} \qquad\qquad \textbf{(2.6)}$$

The value of E_{cell} only indicates if the reaction is thermodynamically possible or impossible, and therefore, the study of kinetics is required to obtain the rates of the corrosion reaction [9].

2.4 Corrosion Measurement Techniques

For evaluation of the corrosion behavior, three main kind of techniques can be found in the literature. The first two tecniques can be classified as non-electrochemical and the last one as electrochemical technique:

- Exposure of samples to a corrosive medium (e.g. in a salt spray test) and detection of the development of defects or corrosion products by visible inspection.

- Quantitative dissolution measurements: the weight loss of material into the corrosive solution is determined. However this method is not suitable for localized corrosion and should be only applied to uniform corrosion attack.

- The most widely used techniques for corrosion measurements of coatings are electrochemical techniques. Different kinds of potential, current or polarization measurements are carried out [10].

2.4.1 Non- electrochemical corrosion testing and analysis techniques

Non-electrochemical teqniques can be summarized as follows:

- Weight loss
- Piting and cracking formation rate
- Surface measurements

- Analitical methods
- Mechanical tests (elongation, breaking and fatigue time)

Weight- loss coupon tests are the simplest and most widely used corrosion and inhibitor testing tools employed to determine 'cumulative' metal thinning and localized forms of corrosion such as pitting, crevice corrosion, weld and heat affected zone corrosion, and erosion corrosion as a function of inhibitor concentration. In corrosion coupon tests, metal coupons of known metallurgy, size, shape and weight are exposed to a corrosive environment with and without the addition of corrosion inhibitors, and are inspected for corrosion after a period of time (e.g. every 14 days). Corroded coupons are subjected to visual and optical or microscopic examination, weight loss measurement, and surface analysis by various surface analytical techniques. Corrosion coupons are an excellent source of corrosion information if monitoring is carried out correctly and maintained continuously. However, coupon tests have limitations: they are considered to be time consuming and labor intensive. They may require periodic removal of the test specimen from the corrosive environment, which is troublesome and may alter the progress of localized corrosion. They only detect the cumulative corrosion damage at the end of the exposure period and provide little information on specific events that may have induced this damage. Although the corrosion coupon test appears to be an easy task, there are problems that often lead to unsuccessful and misleading results. An example is the testing for underdeposit corrosion. If a corrosion coupon is fully covered by sand, it would not simulate important galvanic corrosion effects and thus underdeposit corrosion problems would not be detected [11].

2.4.2 Electrochemical techniques for corrosion inhibitor testing and analysis

Since corrosion is a process involving electrochemical oxidation and reduction reactions, it makes sense that electrochemical methods can be used to study and measure corroding systems [12].

Electrochemical techniques for corrosion testing can be classified as follows:

- Ptentiodynamic Polarization Measurements (Linear polarization, Tafel extrapolation)
- Electrochemical empedance measurements
- Electrochemical noise

- Scanning Kelvin Probe
- Scanning-Vibrating Electrode Technique (SVET) [13].

2.4.2.1 Potentiodynamic polarization measurements

When a metal specimen is immersed in a corrosive medium, both reduction and oxidation processes occur on its surface. Typically, the specimen oxidizes (corrodes) and the medium (solvent) is reduced. In acidic media, hydrogen ions are reduced. The specimen must function as both anode and cathode and both anodic and cathodic currents occur on the specimen surface. Any corrosion processes that occur are usually a result of anodic currents [14].

2.4.2.2 Polarization resistance

An electrode is polarized when its potential is forced away from its value at open circuit or corrosion potential. Polarization of an electrode causes current to flow due to electrochemical reactions it induces at the electrode surface. The polarization resistance (R_p) is defined by the following equation:

$$R_P = (\frac{\Delta E}{\Delta I})_{\Delta E \longrightarrow 0} \qquad \textbf{(2.7)}$$

Where,

- ΔE is the variation of the applied potential around the corrosion potential

- ΔI is the resulting polarization current [15].

The following formula shows the relationship between the R_p value, the Tafel constants and the corrosion current:

$$\frac{\Delta E}{\Delta I} = \frac{\beta a.\beta c}{2.3(I_{CORR})(\beta a + \beta c)} \qquad \textbf{(2.8)}$$

I	is the measured cell current in amps
Icorr	is the corrosion current in amps
E	is the electrode potential
Ecorr	is the corrosion potential in volts
βa	is the anodic Beta Tafel Constant in volts/decade
βc	is the cathodic Beta Tafel Constant in volts/decade

2.4.2.3 Tafel extrapolation methods

Corrosion on metals occurs at a reaction rate determined by opposing electrochemical reaction equilibria established between the metal and an electrolyte solution. One reaction is the anodic reaction, in which the metal is oxidized releasing electrons from its surface. The other is the cathodic reaction, in which solution species like O_2 or H^+ or even the protective coatings and oxide films that cover the metal, are reduced, attracting electrons from the metal.

In a corrosion system, the Tafel equations for both cathodic and anodic reactions can be combined into the Stern-Geary equation:

$$I = I_a + I_c = I_{corr}.(\exp(2.3\frac{E - E_{corr}}{\beta a}) - \exp(-2.3\frac{E - E_{corr}}{\beta c})) \quad\quad \textbf{(2.9)}$$

Where;

I   is the measured cell current in amps

I_{corr} is the corrosion current in amps

E   is the applied electrode potential

E_{corr} is the corrosion potential in volts

β_a is the anodic beta Tafel constant in volts/decade

β_c is the cathodic beta Tafel constant in volts/decade [1].

Figure 2.7 diagrams this process. The vertical axis is potential and the horizontal axis is the logarithm of absolute current. The theoretical current for the anodic and cathodic reactions are shown as straight lines. The curved line is the total current - the sum of the anodic and cathodic currents. This is the current that you measure when you sweep the potential of the metal with potentiostat. The sharp point in the curve is the point where the current changes signs as the reaction changes from anodic to cathodic, or vice versa. The sharp point is due to the use of a logarithmic axis. The use of a log axis is necessary because of the wide range of current values that must be displayed during a corrosion experiment. Because of the phenomenon of passivity, it is not uncommon for the current to change by six orders of magnitude during a corrosion experiment [16].
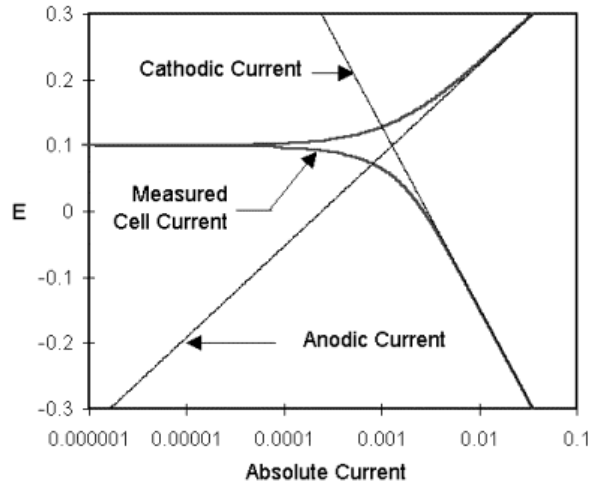
Figure 2.4 : Corrosion Process Showing Anodic and Cathodic Current Components [16].

The equilibrium potential assumed by the metal in the absence of electrical connections to the metal is called the Open Circuit Potential, Eoc. In most electrochemical corrosion experiments, the first step is the measurement of Eoc. The terms Eoc (Open Circuit Potential) and Ecorr (Corrosion Potential) are usually interchangeable, but Eoc is preferred [16].

2.4.2.4 Electrochemical impedance spectroscopy

Electrochemical impedance spectroscopy (EIS) measurements play a vital role in corrosion research. EIS is informative and non-destructive method that is particularly helpful in explanation of mechanisms of electrochemical reactions in corroding systems and in revealing important properties of passivation layers or protective films. The main pillars of the impedance analysis are (i) the physical modelling of the electrochemical interface and (ii) subsequent fitting of experimental spectra to the models in order to extract relevant physico-chemical parameters determining the properties of the electrode/electrolyte boundary [17].

EIS is used to characterize the interface between a metal and an electrolyte. The potentiostat applies both a dc potential and a small superimposed ac excitation to a specimen immersed in an electrolyte. In the experiments, alternating current and ac potential are measured as the excitation frequency varies over several orders of magnitude. The cell voltage and cell current are then converted into a complex impedance by a signal processing instrument such as lock-in amplifier or a frequency

response analyzer. The plot of complex impedance versus frequency can generate information that is difficult to obtain by other types of electrochemical techniques.

Electrochemical impedance spectroscopy is useful in the evaluation of coatings, the elucidation of transport phenomena in electrochemical systems and the determination of corrosion mechanisms and rates. Bode and Nyquist plots are the most common data output formats and an example of each for a simple parallel-connected resistance-capacitance circuit are shown in Figure 2.5 and 2.6 respectively.
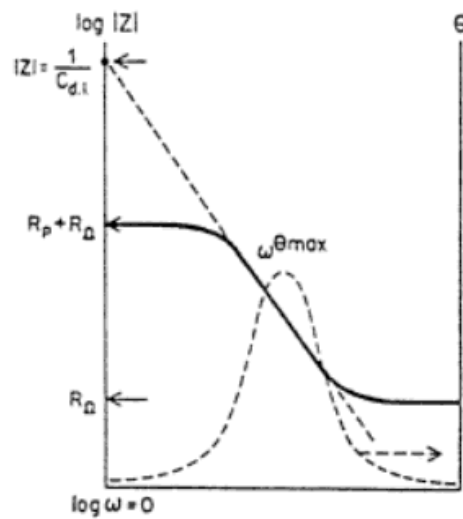
Figure 2.5 : A typical Bode plot of an electrochemical system [1].

The Bode plot format shows the absolute impedance, |Z|, and the phase shift, θ of the impedance, each as a function of frequency f in cycles per second. The log |Z| versus log ω (where $\omega = 2\pi f$) curve can provide values of R_p (polarization resistance) and R_Ω (solution resistance) from the horizontal plateau at low and high frequencies, respectively. At intermediate frequencies, the curve is a straight line with a slope of -1, and extrapolation of this line to the log |Z| axis yields the value of C_{dl} (double layer capacitance) from the following relationship (Equation 2.10):

$$|Z| = \frac{1}{C_{dl}} \qquad\qquad \textbf{(2.10)}$$

The Bode plot format also shows the variations of phase angle θ with log ω. At the high and low frequency limits, where the behaviour is resistor-like, the phase angle is nearly zero. At intermediate frequency ranges, the phase angle increases as the imaginary component of the impedance increases. The expression for Z is composed of a real and an imaginary part (Equation 2.11):

12

$$Z = Z' + jZ'' \qquad\qquad (2.11)$$

In the Nyquist plot shown in Figure 2.6, the real part is plotted on the X axis and the imaginary part on the Y axis. This plot has been annotated to show that low frequency data are on the right side of the plot and higher frequencies are on the left. On the Nyquist plot, the overall impedance can be represented as a vector (arrow) of length |Z|, and the angle between this vector and the X axis is θ, where θ= arg(Z). At this very high frequency, the imaginary component, Z", disappears, leaving a sum of R_Ω and the Faradaic reaction resistance or polarization resistance, P_p. Both the Nyquist and Bode plots should give analogous results of R_Ω and R_p [1].
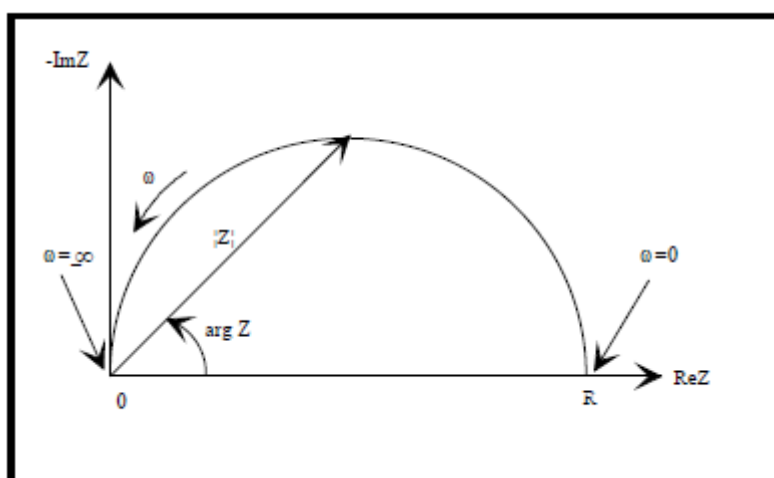
Figure 2.6 : Nyquist plot for a simple electrochemical system with impedance vector [1].

Practically speaking EIS provides a measure of the resistance of the organic coating to aqueous and ionic transport. The technique is based on the measurement of the current response on small sinusoidal perturbations of the electrode potential as a function of the frequency of the perturbation.

Different models have been proposed to analyse EIS measurements obtained for model systems and technical coatings. These models have been applied for industrial screening of organic coatings on bare and phosphated steel in 0.5 M NaCl solution. Figure 2.7 shows a typical impedance spectrum of a quasi-ideal coating which does not exhibit any indication of corrosion attack even after exposure time of up to half a year.
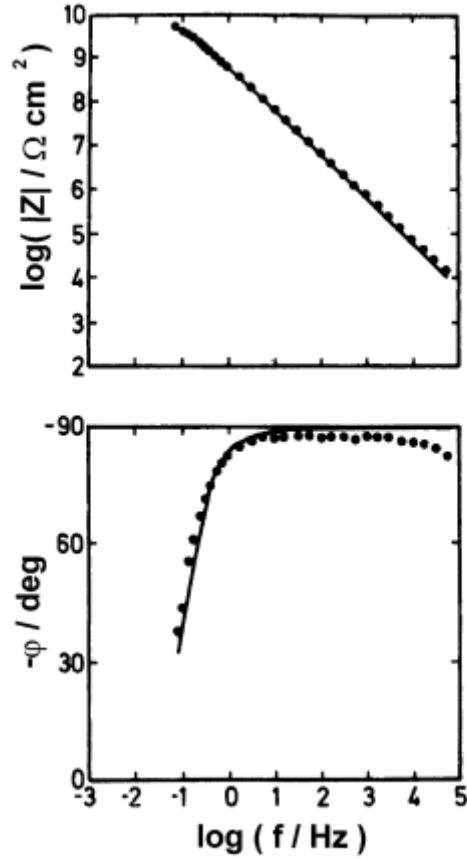
Figure 2.7 : Impedance of a quasi-perfect coating on steel. Experimental data (●)
and optimum fit (–) [18].

The Bode plot shows a pure capacitative behaviour over a wide frequency range and the polarisation resistance at low frequencies is in the order of 10^{11} ohm.cm^2. This is the simple case of a homogeneous 3-D film which is well illustrated in Figure 2.8. The impedance of the coated electrode is described by a parallel combination of the capacitance, C_L; and the resistance, R_L, of the layer which can be given as Equation 2.12.

$$Z_L(j\omega) = \frac{R_L}{1 + j\omega R_L R_C} \tag{2.12}$$

The coating capacitance is given in Equation 2.3.

$$C_C = \varepsilon\varepsilon_0 \frac{A}{d} \tag{2.13}$$

where ε is relative dielectric constant, ε_0 is dielectric constant in vacuum, A is coating area, and d is coating thickness.

14

Thus the capacitance measurement by EIS can provide information on the water uptake, since this incorporation of polar molecules leads to an increase in the dielectric constant of the coating.

Three cases might now be distinguished:

- Corrosion underneath the coating without any defect in the coating itself,
- Partially damaged coating with cracks reaching the metal surface, and
- Partially damaged coating which thereby caused corrosive undermining of the coating [18].
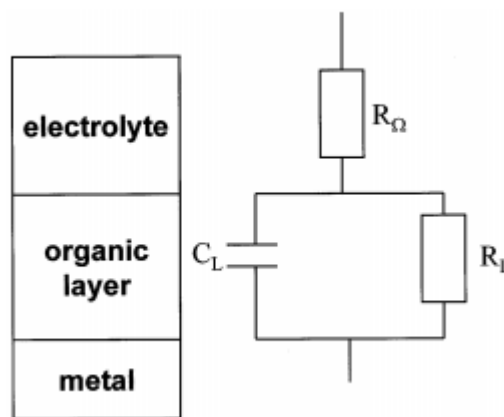
Figure 2.8 : Impedance model of a defect free organic coating on a metal surface in contact with an electrolyte [18].

2.5 Corrosion Control and Protection

Corrosion control is an ongoing, dynamic process in the prevention of metal deterioration in three general ways:

- changing the environment
- changing the material
- placing a barrier between the material and its environment.

The material does not have to be metal – but it is in most cases. Again, the environment is, in most cases, the atmosphere, water, or the earth, and is an important contributor to corrosion chemistry [19].

Two approaches have been used for protecting the metal surface by either metal alloying or by using suitable organic/inorganic coatings. In the presence of corrosive media, a suitable corrosion inhibitor can be applied to decrease the rate of anodic

and/or cathodic reactions. Electrochemical control can be achieved by passing cathodic or anodic current into the metal or by using sacrificial anodes such as zinc, aluminum or magnesium.

2.5.1 Corrosion protection methods

Corrosion prevention methods can be classified into 4 groups:

  - Anode, anode-electrode interface or change in anodic reaction
  - Cathode, cathode-electrode interface or change in cathodic reaction,
  - Change in electrolyte (inhibitor addition or removing oxidizing agent)
  - Usage of electric connection

These methods can be divided into 2 groups as methods with materials and methods with media and interface.

2.5.1.1 Protection methods with material

Basic way of corrosion protection is the appropriate material usage and right design of the material to prevent the corrosive effect of the media. Metal additivies are used to form alloys in case of high corrosion rates of materials. To choose the right metal or alloy, some general rules can be followed. For instance, for acidic or reductive media nickel, copper and their alloys, for oxidative media alloys including chromium or titan and their alloys can be used. On the other hand, noble metals have higher resistance compared to the less noble metals, so noble materials can be preferred in order to reduce corrosion rates. Additionally, natural and synthetic engineering polymers, ceramics, carbon materials and composites are preferred to be used instead of metals to reduce material corrosion.

2.5.1.2 Protection methods with media and interface

During operation, loss due to corrosion can be reduced by preventive methods. These methods can be listed as:

i) Inhibitors
  - Anodic
  - Cathodic
  - Mixed

ii) Protective Coatings

- Metal
- Non-metal inorganic
- Organic

iii) Cathodic protection

- With external current
- Galvanic anodic

iv) Anodic protection

- Passivization

    - Protective film formation via chemical reaction (oxide layer formation, phosphatization, chromatization)

    - With external current [13].

2.6 Organic Coatings

The use of organic coatings is one of the most important approaches for minimizing these enormous corrosion losses. The use of renewable resources in the preparation of various corrosion protective coatings has been revitalized because of environmental concerns [7].

Organic coatings consist of (1) a binder or vehicle, (2) pigments, and (3) additives such as dryers, hardening agents, stabilizing agents, surface activating compounds, and dispersion agents. Coatings can act as a barrier layer to separate the substrate metal from its environment. In some cases, the presence of corrosion inhibiting chemicals in the coatings can further significantly improve their protection performance. In a multi-layer coating system, organic coating is usually used on the top. Organic coating can be applied or formed by a variety of approaches, including painting, powder coating, e-coating, sol–gel coating, and plasma polymerization. The main composition of a coating is resin, which has a variety of types, such as polyvinyl butyral, acrylic polyurethane, vinyl, epoxy and baked phenolic containing zinc chromate or strontium chromate. In order to protect the metal substrate from corrosive environment, the coatings must be uniform, pore free, well-adhered to the substrate and self-healing. These can be accomplished by the presence of corrosion

inhibiting pigments or additives in the coating or by the use of a sacrificial anodic compound in the film [20].

While more and more functionality is introduced into coatings, still the aspect of corrosion protection especially for steel and aluminium are of great interest in research and development. This is due to the fact that hazardous compounds such as Cr(VI) which nowadays guarantee excellent corrosion protection properties have to be replaced with alternative environmentally friendly compounds; the introduction of new light metals such as magnesium with specific corrosion behaviour require specially adopted coatings; use of water based or 100% solvent free coatings will replace solvent based coatings; application of new curing technologies such as UV or electron beam (EB) curing might lead to new specific reactions at the metal/polymer interface; and the trend to sell pre-coated steel sheet to the automotive industry to omit secondary corrosion protection procedures and to reduce the costs caused by expensive paint shops raises new demands for thin organic coatings.

The corrosion protection properties of an organic coating most often result less from the barrier properties but more from the maintenance of adhesion to the substrate under chemical and electrochemical conditions imposed by the environment. It could be shown that for typical organic coatings used for corrosion protection the diffusion rate of H_2O and O_2 far exceeds the diffusion limited value for oxygen reduction. However, ion solubility within the coating is typically very small due to the low dielectric constant of common coatings. The following roles of organic coatings provide corrosion protection:

- Barrier for ions leading to an extended diffusive double layer.
- Adhesion of the coating.
- Blocking of ionic paths between local anodes and cathodes along the metal/polymer interface.
- Vehicle of corrosion active pigments and inhibitors which are released in the case of coating damage [18].

2.6.1 Role of conducting polymers in corrosion protection

Intrinsically conducting polymers (ICPs) were discovered in 1976 by Heeger, MacDiarmid and Shirakawa, for which they were awarded the Nobel Prize in Chemistry in 2000. ICPs belong to those classes of polymers which have π

conjugation along the polymer backbone such as polyaniline (PANI), polypyrrole (PPy) and polythiophene (PTh), as shown in Figure 2.9.

(a) Polyaniline   (b) Polypyrrole   (c) Polythiophene
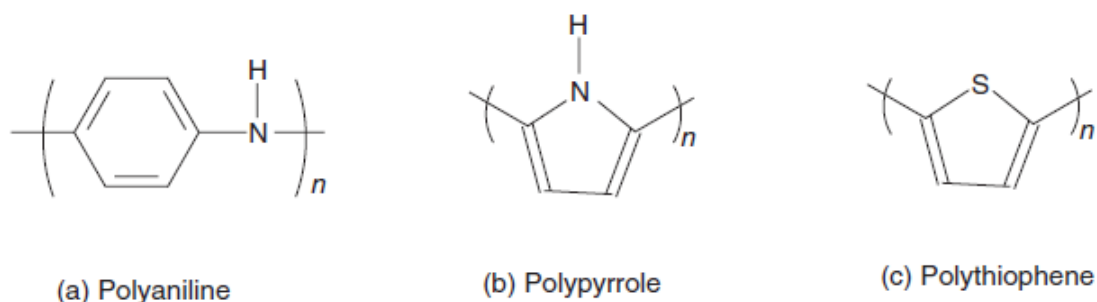
Figure 2.9 : Chemical structure of some heterocyclic ICPs [21].

CPs represent a new class of 'synthetic metals' which have attracted the attention of many researchers in areas such as separation membranes, gas sensors, electrocatalysis, actuators, rechargeable batteries and biosensors. One of the unique characteristics of CPs is their ability to undergo oxidation–reduction reactions, by gaining or losing electrons from the surrounding environment. Because of this interesting feature, CPs have been proposed as novel anti-corrosion coatings for different metals and alloys [21].

There is an increasing interest on the use of CP to protect reactive metals against corrosion. At least four different configurations to apply CP coatings have been reported:

(i) as a coatings alone;

(ii) as a primer coating with a conventional topcoat;

(iii) blended with a conventional polymer coating;

(iv) as an additive to modify a conventional organic coating.

The first studies devoted to examine the protection imparted by CP coating on active metals were published at the beginning of eighties [6].

2.6.2 PANI

PANI is a quite established material having been prepared over 150 years ago by H. Letheby. Clearly, at that time the polymeric nature of PANI was not understood; the material was called 'aniline black' and was used in textiles as dyes and in printing. Currently, the preparation of PANI is accomplished via oxidation under mild conditions [5].

PANI can be represented in three different convertible structures, leucoemeraldine, pernigraniline and the emeraldine base (EB) as shown in Figure 2.10. The most useful structure is the non-conducting EB which can be converted into the conducting emeraldine salt (ES) by acid treatment through a process known as 'doping'. The associated ionic materials/electrolytes are called 'dopants'. The conductivity increases as the doping level increases. PANI in its conductive ES and non-conductive EB was utilized as anti-corrosion coating for ferrous and non-ferrous metals and alloys; including iron, steel, stainless steel, aluminum, aluminum alloys, copper, zinc, titanium and magnesium [21].
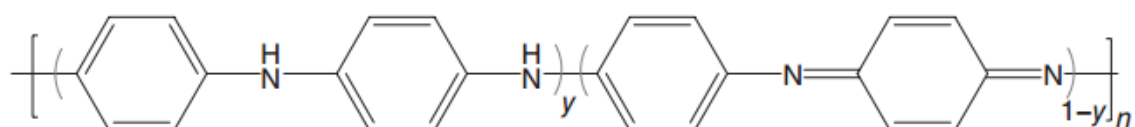
y= 0,5 Emeraldine (EB)

y= 0 Pernigraniline (PB)

y= 1 Leucoemeraldine (LEB)

Figure 2.10 : Different convertible structures of PANI.

Electrochemical and chemical synthesis of conducting PANI by oxidative polymerization is usually described by the scheme in Figure 2.11 (Wei at al., 1989). It involves:

1) Oxidation of nitrogen atom of monomer followed by oxidation of end nitrogen atom of oligomer and polymer;

2) Addition of monomer in the "nitrogen-carbon" fashion as a result of chain reaction (electrophilic substitution of proton in aromatic ring of monomer by oxidized polymer fragment).
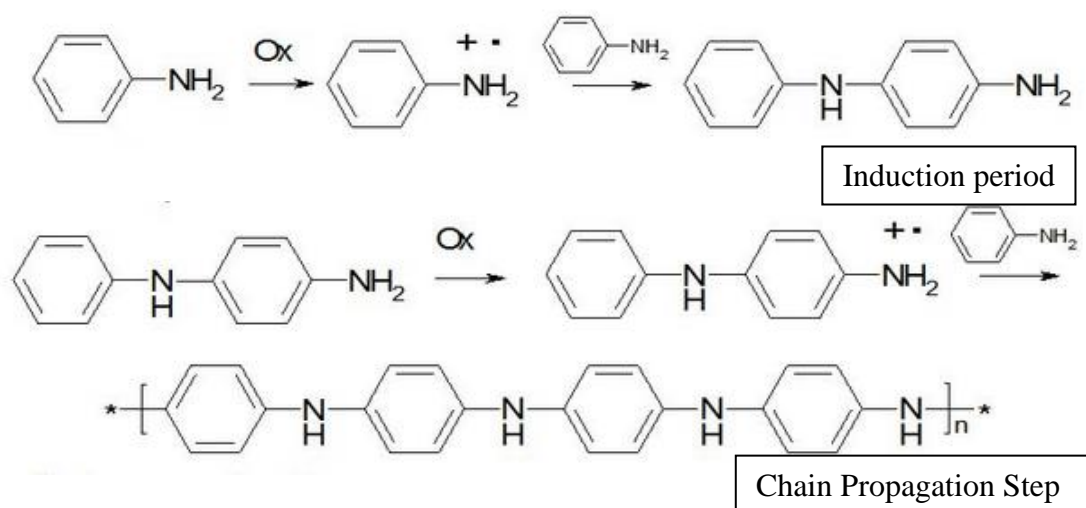
Figure 2.11 : Aniline oxidative polymerization [22].

In the induction period, aniline radical cations are formed; this process is followed by their recombination (according to the electrophilic substitution mechanism) to afford a dimer, namely, N-phenylphenylene-1,4-diamine (p-semidine). The following propagation step is assumed to be similar to the electrophilic substitution process where the oxidized terminal amino group of oligomer (polymer) attacks para-position in monomer. It is assumed that the reaction involves monomer in its most reactive deprotonated form. The oxidation rate-limiting step is considered to be either the formation of aniline radical cations or their dimerization [22].

As an intrinsically conducting polymer, PANI has received considerable attention over the past two decades because of its relatively easy preparation, excellent environmental and thermal stabilities, low cost, as well as interesting electronic properties. One of the applications of PANI is corrosion protection. Numerous studies have revealed that PANI can improve the corrosion resistance of stainless steel, iron, mild steel, copper, aluminum, and zinc [23].

An interesting alternative to avoid multilayer coatings is the mixing of CP with conventional resins to prepare blend materials for corrosion protection. In this context, blended coatings formed by PANI or poly-o-ethoxyaniline mixed with an equal amount of epoxy, polymethylmetacrylate or water soluble epoxy showed better corrosion protection of iron than single component coatings. Furthermore, excellent anticorrosion effects were also found in coatings constituted by PANI blended with polyimide or poly(esteramide urethane), even although in these cases the CP only

reached 8–15 wt%. Unfortunately, no information about the anticorrosive properties of blends containing PPy or PTh derivatives is available to our knowledge.

On the other hand, paint formulations modified by the addition of low concentration of CP, i.e. typically 0.2–0.3% w/w, have been shown to impart in some cases better corrosion resistance than unmodified paints. Thus, paints prevent steel from corrosion by isolating the substrate from the environment, i.e. limiting the access of oxygen, water or other pollutants to the steel surface. In order to make the paint more effective, some corrosion inhibitors are often added: zinc powders, iron oxide, chromium compounds, calcium ion exchanged amorphous silica, organic amines, etc. However, some of these anticorrosive additives reduce the performance of the paint and even can result in environmental and health problems. Accordingly, at present time CP are considered an alternative to replace conventional anticorrosive pigments [6].

Various corrosion protection mechanisms using PANI ICP have been proposed as summarized in Figure 2.12. These include cathodic protection, passivation (anodic protection), barrier protection (coatings) and corrosion inhibitor [21].
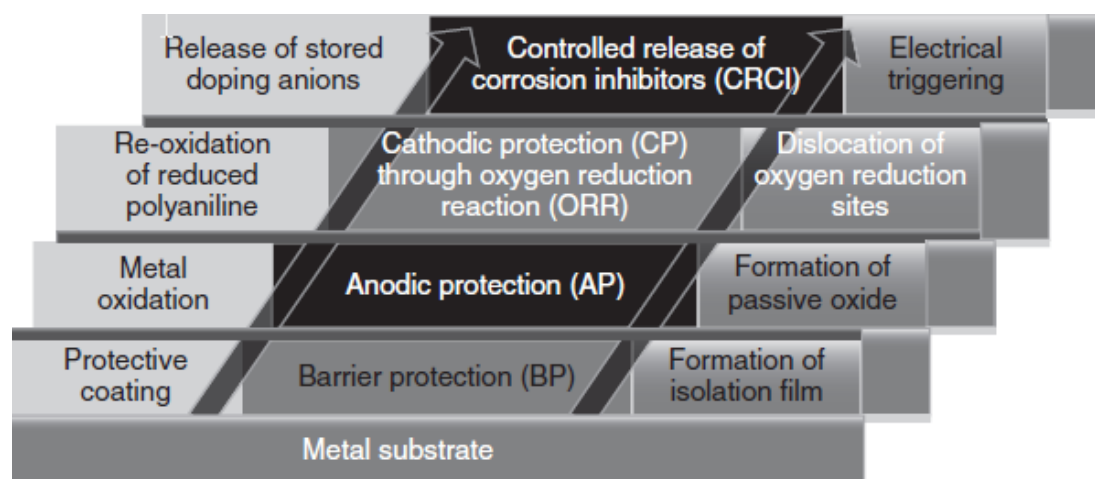
Figure 2.12 : Schematic illustration of various possible corrosion protection mechanisms by ICPs [21].

2.6.3 Cerium oxide

Based on present literature, several different strategies and materials were exploited for storage and prolonged release of corrosion inhibitors. Among the novel materials developed as corrosion inhibitors, the interest for the use of lanthanide compounds is growing over the last years. The success of these compounds is attributed to the

corrosion potential efficiency of cerium salts, in particular chlorides and nitrites. It has been demonstrated that they promoted protection to a significant number of metals and alloys, for example steel, hot dip galvanized steel, tin, aluminum and their alloys, etc. In fact, because of the local pH increase at the cathodic sites due to the generation of OH^- ions via Equation 2.14.

$$2H_2O + O_2 + 2e^- \rightarrow 4OH^- \tag{2.14}$$

OH^- ions occur when a corrosion process takes place, insoluble cerium compounds such as $Ce(OH)_4$ and $CeO_2 \cdot xH_2O$ are formed. These compounds are believed to precipitate on the surface of the metal, reducing the cathodic reaction rate and, thus, the overall corrosion extent. Following the success of soluble cerium salts as corrosion inhibitors, cerium oxides particles have been likewise studied as pigments inside protective coatings for corrosion mitigation purposes. Cerium oxides are widely used as a reducible oxide support material in the field of emission control catalysis for the purification of exhaust gases for different combustion systems, mainly due to their oxygen storage capacity (OSC). Owing to the ease of the $Ce^{4+} \leftrightarrow Ce^{3+}$ redox shuttle, the exchange process in Equation 2.15 is   is favored.

$$2CeO_2 \leftrightarrow Ce_2O_3 + 1/2O_2 \tag{2.15}$$

Thus, the material is suitable for storing and releasing oxygen under conditions fluctuating between oxidizing and reducing state of cerium ions. In fact, the $Ce^{3+} \leftrightarrow Ce^{4+}$ shift leads to a high oxygen mobility in the ceria lattice that is responsible for its high catalytic activity. The particular behavior of the cerium oxides was attributed to the unstable fluorite structure of the lattice where some Ce^{4+} have a tendency to be reduced to Ce^{3+}, which has a larger ionic size than Ce^{4+}, followed by oxygen molecules release with subsequent formation of oxygen vacancies [24].

3. EXPERIMENTAL STUDY

3.1 Chemicals

Aniline monomer, cerium (IV) oxide and ammonium peroxidisulfate and acetone was supplied from Sigma-Aldrich, aniline monomer and hydrochloric acid was supplied from Carlo Erba. Dimethyl formamide was supplied from Alfa Easer. Sulfuric acid was supplied from Riedel.

3.2 Metal Electrodes

For corrosion prevention detection, phenol-formaldehyde resin based paint including PANI and PANI/CeO_2 nanocomposite was coated over 2 types of cylindrical electrodes of aluminium and carbon steel, 8 mm in diameter both. Electrodes were placed in glass tubes which prohibit connection of uncoated surface with the solution and the other electrodes used in the cell during electrochemical measurements. Glass tube was attached at the metal surface by using two component epoxy resin system, which is durable inside the acidic medium and prevents the solution in the cell to leak inside the glass tube. Aliminum electrodes contain (%*w/w*) 0.40 Fe, 0.30 Si, 0.05 Cu, 0.20-0.60 Mn, 2.70-3.70 Mg, 0.20 Zn, 0.20 Ti, 0.30 Cr and carbon steel electrodes contain 0.35 C, 0,65 Mn, 0.25 Si, 0.035 P, 0.035 S and Fe to 100.

3.3 Polyaniline and Polyaniline/CeO_2 Nanocomposite Synthesis

Polyaniline and polyaniline/CeO_2 nanocomposite were synthesized as proposed by E. Kumar and co-workers. The following synthesis method was applied:

For synthesis of PANI/CeO_2 4.5 ml aniline was injected into 70 ml of 2 M HCl containing 2 g of CeO_2 nanoparticles under ultrasonic action to reduce the aggregation of nanoparticles. After 12h, 4.5 g of APS was dissolved in 20 ml deionized water and it was dropped into solution with constant stirring for about 10 min. Polymerization was allowed to proceed for 3 h at 30 C. Reaction mixture was

filtered under gravity and washed with 2 M HCl and deionized water, afterwards dried at 90 C for 12 h in vacuum to obtain a fine tint green powder.

For synthesis of PANI without CeO_2, the same procedure was applied without adding CeO_2 nanoparticles.

PANI and PANI/CeO_2 nanocomposite were used both in protonated emeraldine salt (green color) forms as recived from the reaction and deprotonated emeraldine base (EB) forms by reacting with NH_4OH (blue color).

In order to obtain EB forms PANI and PANI/CeO_2 were dissolved in DMF and NH_4OH was added to solution. The color of solution changed from green to dark blue as the emeraldine base form occurred (Figure 3.1) [7].

Transition from emeraldine salt form to base form was also determined by UV-Visible spectrophotometric measurements.
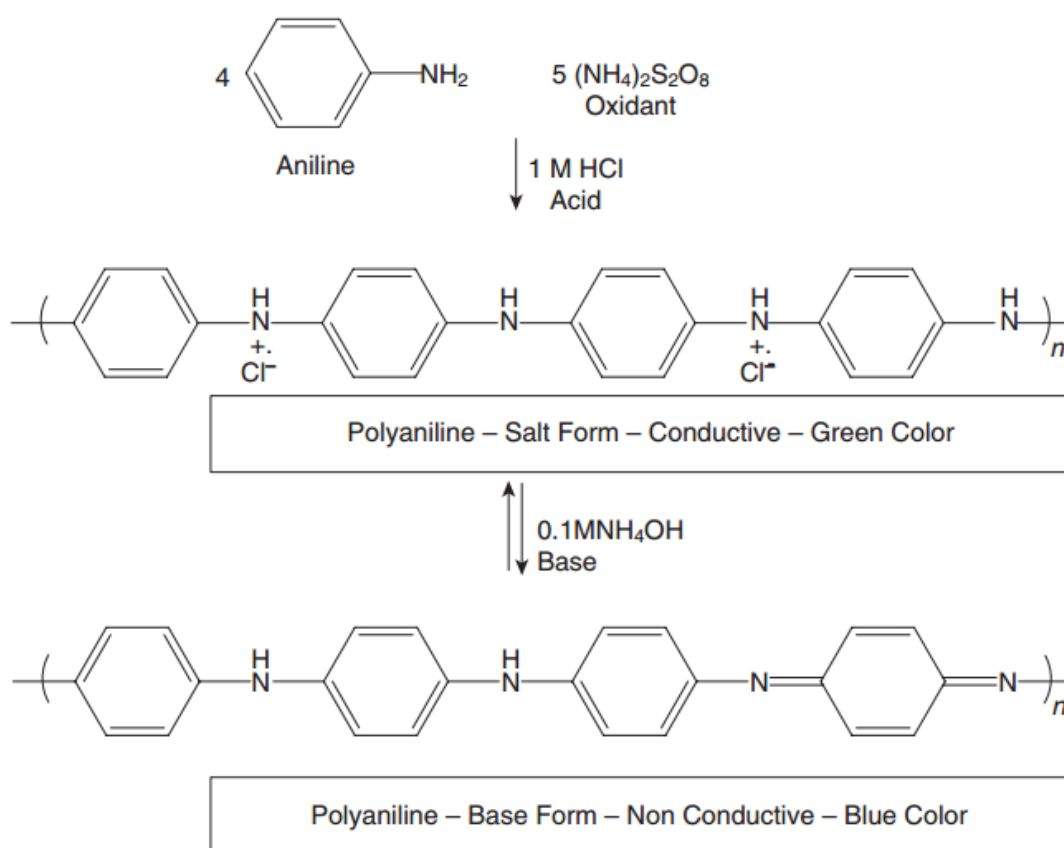
Figure 3.1 : Oxidative polymerization of PANI [7].

3.4 Corrosion Medium

Measurements were carried out with 2 different type of solutions:

- 0.1 M H_2SO_4
- Seawater

3.4.1 Seawater preparation

Through the experiments, artificial seawater was prepared as indicated at Table 3.1. The ion content for the 3,5% w/w artificial seawater is seen at Table 3.2 and the approximate pH value of this formulation is 8 and conductivity is 60.000 µs/cm.

Table 3.1: Formula of 1 kg of 3.5% w/w artificial seawater [25].

Gravimetric salts	Molecular wt	g/kg of solution
NaCl	58.44	23.926
Na_2SO_4	142.04	4.008
KCl	74.56	0.677
$NaHCO_3$	84.00	0.196
KBr	119.01	0.098
H_3BO_3	61.83	0.026
NaF	41.99	0.003
Volumetric Salts	**Molecular wt**	**moles/kg of solution**
$MgCl_2.6H_2O$	203.33	0.053
$CaCl_2.2H_2O$	147.03	0.010
$SrCl_2.6H_2O$	266.64	0.00009
Distilled water to 1,000 g		

Table 3.2: The ion content for 3.5% w/w artificial seawater [25].

Ion	Artificial Seawater (g/kg)
Cl^-	19.353
Na^+	10.765
SO_4^{2-}	2.711
Mg^{2+}	1.295
Ca^{2+}	0.414
K^+	0.387
HCO_3^-	0.142
Br^-	0.066
Sr^{2+}	0.008
H_3BO_3	0.026
F^-	0.001

3.5 Paint Solution Preparation

1 gram phenol-formaldehyde resin was dissolved in 2 ml acetone and 0.05g PANI or 0.05 g PANI/CeO_2 nanocomposite were dissolved in 5 ml dimethyl formamide (DMF) ultrasonically. PANI and PANI/CeO_2 nanocomposites were not completely soluble and insoluble part were separated by filtration. Emeraldine base (EB) forms of PANI polymers were prepared by dissolving 0.005g polymer in DMF solution and by reacting these solutions with NH_4OH. Insoluble part was eliminated by filtration. The final saturated concentration of all solutions were given in Table 3.3 Coating were prepared by mixing these solutions in different ratios and the volume of resin and PANI polymers used for coatings and the abbreviation of coating names were summarized in Table 3.4.

Table 3.3 : Polymer solution concentrations

Polymer	Concentration (g/ml)
PANI	1.6×10^{-3}
PANI/CeO_2	9.29×10^{-4}
PANI-EB	8.10×10^{-3}
PANI/CeO_2.EB	5.88×10^{-3}

Table 3.4 : PANI and resin contents and abbreviation of coatings

Abr.of Coating	Polymer	PANI or PANI/CeO_2 (μl)	Resin (μl)	Concentration % (g/g)*
$P_{50}R_{50}$-032	PANI	50	50	0.32
$PC_{85}R_{50}$-032	PANI/CeO_2	85	50	0.32
PC_{50}-R_{50}-019	PANI/CeO_2	50	50	0.19
$P_{50}R_{50}$EB-162	PANI-EB	50	50	1.62
$PC_{68}R_{50}$EB-162	PANI/CeO_2.EB	68	50	1.62
$PC_{50}R_{50}$EB-118	PANI/CeO_2.EB	50	50	1.18

*Concentration % of PANI or PANI/CeO_2 to resin

3.6 Coating Preparation Procedure

Electrodes were mechanically polished with emery papers of 400, 600 and 1200 grids and then with aluminium paste. Then the electrodes were washed with isopropyl alcohol in an ultrasonic bath and dried before use. Deposition were carried

out by dropping 3 µl coating solution on metal electrodes. After deposition of each layer, the substrate was allowed to dry completely. Film thickness was calculated based on the concentration of the polymer solution, polymer density (d= 1.36 g/ml), weight and surface area of the electrode as suggested in literature [26, 27]. The average thickness of all coatings are summarized in the Table 3.5.

Table 3.5: Thickness of coatings

Coating	Thickness (µm)
$P_{50}R_{50}$-032	14.9±0.2
$PC_{85}R_{50}$-032	11.1±0.2
PC_{50}-R_{50}-019	14.9±0.2
$P_{50}R_{50}EB$-162	14.9±0.2
$PC_{68}R_{50}EB$-162	12.6±0.2
$PC_{50}R_{50}EB$-118	14.9±0.2

3.7 Methods

Electrochemical measurements including potentiodynamic polarization curves and electrochemical impedance spectroscopy (EIS) were performed in a three-electrode cell (Figure 3.2). A glass cell of 100 ml capacity which contains three electrodes; steel/aluminium as working, platinum as counter and silver/silver chloride (Ag/AgCl) as reference electrodes was used.

Gamry Reference 600 Model Potentiostat with a software version 5.67 was used. The potentiodynamic current−potential curves were measured at a scan rate of 1 mV/s. Impedance measurements were carried out using AC signals of amplitude of ±10 mV (peak to peak) at open circuit potential in the frequency range from 10 mHz to 1 MHz. Prior to the potential sweep. the electrode was left under open-circuit in the respective solution for ~1 h until a steady free corrosion potential was recorded.
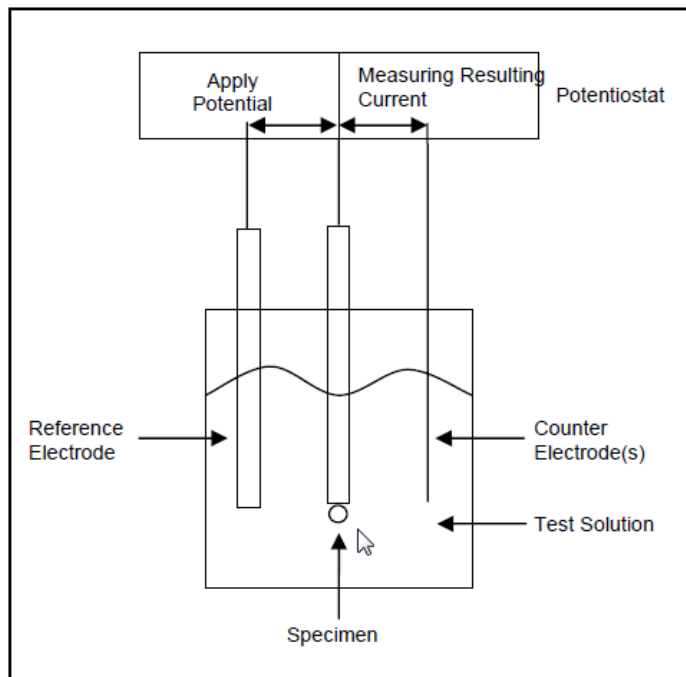
Figure 3.2 : Potentiostat operation

4. RESULTS AND DISCUSSION

Before application as coating material synthesized PANI and PANI/CeO$_2$ were characterized by Fourier Transform Infrared (FTIR) and UV-Visible absorption measurements. Then anticorrosion effects of coatings constituted by PANI polymers blended with cyclohexane formaldehyde resin were tested both in acidic (H$_2$SO$_4$) and neutral corrosive (sea water) media for carbon steel and aluminum by polarization and EIS measurements. EIS measurements were also supported by equivalent circuit models.

4.1 FTIR Spectral Analysis

The infrared spectroscopy is used to identify the functional groups of the synthesized compounds. The FTIR spectrum of the nanoparticles of CeO$_2$ is shown in Figure 4.1. From the results. it is observed that FTIR spectra of PANI/CeO$_2$ nanocomposites contain contributions from both the CeO$_2$ nanoparticles and PANI.
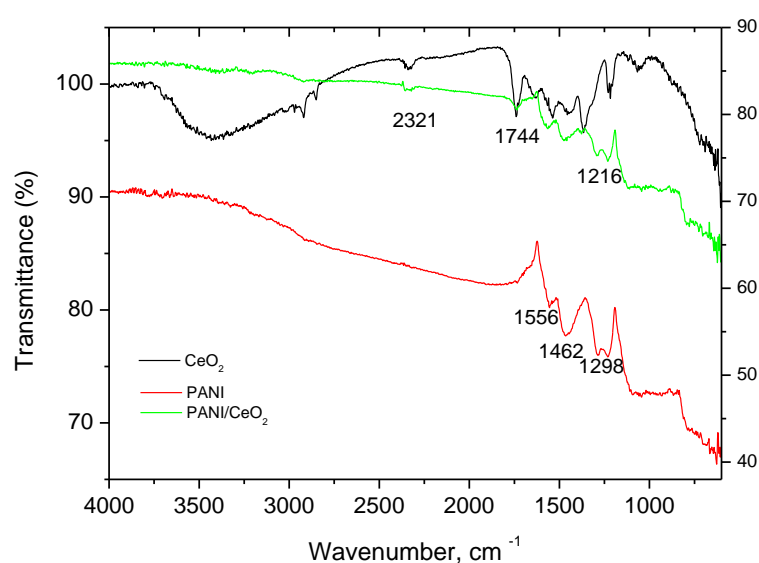
Figure 4.1 : FTIR pattern of PANI, CeO$_2$ and PANI/CeO$_2$ nanoparticles

The bands due to scretching frequency of Ce-O can be seen in 850-1750 cm^{-1}. The characteristic scretching mode of N-N. C-C of PANI were observed at the 1556, 1462, 1298 cm^{-1}. In addition to the characteristic peak of PANI. Ce-O scretching frequency in 850-1750 cm^{-1} and the characteristic peak at 2321 were also observed for PANI/CeO$_2$ nanocomposite indicating the contrubition of CeO$_2$ to the PANI structure.

4.2 UV–Visible Spectrofotometric Analysis

UV–Visible absorption spectra of emeraldine salt and emeraldine base (EB) forms of PANI and PANI/CeO$_2$ nanocomposite in DMF solution were compared (Figure 4.2). For the emeraldine salt forms three characteristic absorbance peaks at $\lambda= 275$ nm, $\lambda= 375$ nm, $\lambda=550$ nm arises from the π-π* transition, polaron-π* transition, polaron-π respectively. When NH$_4$OH is added to PANI and PANI/CeO$_2$ solutions the color is changed from green to blue due to transition of emeraldindine salt forms to emeraldine base forms. In this form absorbance peaks at $\lambda= 275$ nm, $\lambda= 375$ nm, become a single peak at $\lambda= 325$ nm and peak at $\lambda=550$ nm shifts to $\lambda=600$ nm and its intensity increases. In the case of EB form the ratio of peak intensities at $\lambda_{325}/ \lambda_{600}$ shows the benzonoid/quinoid ratio. For PANI and PANI/CeO$_2$ nanocomposites the ratios were obtained as 0.47 and 0.43 respectively, which is very close to each other. UV–Visible absorption spectra of pure CeO$_2$ in DMF solution were also recorded and compared with PANI/CeO$_2$ nanocomposite (Figure 4.2.D). As it can be seen well-defined absorption peak located at $\lambda=270$ nm and the sharp and strong absorption spectrum is in good accordance with the narrow size distribution of ceria nanocrystal. The optical absorption value around 270 nm has higher intensity in the case PANI/CeO$_2$ nanocomposite with the conribution of CeO$_2$.
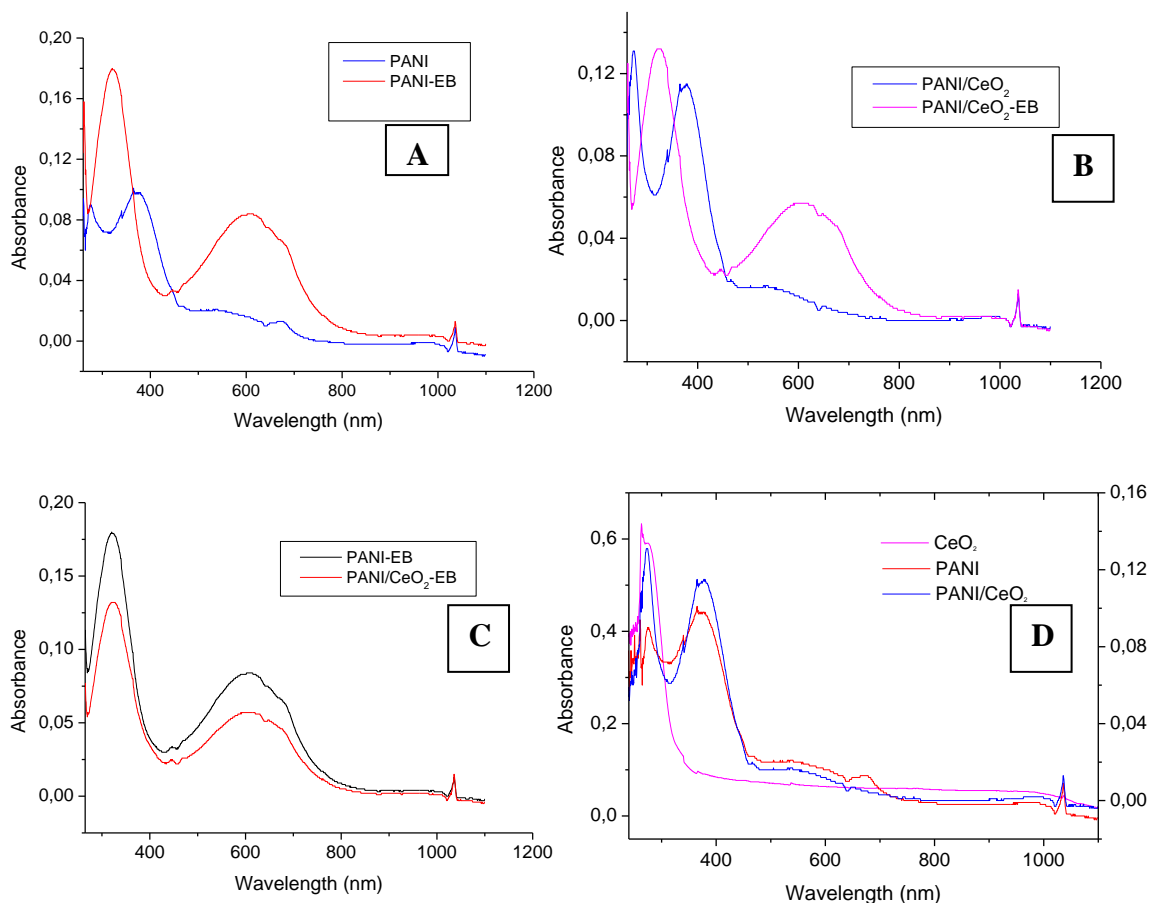
Figure 4.2 : Comparison of UV-visible spectra of emeraldine salt and emeraldine base (EB) forms of PANI **(A),** PANI/CeO$_2$ nanocomposite **(B),** EB form of PANI and PANI/CeO$_2$ **(C),** PANI, PANI/CeO$_2$ and CeO$_2$ **(D)** in DMF solution.

4.3 Measurements in 0.1 M H$_2$SO$_4$ Solution

In this part of the study, corrosion phenomena of carbon steel and aluminum was examined by polarization curves and EIS in 0.1 M H$_2$SO$_4$. Electrodes were kept in electrolyte solutions for 1 hour before each run.

4.3.1 Measurements of bare electrodes in 0.1 M H$_2$SO$_4$

Figure 4.3 shows the Nyquist diagrams plotted at the corrosion potential of bare aluminum and carbon steel electrodes in 0.1 M H$_2$SO$_4$ in the absence of coating.

The high frequency intercept of the semi-circle on the real axis yields the solution resistance (R$_s$) while low frequency region yields the sum of R$_s$ and polarization resistance (R$_p$) of the electrode/electrolyte interface. The semicircles are generally

associated with the relaxation of the capacitors of electrical double layers with their diameters representing the charge transfer resistance [27].

Polarization resistance of bare aluminum electrode and bare carbon steel electrode were obtained as 2.490 ohms 293 ohms respectively. Since the oxide formation energy of aluminium (Al) is much higher than steel, higher value of Rp for Al was observed.
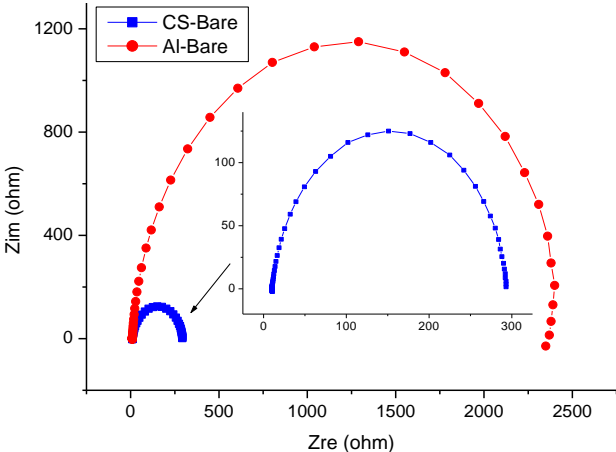
Figure 4.3 : Nyquist plots of bare aluminium and carbon steel electrodes in 0.1 M H$_2$SO$_4$ solution

Tafel-extrapolation measurements were done in the potentials region $\pm$ 250 mV from corrosion potential, E$_{corr}$. All the measurements were conducted after 1 hour of exposure to the electrolyte solution, in order to ensure steady-state conditions. Figure 4.4 shows the current voltage curves obtained with bare electrodes after 1 h exposure to 0.1 M H$_2$SO$_4$.
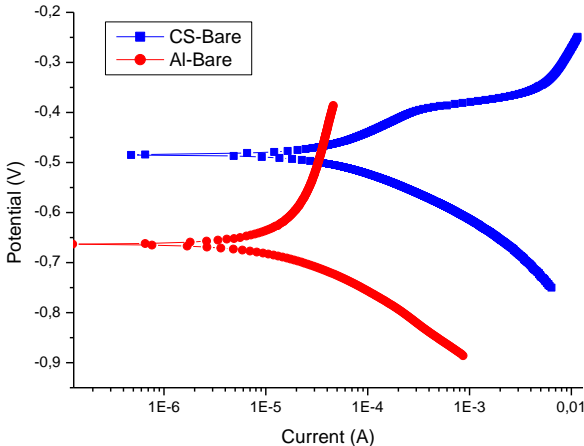
Figure 4.4 : Tafel plots of bare aluminum and carbon steel electrodes in 0.1 M H$_2$SO$_4$ solution

As expected, due to the oxide film formation of aluminium which has a greater cathodic potential resulted in lower corrosion currents.

EIS data is also analyzed graphically by fitting it to an equivalent electrical circuit model using ZSimp-Win software. Figure 4.5 depicts the equivalent circuits to model electrochemical behavior of bare carbon steel electrode after 1 hour immersion in 0.1 M H_2SO_4 solution. The simplified Randles circuit with a CPE is used to represent the corroding system where Rs represents solution resistance. Rp charge transfer resistance. CPE_{dl} a constant phase element, non-ideal double layer capacitive element to give a more accurate fit [28].

It is observed that a reasonable accuracy of the fitting was obtained. As evidence, chi-square is in the order of 10^{-3} and 10^{-4} for the experimental data. Rp values obtained by equivalent curcuits and experiments are in agreement with each other.
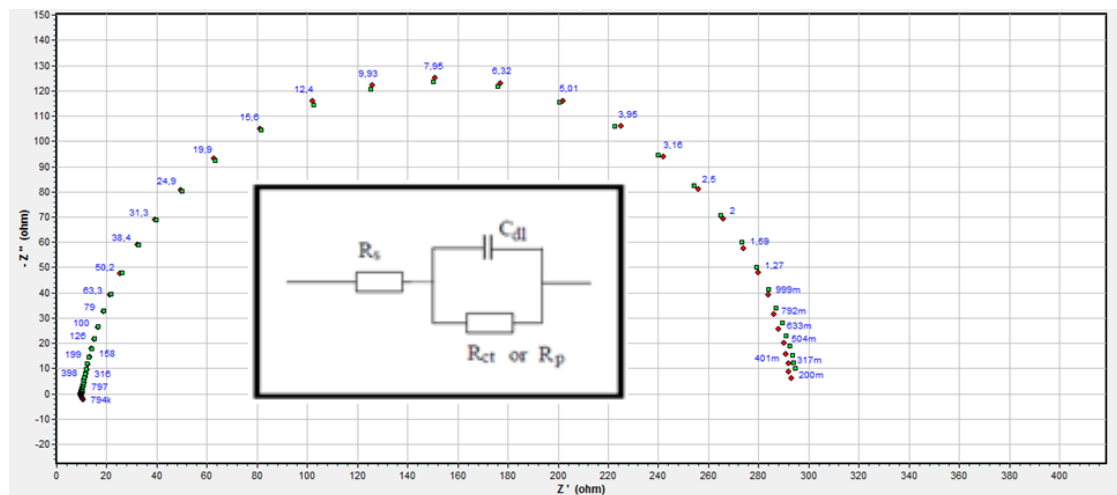
Figure 4.5 : Values of equivalent circuit elements required for fitting the EIS values of bare carbon steel in 0.1 M H_2SO_4 solution.

4.3.2 Measurements with carbon Steel in 0.1 M H_2SO_4

In order to analyze the effect of PANI and PANI/CeO_2 nanocomposite to corrosion resistance of carbon steel, paint solutions with different concentrations including different ratios of PANI polymer and PANI/CeO_2 nanocomposite which had been synthesized previously were applied on electrode surfaces to obtain coatings. Polarization and EIS measurements were conducted after having the coatings dried.

Figure 4.6 shows the Nyquist plots for the impedance of the bare, $P_{50}R_{50}$-032 and $PC_{85}R_{50}$-032 coatings on carbon steel after 1 hour of exposure to 0.1 M H_2SO_4. Loop

sizes of both of the coatings are approximately 3 times larger than the bare electrode which clearly shows the inhibition efficiency of the polymer coatings on carbon steel substrate. R_p values obtained from Nyquist diagrams were summarized in Table 4.1.
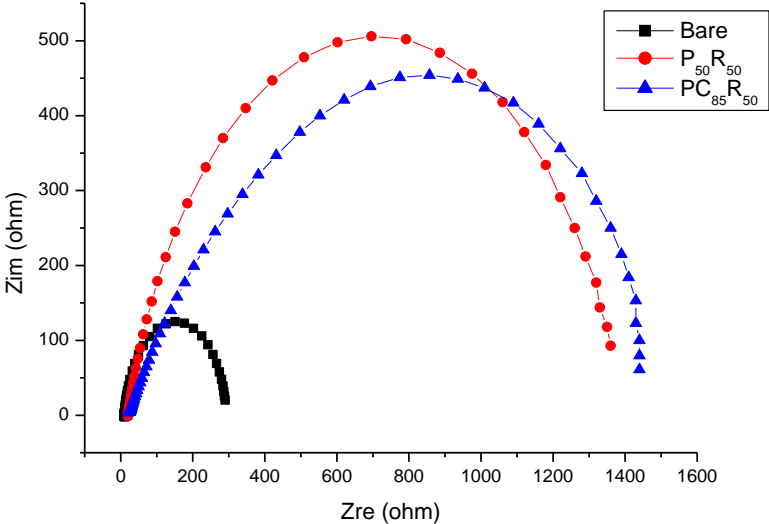
Figure 4.6 : Nyquist plot of bare, $P_{50}R_{50}$-032 and $PC_{85}R_{50}$-032 coatings on carbon steel in 0.1 M H_2SO_4

Figure 4.7 depicts the equivalent circuits to model electrochemical behavior of $P_{50}R_{50}$-032 and $PC_{85}R_{50}$-032 coatings on carbon steel coatings after 1 hour immersion in 0.1 M H_2SO_4 solution. The electrochemical circuit model is represented by the conventional equivalent circuit consists of a series of a resistor and capacitor. Rs(Q(RpW)) where Rs is the uncompensated ohmic resistance between the working electrode and the reference electrode, Rp is the polarization resistance and Q is the constant phase element which represents the total capacitance at the metal/electrolyte interface and Zw is the Warburg impedance which represents the diffusion processes within the pores in case of coated metal/solution interface [1, 27].
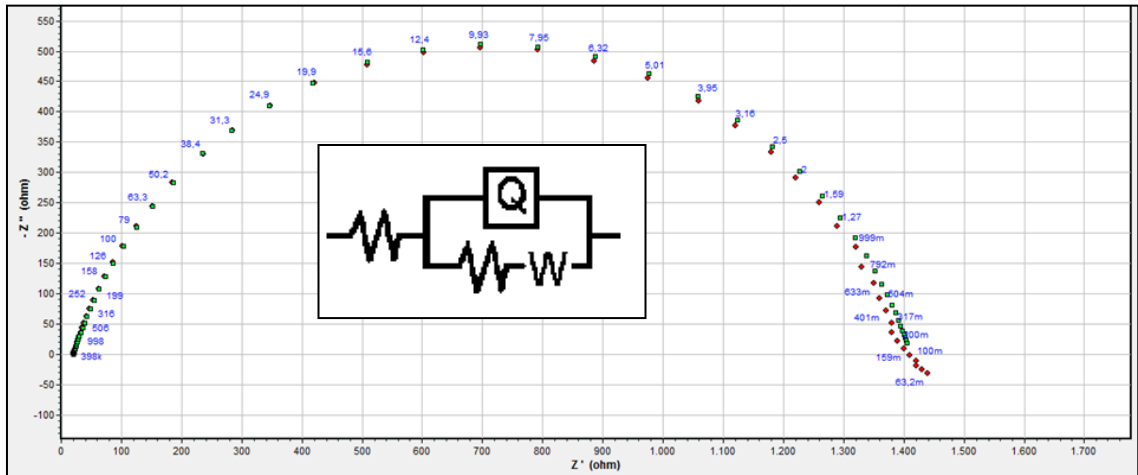
Figure 4.7 : Values of the elements of equivalent circuit required for fitting the EIS of $P_{50}R_{50}$-032 and $PC_{85}R_{50}$-032 coatings on carbon steel electrode in 0.1 M H_2SO_4

The polarization curves of uncoated, $P_{50}R_{50}$-032 and $PC_{85}R_{50}$-032 coated carbon steel in 0.1 M H_2SO_4 are shown in Figure 4.8.
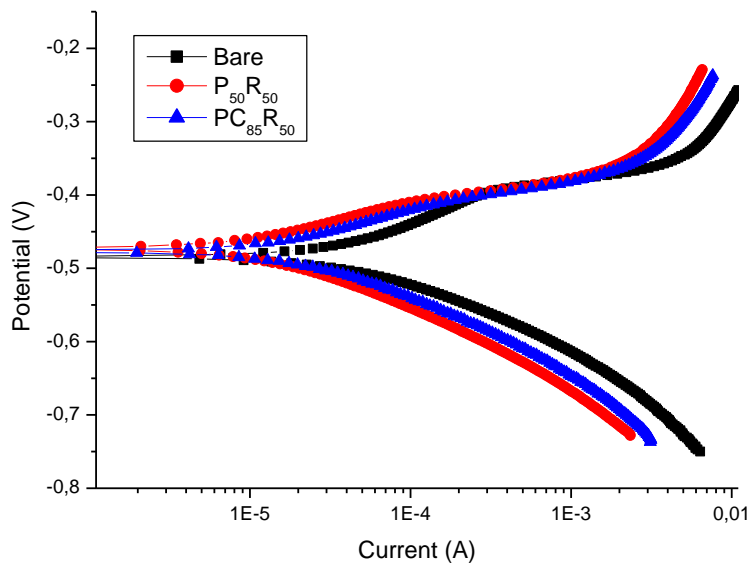
Figure 4.8: Polarization curves of bare, $P_{50}R_{50}$-032 and $PC_{85}R_{50}$-032 coated carbon steel in 0.1 M H_2SO_4

Ecorr, icorr and Tafel slopes were determined from the Tafel plots of potentiodynamic measurements by extrapolation. The values of Rp and CR were calculated using Equation 4.1 and 4.2 [29]. Ecorr, icorr, β_a, β_c, Rp and CR values for uncoated and PANI coated carbon steel electrodes are summarized in Table 4.1.

$$Icorr = \frac{C_R.A.d}{0,129.(EW)} \qquad \textbf{(4.1)}$$

$$Icorr = \frac{\beta_a.\beta_c}{2,303(\beta_a + \beta_c)} \cdot \frac{1}{R_p.A} \qquad \textbf{(4.2)}$$

Table 4.1 : Polarization parameters for BARE, $P_{50}R_{50}$-032and $PC_{85}R_{50}$-032 coated carbon steel in 0.1 M H_2SO_4

Coating	Ecorr (mV)	Icorr ($\mu A.cm^{-2}$)	CR (mpy)	βa (mV)	βc (mV)	Rp ($\Omega.cm^2$)	IEIcorr (%)	IERp (%)
BARE	-484	59.48	27.29	86	68	147		
$P_{50}R_{50}$-032	-473	24.27	11.09	70	88	709	59	79
$PC_{85}R_{50}$-032	-477	25.06	11.47	62	63	744	58	80

As it can be seen from Table 4.1 although corrosion potentials stayed almost constant, corrosion currents decrease and R_p values increase in case of $P_{50}R_{50}$-032 and $PC_{85}R_{50}$-032 coatings compared to bare and CF-R coated electrodes. Both coatings have similar corrosion inhibition efficiencies.

4.3.2.1 Measurements with PANI-EB form coatings on carbon steel

Depending on the oxidation state and degree of protonation by acids, PANI may exist in various forms related by reversible transitions (Figure 4.9) [22]. This transition causes some change in properties of PANI. For example, in protonated emeraldine salt form, the conductivity increases, however solubility decreases. Emeraldine base form of PANI was obtained by adding NH_4OH and both form were used in paint formulation in order to observe their effect on the coating properties.
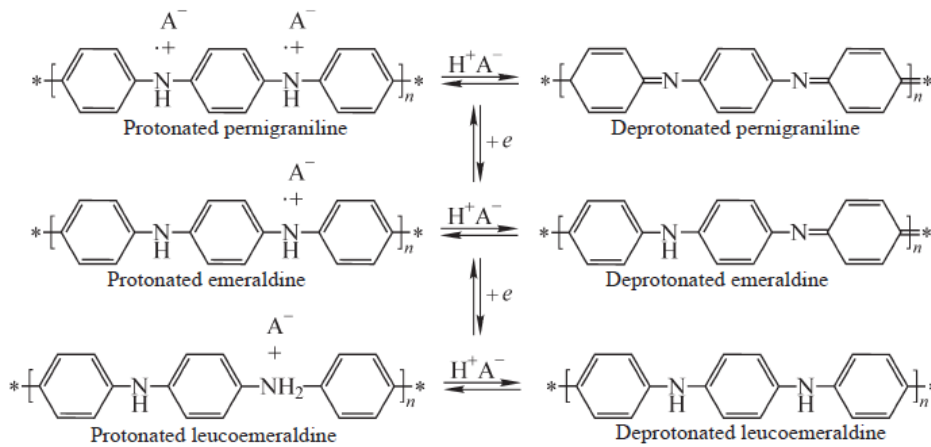
Figure 4.9 Different forms of polyaniline [22].

Coating solutions containing similar PANI polymer-resin content (Table 3.4) were prepared and their corrosion behavior was investigated in order to observe the effect of polymer solubility and the conductivity on the paint formulation. Conductivities of polymers are listed in Table 4.2.

Table 4.2 : Solid state conductivities of polymers

Polymer	Conductivity (S/cm)
PANI	2.2×10^{-5}
PANI/CeO$_2$	8.3×10^{-6}
PANI-EB	1.42×10^{-7}
PANI/CeO$_2$.EB	7.05×10^{-8}

Figure 4.10 shows the Nyquist plots of bare, CF resin (CF-R) coated, $P_{50}R_{50}$-032, $PC_{85}R_{50}$-032, $P_{50}R_{50}EB$-162, $PC_{68}R_{50}EB$-162 and $PC_{50}R_{50}EB$-118 coatings on carbon steel. The better inhibition efficiency of the coating $PC_{68}R_{50}EB$-162 can be seen by an almost double semi-circle in comparison with $P_{50}R_{50}EB$-162 coating. This result suggests that inclusion of CeO$_2$ into PANI structure provided additional protection efficiency. Furthermore, it can be observed that increase in concentration from 1.18% to 1.62% for PANI/CeO$_2$ nanocomposite results increase in the inhibition efficiency of the coating.
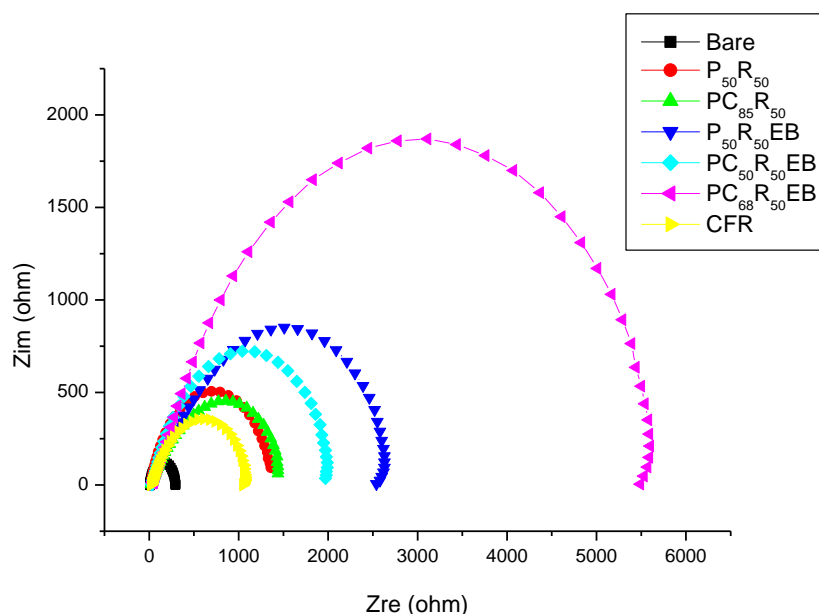
Figure 4.10 : Nyquist plot of bare, CF-R, $P_{50}R_{50}$-032, $PC_{85}R_{50}$-032, $P_{50}R_{50}EB$-162, $PC_{68}R_{50}EB$-162 and $PC_{50}R_{50}EB$-118 coated carbon steel electrode in 0.1 M H$_2$SO$_4$

Figure 4.11 depicts the equivalent circuits to model electrochemical behavior belonging to $P_{50}R_{50}EB$-162, $PC_{68}R_{50}EB$-162 and $PC_{50}R_{50}EB$-118 coatings on carbon steel after 1 hour immersion in 0.1 M H_2SO_4 solution. The electrochemical circuit model which was also used also for $P_{50}R_{50}$-032 and $PC_{85}R_{50}$-032 coatings [Rs(Q (Rp W))] fits with the minimum chi square value.

It is observed that a reasonable accuracy of the fitting was obtained. As evidence, chi-square is in the order of 10^{-3} and 10^{-4} for the experimental data. Rp values obtained by equivalent curcuits and experiments are in agreement with each other.
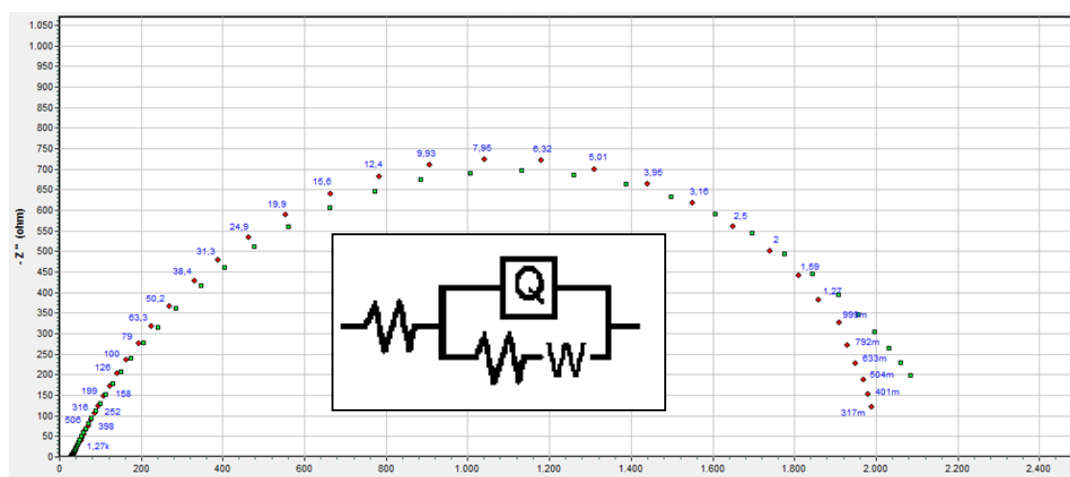
Figure 4.11 : Values of the elements of equivalent circuit required for fitting the EIS of $P_{50}R_{50}EB$-162, $PC_{68}R_{50}EB$-162 and $PC_{50}R_{50}EB$-118 coatings on carbon steel electrode in 0.1 M H_2SO_4

From Table 4.3, it is clear that the addition of CeO_2 and switching to emeraldine base form of PANI results in increase in Rp which gives highest inhibition effect. Diffusion can create an impedance known as the Warburg impedance. This impedance depends on the frequency of the potential perturbation. At high frequencies the Warburg impedance is small since diffusing reactants don't have to move very far. At low frequencies the reactants have to diffuse farther thereby increasing the Warburg impedance [16].

The percent of the inhibition effect (IE %) values were calculated from polarization and impedance measurements according to the following equations [27].

$$IE\% = (\frac{I_{corr}(coated) - I_{corr}(bare)}{I_{corr}(bare)})x100 = (\frac{R_p(coated) - R_p(bare)}{R_p(coated)})x100 \quad \textbf{(4.3)}$$

Table 4.3 : Values of equivalent circuit elements required for fitting EIS results of carbon steel in 0.1 M H_2SO_4 solution for bare electrode and various coating types.

Circuit Model	Carbon Steel Electrode - 0.1 M H_2SO_4	Rs ($\Omega.cm^2$)	Rp ($\Omega.cm^2$)	CPEdl. Yo.10^5 ($\Omega^{-1}.s^n.cm^{-2}$)	n_{dl}	W.Yo 10^{-6} ($\Omega^{-1}.s^5$)	IE%
R(QR)	BARE	5.00	144	20.55	0.91		
R(Q(RW))	$P_{50}R_{50}$-032	10.02	699	5.26	0.81	6722	79
R(Q(RW))	$PC_{85}R_{50}$-032	11.15	790	7.86	0.62	24130	82
R(Q(RW))	$P_{50}R_{50}EB$-162	16.42	1472	6.05	0.62	1.53	90
R(Q(RW))	$PC_{68}R_{50}EB$-162	22.42	3096	2.15	0.67	21	95
R(Q(RW))	$PC_{50}R_{50}EB$-118	14.61	1090	6.17	0.73	5754	87

Bode magnitude plots of CF-Resin coated with $P_{50}R_{50}$-032, $PC_{85}R_{50}$-032, $P_{50}R_{50}EB$-162, $PC_{68}R_{50}EB$-162 and $PC_{50}R_{50}EB$-118 carbon steel electrode after 1 hour immersion in 0.1 M H_2SO_4 are given in Figure 4.12. It is obvious that Z magnitude values of coatings are increasing in the same tendency as Rp values, indicating the efficiency of the coatings. The coating $PC_{68}R_{50}EB$-162 whose Rp is the highest also has the highest Z value.
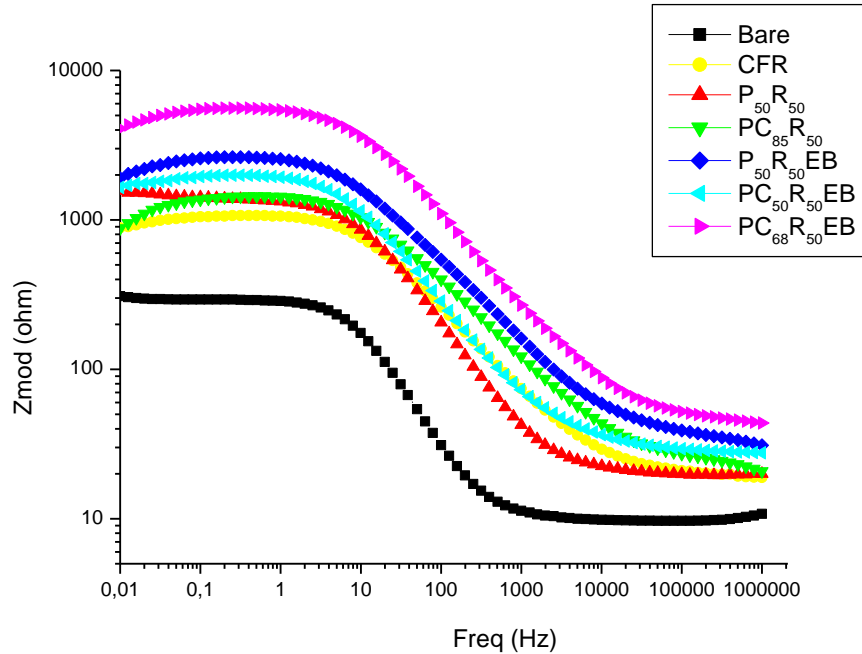
Figure 4.12 : Bode plot of bare, CF-Resin coated $P_{50}R_{50}$-032, $PC_{85}R_{50}$-032, $P_{50}R_{50}EB$-162, $PC_{68}R_{50}EB$-162 and $PC_{50}R_{50}EB$-118 carbon steel electrode in 0.1 M H_2SO_4

Tafel curves of the coatings exposed to 0.1 M H_2SO_4 were obtained after one hour immersion in corrosion media are shown in Figure 4.13. Corrosion parameters obtained from these polarization measurements are listed in Table 4.4. Corrosion current and corrosion rate decreased with increasing PANI and PANI/CeO_2 concentration. There are slight decreases in I_{corr} values of PANI/CeO_2 coatings over pure PANI coatings. The minimum I_{corr} value and best efficiency (95%) is obtained with the $PC_{68}R_{50}EB$-162 coating which is the coating obtained with the highest polymer concentration used in this study. All results in agreement with EIS results. The decrease in corrosion rates and increase in Rp indicates the formation of protective films on metal surfaces [27].

Although Rp values of PANI and PANI/CeO_2 nanocomposite coatings increase and corrosion currents decrease, the change in Ecorr values are small in comparison with the bare electrode. This result indicates that the coatings retard both anodic and cathodic reactions. In other words, they reduce the anodic dissolution and also retards the hydrogen evolution reaction.
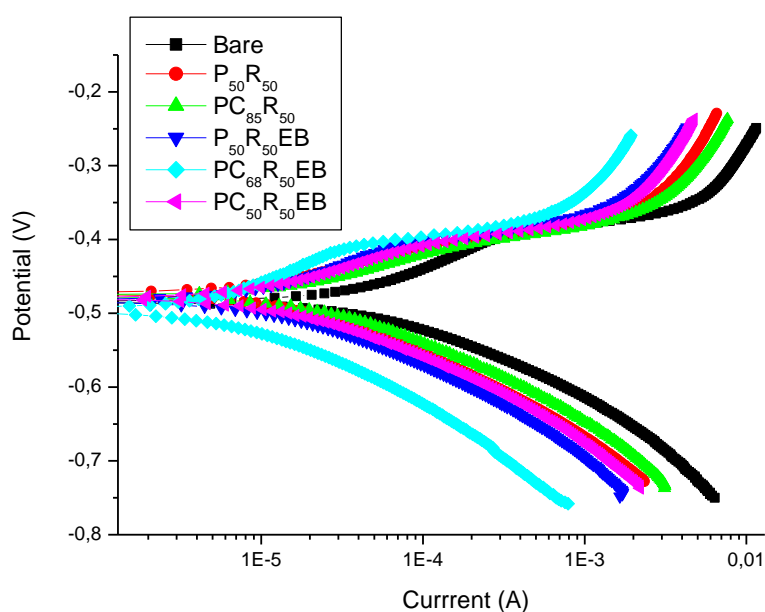
Figure 4.13 : Polarization curves of bare, $P_{50}R_{50}$-032, $PC_{85}R_{50}$-032, $P_{50}R_{50}EB$-162, $PC_{68}R_{50}EB$-162 and $PC_{50}R_{50}EB$-118 coatings on carbon steel.

Table 4.4 : Polarization parameters of CF-R, $P_{50}R_{50}$-032, $PC_{85}R_{50}$-032, $P_{50}R_{50}EB$-162, $PC_{68}R_{50}EB$-162 and $PC_{50}R_{50}EB$-118 coatings and bare carbon steel electrode in 0.1 M H_2SO_4.

Coating	Ecorr (mV)	I_{corr} ($\mu A.cm^{-2}$)	CR (mpy)	βa (mV)	βc (mV)	R_p ($\Omega.cm^2$)	IEI_{corr} (%)	IER_p (%)
BARE	-484	59.48	27.29	86	68	147		
CF-R	-491	43.56	19.97	116	95	528	27	72
$P_{50}R_{50}$-032	-473	24.27	11.09	70	88	709	59	79
$PC_{85}R_{50}$-032	-477	25.06	11.47	62	63	744	58	80
$P_{50}R_{50}EB$-162	-483	20.49	9.352	93	81	1327	66	89
$PC_{68}R_{50}EB$-162	-496	11.96	5.475	118	95	2926	80	95
$PC_{50}R_{50}EB$-118	-480	24.07	11.01	86	84	1020	60	86

4.3.2.2 Measurements of carbon steel in H_2SO_4 with increasing exposure time

In order to analyses the change in corrosion resistance of coatings with increasing exposure time to corrosive environment, measurements at different exposure time was conducted in 0.1 M H_2SO_4. The coatings were almost completely degraded after 24 hours when they left in corrosion media. In order to eliminate the measurement differences that might come from preparation of coating the same coating was used for all measurements. Coating degradation accelerated during measurements and the coatings were durable for approximately 6 hours of measurement. All the coatings were exposed to electrolyte solution for 1 hour before starting the measurements.

Figure 4.14-4.16 show the Nyquist plots of the coatings $P_{50}R_{50}EB$-162, $P_{68}R_{50}EB$-162 and $P_{50}R_{50}EB$-118 respectively on carbon steel substrate for an exposure time of 6 hours. Rp values for the measurements with time are summarized in Table 4.6-4.8.

It is again obvious that corrosion resistances of the substrate decreases with time due to electrolyte penetration. There is a slight increase in the R_p values of the coatings $P_{50}R_{50}EB$-162 after 6th hours, which can be attributed to the passivation effect of corrosion products.
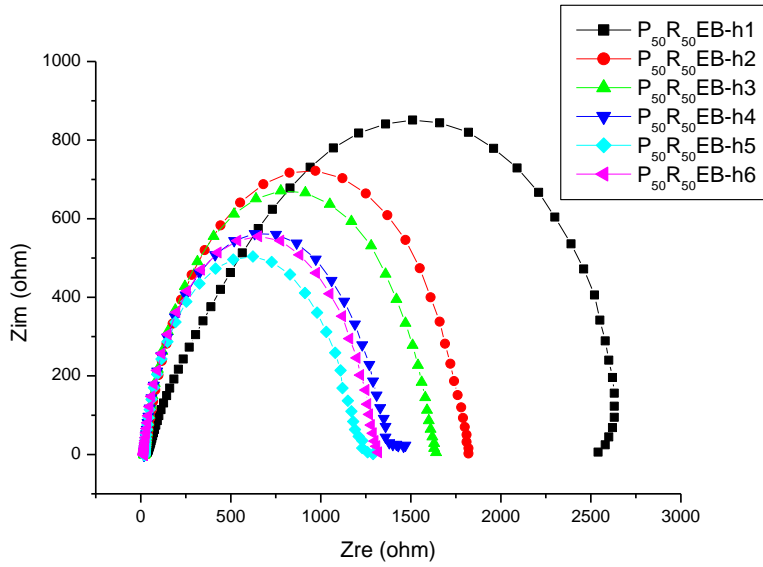
Figure 4.14 : Nyquist plot of carbon steel electrode coated with $P_{50}R_{50}EB$-162 coating in 6 hours of exposure to 0.1 M H_2SO_4
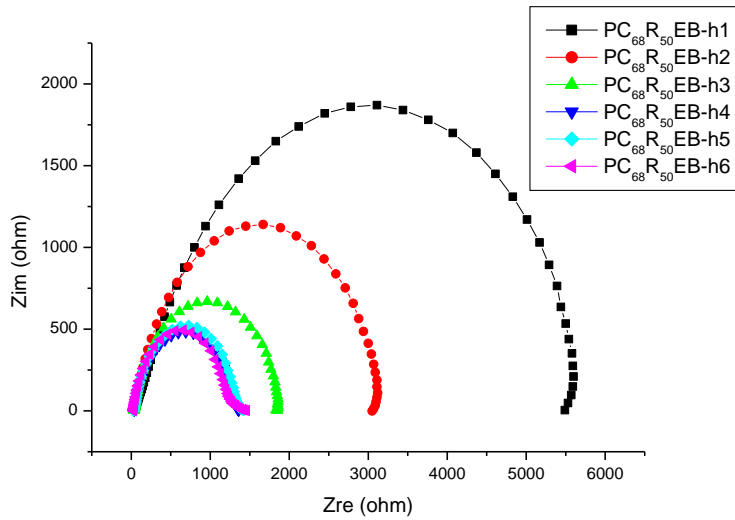
Figure 4.15 : Nyquist plot of carbon steel electrode in 0.1 M H_2SO_4 coated with $P_{68}R_{50}EB$-162 in 6 hours of exposure to 0.1 M H_2SO_4
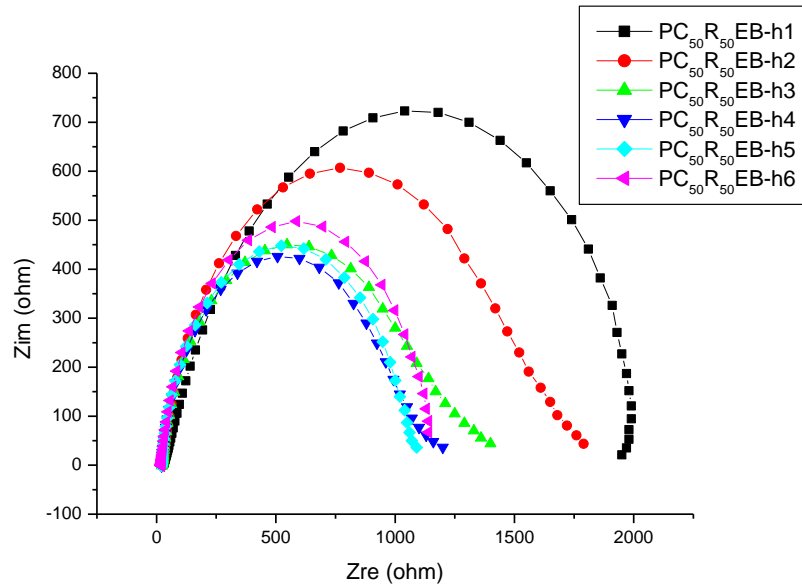
Figure 4.16 : Nyquist plot of carbon steel electrode in H_2SO_4 coated with $P_{50}R_{50}EB$-118 in 6 hours of exposure to 0.1 M H_2SO_4

Figure 4.17 shows the change in Rp values of bare, $P_{50}R_{50}EB$-162, $PC_{68}R_{50}EB$-162 and $PC_{50}R_{50}EB$-118 comperatively with increasing exposure time. When two different PANI/CeO_2 nanocomposite coatings ($P_{50}R_{50}EB$-162 and $PC_{50}R_{50}EB$-118) are compared it can be seen that at the begining, coating with higher concentration ($PC_{68}R_{50}EB$-162) has better protection and their effect become almost similar after 6 hours.

On the other hand Rp values of CeO_2 containing coating ($PC_{68}R_{50}EB$-162) is higher than the $P_{50}R_{50}EB$-162 coating. These results shows the advantage of CeO_2 nanoparticle contrubition in the coating. All coatings have higher polarization resistance values in comparison to bare electrode at the begining and after 6 hour indicating barier effect of coatings.
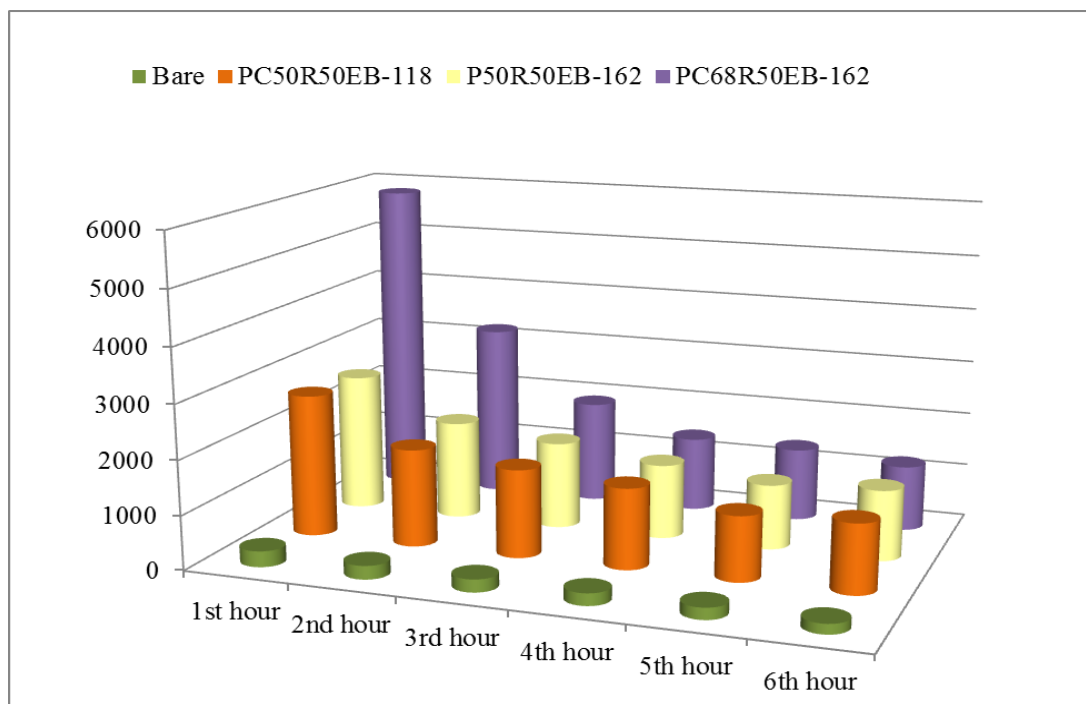
Figure 4.17 : Rp values of $P_{50}R_{50}EB$-162, $PC_{68}R_{50}EB$-162 and $PC_{50}R_{50}EB$-118 coatings in 0.1 M H_2SO_4 with increasing exposure time

Figure 4.18-4.20 show the Tafel plots of $P_{50}R_{50}EB$-162, $PC_{50}R_{50}EB$-118 and $PC_{68}R_{50}EB$-118 coated elerectrodes in 0.1 M H_2SO_4 with time, respectively. Ecorr, Icorr, β_a, β_c and CR values obtained from these graphs are listed in Table 4.5-4.8. These results were also compared with bare electrode. Icorr values increases with time for all types of coatings.
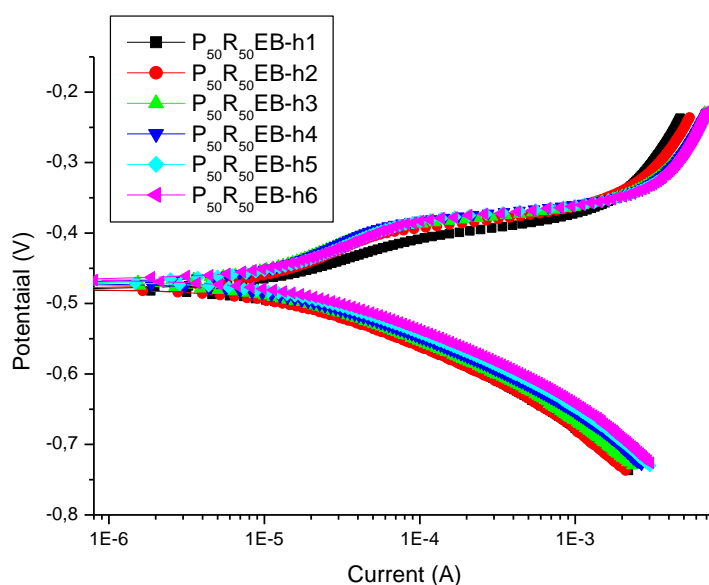
Figure 4.18 : Polarization curves of $P_{50}R_{50}EB$-162 coating on carbon steel electrode in 0.1 M H_2SO_4 with increasing exposure time
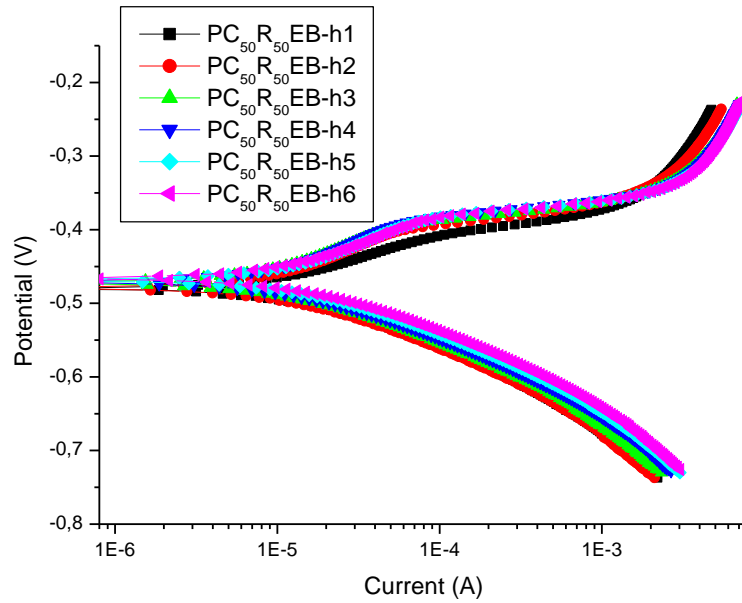
Figure 4.19 : Polarization curves of $PC_{50}R_{50}EB$-118 coating on carbon steel electrode in 0.1 M H_2SO_4 with increasing exposure time
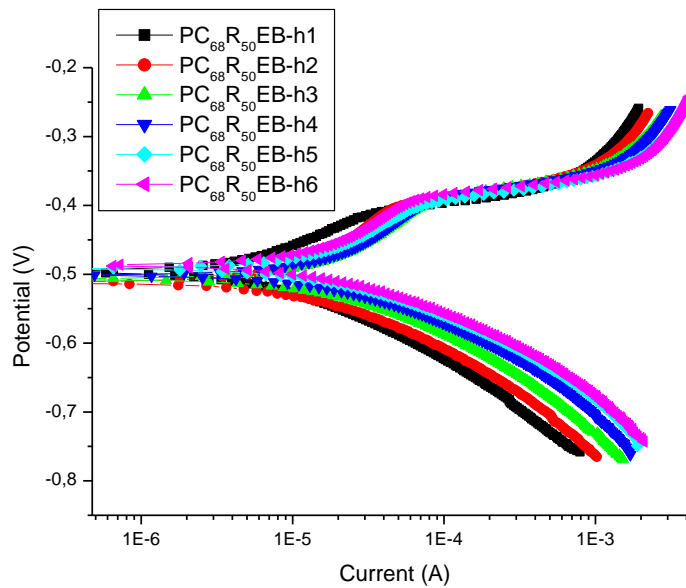
Figure 4.20 : Polarization curves of $PC_{68}R_{50}EB$-162 coating on carbon steel electrode in 0.1 M H_2SO_4 with increasing exposure time

For bare electrode, I_{corr} values in 0.1 M H_2SO_4 increases and Rp values decreases with time as expected (Table 4.5).

Although there is a difference in the I_{corr} and Rp values of $PC_{68}R_{50}EB$-162 and the other two coatings ($P_{50}R_{50}EB$-162 and $PC_{50}R_{50}EB$-118) at the beginning of measurements, they become very close to each other for the three coatings after 6

hour of exposure to 0.1 M H_2SO_4. This might be due to formation of corrosion products on the surface. Since all the coatings produce the same type of corrosion products by oxidation, the passive film behaves in the same way and measured values become closer to each other.

Table 4.5 : Polarization parameters for bare carbon steel electrode in 0.1 M H_2SO_4

	Ecorr (mV)	I_{corr} ($\mu A.cm^{-2}$)	CR (mpy)	βa (mV)	βc (mV)	R_p ($\Omega.cm^2$)
BARE / h1	-484	59.5	27.3	86	68	147
BARE / h2	-480	84.3	38.7	108	83	126
BARE / h3	-479	93.1	42.7	113	81	118
BARE / h4	-478	95.3	43.7	107	74	113
BARE / h5	-479	116.2	53.2	117	77	108
BARE / h6	-479	126.1	57.8	115	76	92

Table 4.6 : Polarization parameters for $P_{50}R_{50}EB$-162 coating on carbon steel with increasing exposure time in 0.1 M H_2SO_4

	Ecorr (mV)	I_{corr} ($\mu A.cm^{-2}$)	CR (mpy)	βa (mV)	βc (mV)	R_p ($\Omega.cm^2$)
$P_{50}R_{50}EB$-162 / h1	-483	20.5	9.4	94	81	1327
$P_{50}R_{50}EB$-162 / h2	-474	24.7	11.3	104	94	910
$P_{50}R_{50}EB$-162 / h3	-464	20.3	9.3	91	83	819
$P_{50}R_{50}EB$-162 / h4	-459	20.5	9.4	103	84	749
$P_{50}R_{50}EB$-162 / h5	-462	21.9	10.1	98	78	603
$P_{50}R_{50}EB$-162 / h6	-463	26.7	12.2	107	85	643

Table 4.7 : Polarization parameters for $PC_{68}R_{50}EB$-162 coating on carbon steel with increasing exposure time in 0.1 M H_2SO_4

	Ecorr (mV)	I_{corr} ($\mu A.cm^{-2}$)	CR (mpy)	βa (mV)	βc (mV)	R_p ($\Omega.cm^2$)
$PC_{68}R_{50}EB$-162 / h1	-496	12.0	5.5	118	95	2926
$PC_{68}R_{50}EB$-162 / h2	-512	26.5	12.1	203	103	1609
$PC_{68}R_{50}EB$-162 / h3	-507	38.4	17.6	188	105	955
$PC_{68}R_{50}EB$-162 / h4	-501	42.6	19.5	200	96	694
$PC_{68}R_{50}EB$-162 / h5	-492	34.4	15.8	162	83	664
$PC_{68}R_{50}EB$-162 / h6	-487	35.6	16.3	185	87	608

Table 4.8 : Polarization parameters for $PC_{50}R_{50}EB$-118 coating on carbon steel with increasing exposure time to 0.1 M H_2SO_4

	Ecorr (mV)	I_{corr} ($\mu A.cm^{-2}$)	CR (mpy)	βa (mV)	βc (mV)	R_p ($\Omega.cm^2$)
$PC_{50}R_{50}EB$-118 / h1	-480	24.1	11.0	86	84	1020
$PC_{50}R_{50}EB$-118 / h2	-479	23.7	10.8	11	85	809
$PC_{50}R_{50}EB$-118 / h3	-472	20.9	9.5	110	80	603
$PC_{50}R_{50}EB$-118 / h4	-471	21.7	9.9	115	76	553
$PC_{50}R_{50}EB$-118 / h5	-469	25.9	11.8	112	78	543
$PC_{50}R_{50}EB$-118 / h6	-466	27.8	12.8	113	80	563

Figure 4.21-4.23 show the Bode plots of the coatings $P_{50}R_{50}EB$-162, $P_{68}R_{50}EB$-162 and $P_{50}R_{50}EB$-118 respectively on carbon steel substrate for an exposure time of 6 hours. Z values are decreasing with increasing exposure time as expected.
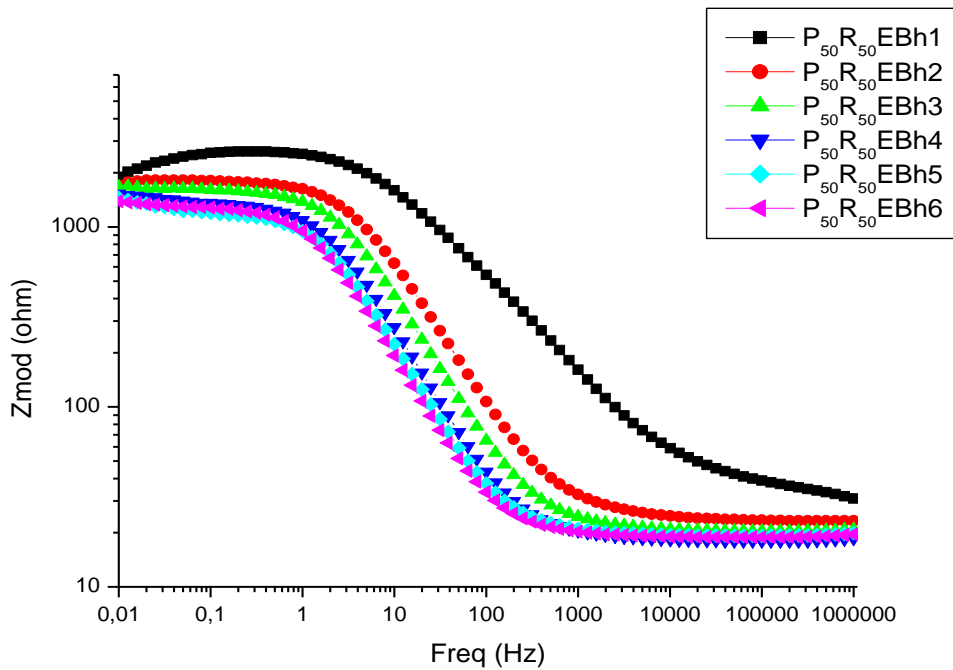
Figure 4.21 : Bode plot of carbon steel electrode in H_2SO_4 coated with $P_{50}R_{50}EB$-162 in 6 hours of exposure to 0.1 M H_2SO_4
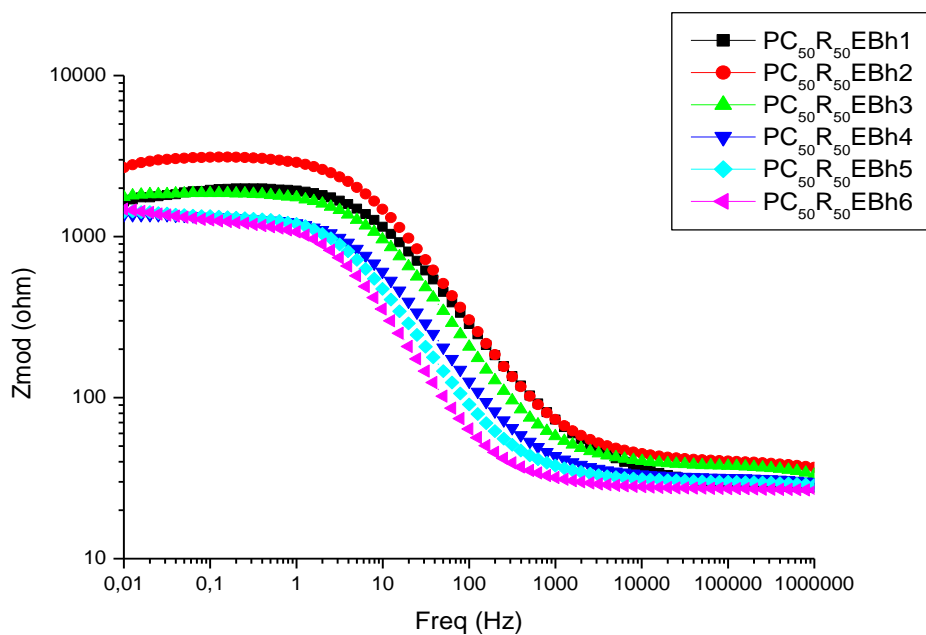
Figure 4.22 : Bode plot of carbon steel electrode in H_2SO_4 coated with $PC_{50}R_{50}EB$-118 in 6 hours of exposure to 0.1 M H_2SO_4
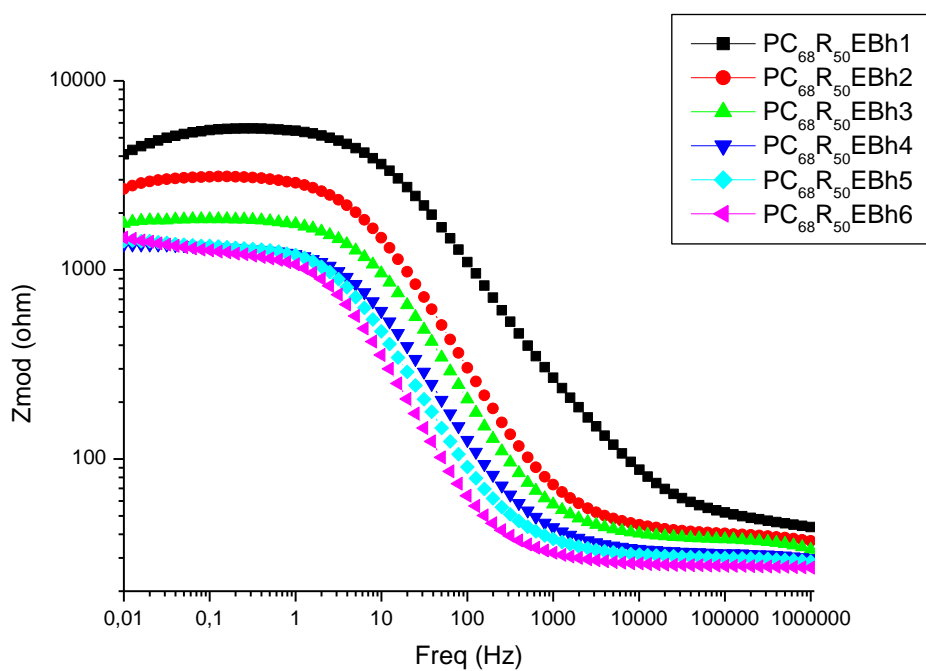
Figure 4.23 : Bode plot of carbon steel electrode in H_2SO_4 coated with $PC_{68}R_{50}EB$-162 in 6 hours of exposure to 0.1 M H_2SO_4

Table 4.9 lists the data obtained from equivalent curcit model. All Rp data is in agreement with experimental values. Rp values decreases with increasing exposure time. When coating type is compared, addition of CeO_2 in the structure and using emeraldine base form increases protection efficiency.

Table 4.9 : Values of equivalent circuit elements required for fitting the EIS results of carbon steel in 0.1 M H_2SO_4 solution in bare electrode and varying coating types with increasing exposure time.

Circuit Model	Carbon Steel Electrode - 0.1 M H_2SO_4	Rs ($\Omega.cm^2$)	Rp ($\Omega.cm^2$)	CPEdl. $Yo.10^5$ ($\Omega^{-1}.s^n.cm^{-2}$)	n_{dl}	$W.Yo.10^6$ ($\Omega^{-1}.s^5$)	IE%
R(QR)	BARE-h 1	5.00	144	20.55	0.91		
R(QR)	BARE-h 6	6.09	87	81.76	0.92	0.84	
R(Q(RW))	$P_{50}R_{50}EB$-162 /h1	16.42	1472	6.05	0.62	1.53	90
R(Q(RW))	$P_{50}R_{50}EB$-162 /h6	9.66	646	24.65	0.90	7.65	87
R(Q(RW))	$PC_{68}R_{50}EB$-162/h1	22.42	3096	2.15	0.67	21	95
R(Q(RW))	$PC_{68}R_{50}EB$-162/h6	14.01	623	15.50	0.85	0.03	86
R(Q(RW))	$PC_{50}R_{50}EB$-118/ h1	14.61	1090	6.17	0.73	5754	87
R(Q(RW))	$PC_{50}R_{50}EB$-118/ h1	10.06	576	27.33	0.90	194.3	85

4.3.2.3 Measurements of aluminium in 0.1 M H_2SO_4

Similar to the study with carbon steel, in order to analyze the effect of PANI and PANI/CeO_2 nanocomposite to corrosion resistance of aluminium, paint solutions with different concentrations including different ratios of PANI polymer and PANI/CeO_2 nanocomposite were applied on electrode surfaces. Polarization and EIS measurements were conducted after 1 hour immersion time.

Figure 4.24 shows the empedance plot of bare and CF resin coated aluminium electrodes. Bare aluminium electrode has a Rp value of 2300 ohm and its value increased up to 22622 ohm by applying pure CF-R coating.
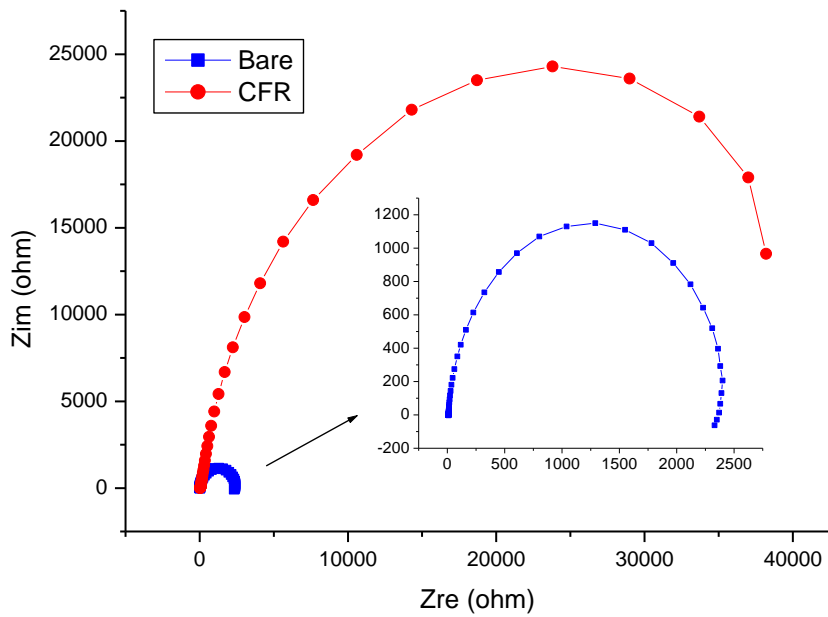
Figure 4.24 : Nyquist plot of bare and CF-R coated aluminium electrode in H_2SO_4

Figure 4.25 shows the Nyquist plot of $P_{50}R_{50}EB$-162, $PC_{68}R_{50}EB$-162, $PC_{50}R_{50}EB$-118 and CF resin coatings. The coating $PC_{68}R_{50}EB$-162 has the biggest Rp value which shows that the coating with 1.62 % concentration PANI/CeO$_2$ coating is the most efficient coating as in the case of carbon steel.
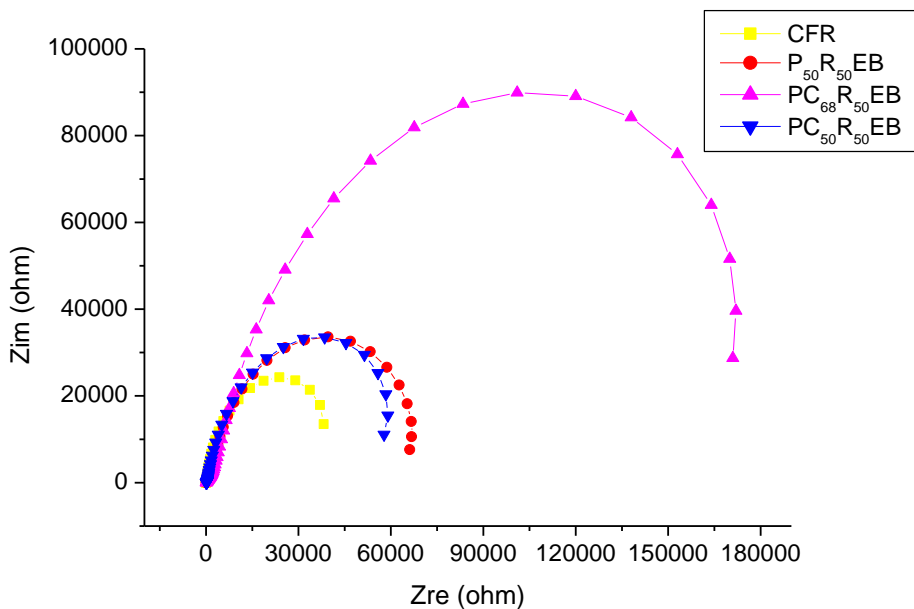
Figure 4.25 : Nyquist plot of $P_{50}R_{50}EB$-162, $PC_{68}R_{50}EB$-162, $PC_{50}R_{50}EB$-118 and CF resin coated aluminium electrode in 0.1 M H_2SO_4

Figure 4.26 shows the Bode plot of $P_{50}R_{50}EB-162$, $PC_{68}R_{50}EB-162$, $PC_{50}R_{50}EB-118$ and CFR coatings on aluminium after 1 h of immersion in H_2SO_4. The coating $PC_{68}R_{50}EB-162$ has the biggest Z value which shows that the coating with 1.62 % concentration $PANI/CeO_2$ coating is the most efficient coating as in the case of carbon steel.
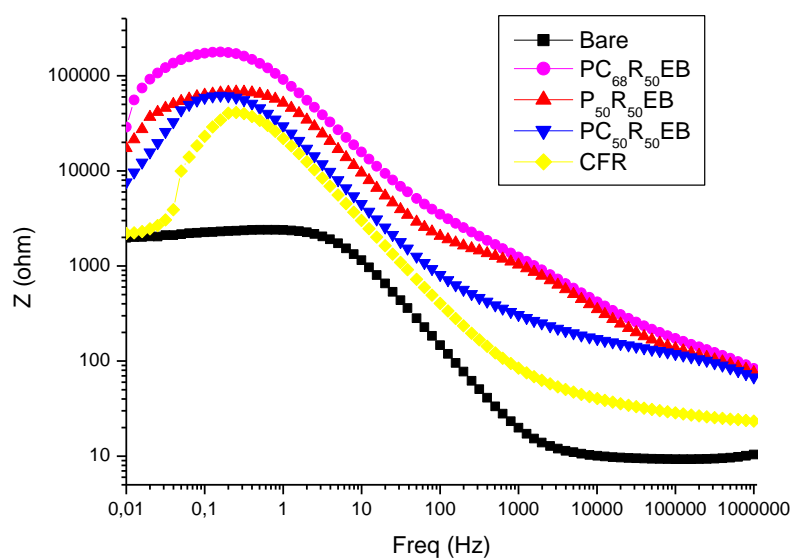
Figure 4.26 : Bode plot of $P_{50}R_{50}EB-162$, $PC_{68}R_{50}EB-162$, $PC_{50}R_{50}EB-118$ and CF resin coated and bare aluminium electrode in 0.1 M H_2SO_4
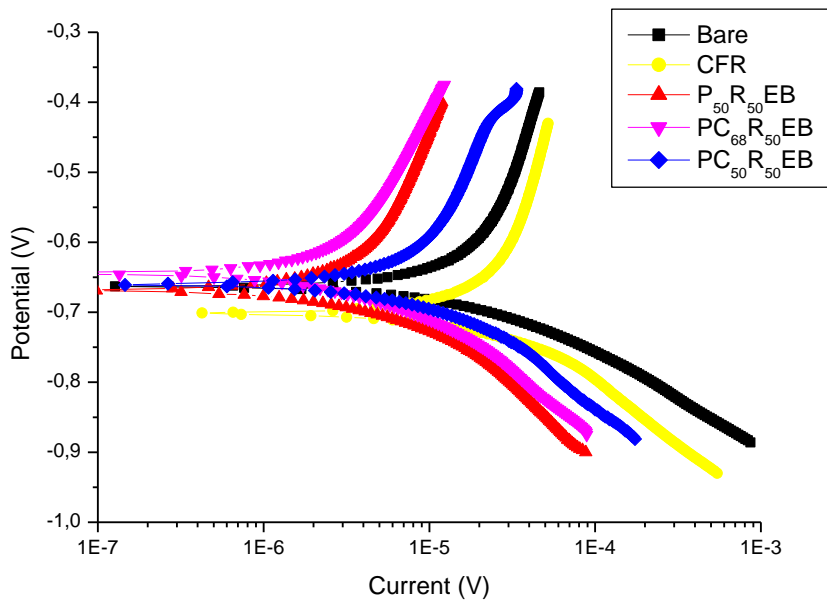
Figure 4.27 shows Tafel plots of $P_{50}R_{50}EB-162$, $PC_{68}R_{50}EB-162$, $PC_{50}R_{50}EB-118$ and CF resin coated and bare aluminium electrodes after 1 hour exposure to 0.1 M H_2SO_4. Ecorr, Icorr, β_a, β_c and CR values obtained from these graphs are listed in Table 4.10. Icorr values effectively decrease in comparison with the bare electrode showing that corrosion protection is provided. There is a slight shift in Ecorr values to anodic region for $PC_{68}R_{50}EB-162$ coating which indicates the barrier effect and retarding anodic reaction. The lowest Icorr value belongs to the coating $PC_{68}R_{50}EB-162$, $P_{50}R_{50}EB-162$ has a lower corrosion current than $PC_{50}R_{50}EB-118$ so the corrosion protection efficiency of $P_{50}R_{50}EB-162$ is higher than $PC_{50}R_{50}EB-118$ for aluminium in 0.1 M H_2SO_4 (Table 4.A).

Figure 4.27 : Polarization curves of $P_{50}R_{50}EB$-162, $PC_{68}R_{50}EB$-162, $PC_{50}R_{50}EB$-118 and CF resin coated and bare aluminium electrodes in 0.1 M H_2SO_4

Table 4.10 : Polarization parameters for $P_{50}R_{50}EB$-162, $PC_{68}R_{50}EB$-162, $PC_{50}R_{50}EB$-118 CF resin coated and bare aluminium electrodes in 0.1 M H_2SO_4 solution

	Ecorr (mV)	I_{corr} (µA.cm^{-2})	CR (mpy)	βa (mV)	βc (mV)	R_p (Ω.cm^2)	IEI$_{corr}$ (%)	IER$_p$ (%)
BARE	-663	34.8	15.0	512	111	1206		
CF-R	-702	22.3	19.1	513	109	22622	36	95
$P_{50}R_{50}EB$-162	-668	9.1	3.9	714	120	36697	74	97
$PC_{68}R_{50}EB$-162	-645	4.1	1.8	217	83	92497	88	99
$PC_{50}R_{50}EB$-118	-660	21.5	9.3	753	134	34184	38	96

Figure 4.28 depicts the equivalent circuit to model electrochemical behavior belonging to $P_{50}R_{50}EB$-162, $PC_{68}R_{50}EB$-162 and $PC_{50}R_{50}EB$-118 coatings on aluminium after 1 hour immersion in 0.1 M H_2SO_4 solution. Equivalent circuit model represented by R(Q(R(C(R(C(RW)))))))(CR) fits better and the first part of the circuit represents the solution resistanceof the polymer and electrolyte, Rs, the second part is the parallel combination of the double layer capacitance, C1 and, third part is the pore resistance of the polymer film R1 deposited on aluminium. A series connection to R1 constructed using a constant phase element Q (Yo, CPE), in parallel to the redox process taking place at the polymer/solution interface is described by the

charge transfer resistance R2. The CPE represented as Q takes into account the interfacial irregularities such as porosity, roughness, and geometry. A series connection to R2 was constituted using C2, having a paralel connection to R3 and W. The low frequency behavior was determined by the adsorption of cations and could be described by adsorption resistance R3 parallel to an adsorption capacitance C2. Diffusion processes arising in systems explained by W is the Warburg diffusion impedance element. The last component corresponds to the polymer coated aluminium capacitance and resistance. Circuit elements are listed in Table 4.14 [30].
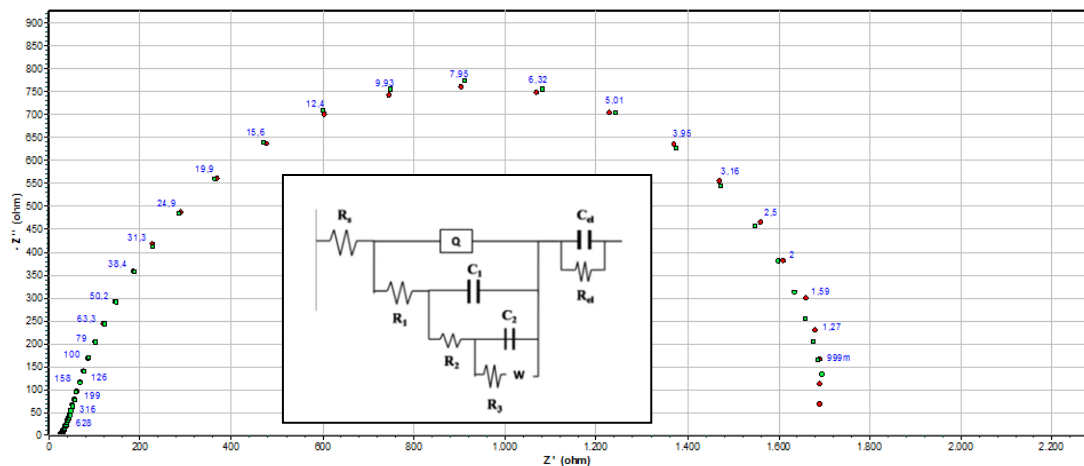
Figure 4.28 : Values of the elements of equivalent circuit required for fitting the EIS of $P_{50}R_{50}EB$-162, $PC_{68}R_{50}EB$-162 and $PC_{50}R_{50}EB$-118 coatings on aluminium electrode in 0.1 M H_2SO_4

4.3.2.4 Measurements of aluminium in H_2SO_4 with increasing exposure time

In order to analyze the change in corrosion resistance of coatings with increasing exposure time to corrosive environment measurement sets of 5 hour were conducted. All the coatings were exposed to electrolyte solution for 1 hour before starting measurements.

Figure 4.29-4.31 show the Nyquist plots of the coatings $P_{50}R_{50}EB$-162, $P_{68}R_{50}EB$-162 and $P_{50}R_{50}EB$-118 respectively on aluminium substrate for an exposure time of 5 hours. Rp values for the measurements with time are summarized in Table 4.11-4.13.
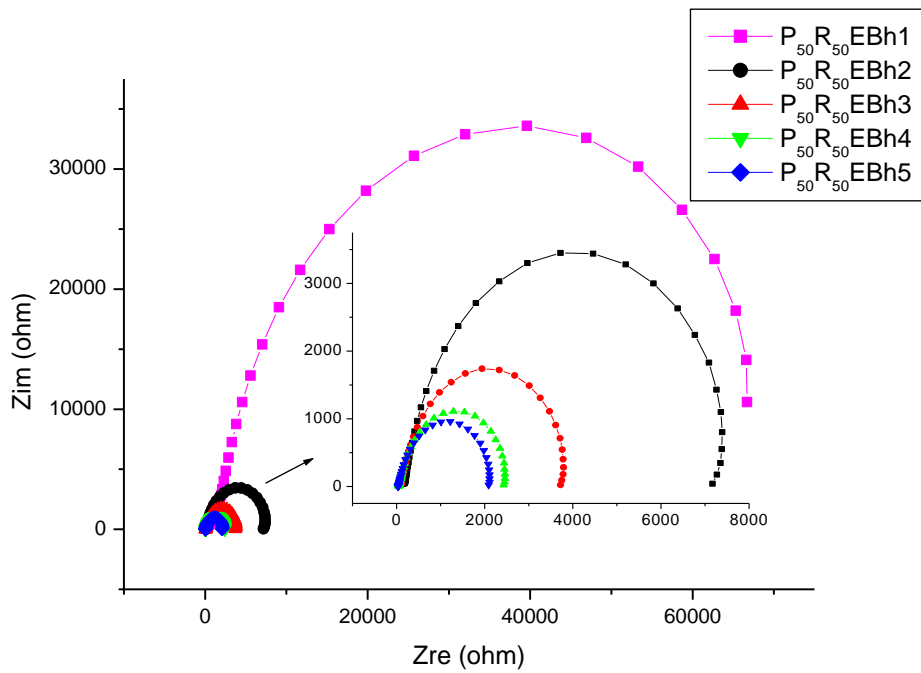
Figure 4.29 : Nyquist plot of coating $P_{50}R_{50}EB$-162 on aluminium electrode in 0.1 M H_2SO_4 with increasing exposure time
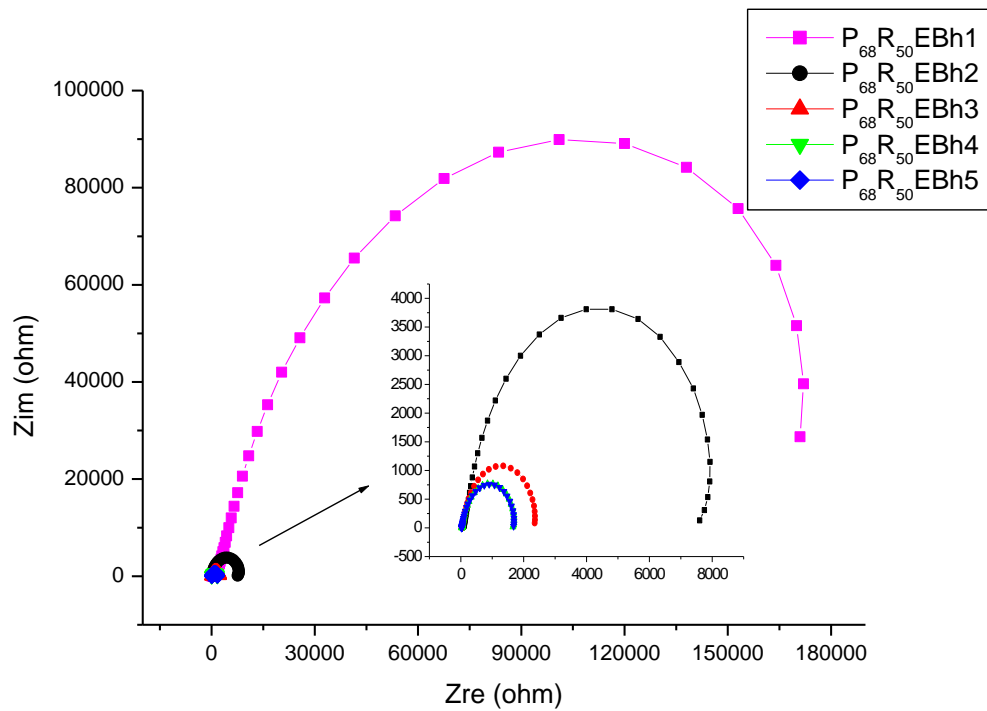
Figure 4.30 : Nyquist plot of coating $PC_{68}R_{50}EB$-162 on aluminium electrode in 0.1 M H_2SO_4 with increasing exposure time
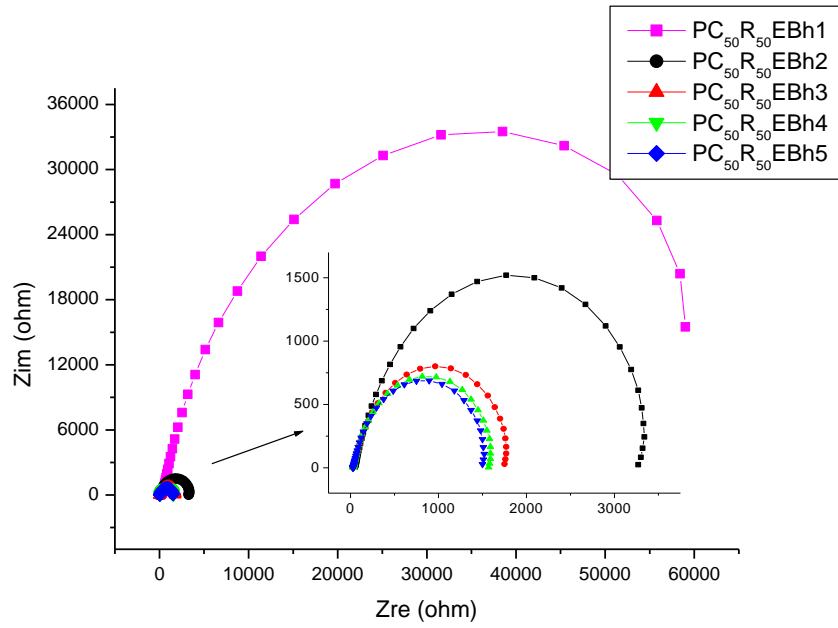
Figure 4.31 : Nyquist plot of coating $PC_{50}R_{50}EB$-118 on aluminium electrode in 0.1 M H_2SO_4 with increasing exposure time

Figure 4.32 shows the change in Rp values of $P_{50}R_{50}EB$-162, $PC_{68}R_{50}EB$-162 and $PC_{50}R_{50}EB$-118 comperatively with increasing exposure time starting from 2nd hour of exposure time until 5th hour.
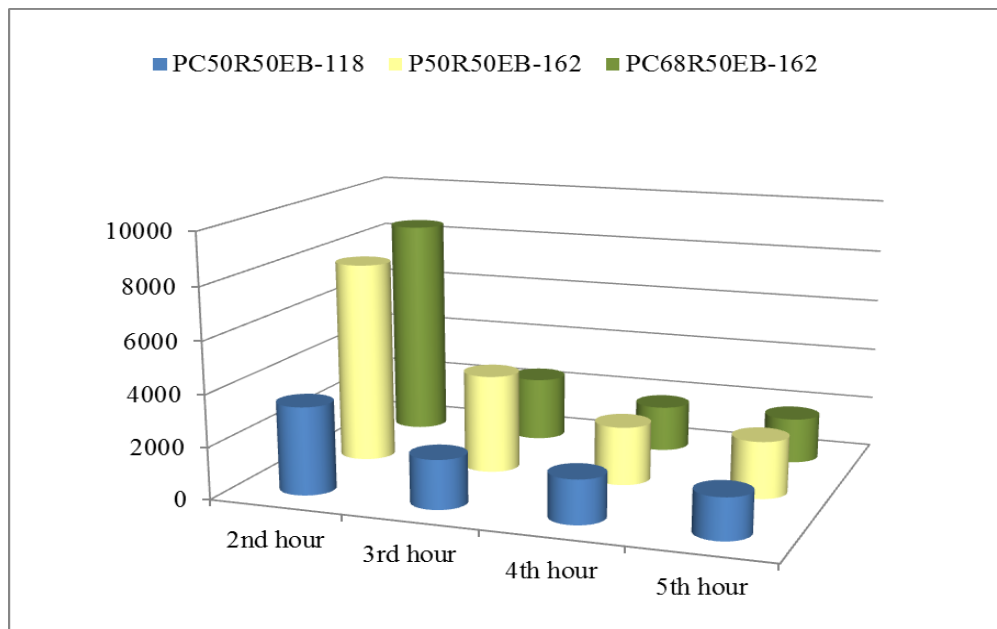
Figure 4.32 : Comparison of Rp values of $P_{50}R_{50}EB$-162, $PC_{68}R_{50}EB$-162 and $PC_{50}R_{50}EB$-118 on aluminium substrate

Bode plots of $P_{50}R_{50}EB$-162, $PC_{68}R_{50}EB$-162 and $PC_{50}R_{50}EB$-118 on aluminium substrate are shown in Figures 4.33-4.35. Although there is a significant differanace in Rp and Z values of the coating until 2 hours of exposure time, changes become smaller after 2nd hour and the coatings become stable and all the curves obtained by electrochemical measurements show similar behavior.

Figure 4.33 : Bode plot of coating $P_{50}R_{50}EB$-162 on aluminium electrode in 0.1 M H_2SO_4 with increasing exposure time
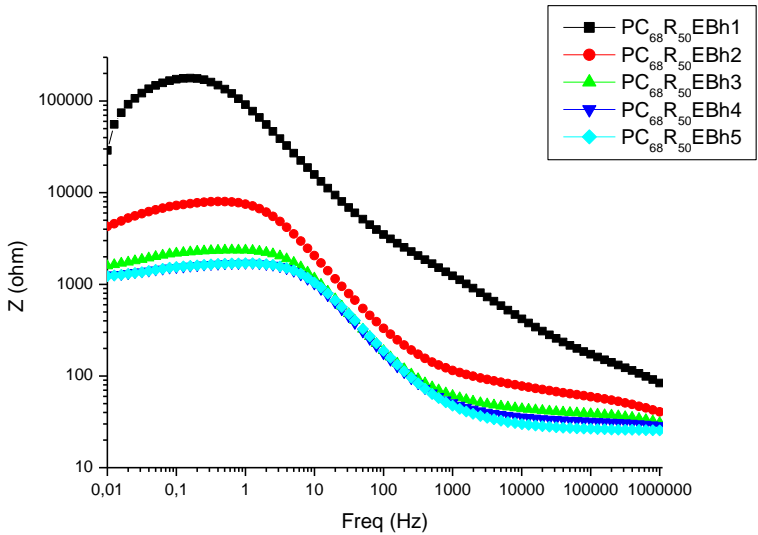

Figure 4.34 : Bode plot of coating $PC_{68}R_{50}EB$-162 on aluminium electrode in 0.1 M H_2SO_4 with increasing exposure time
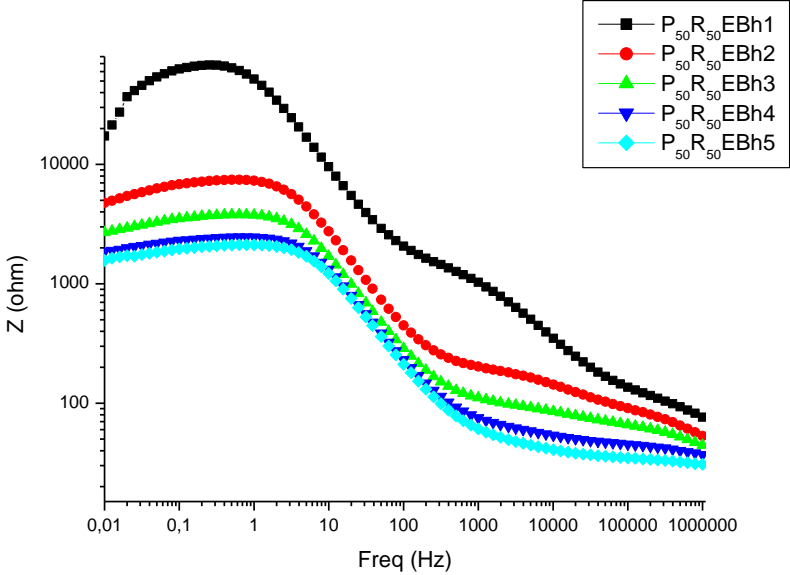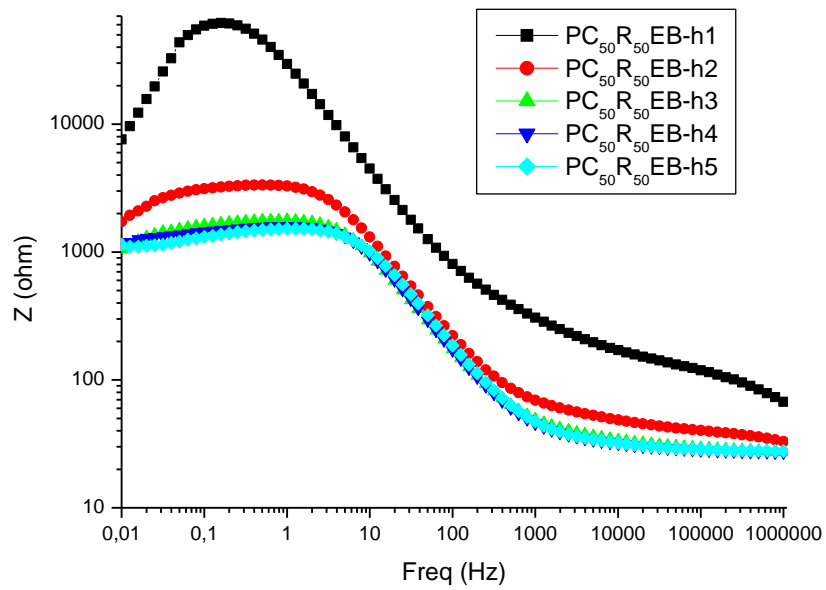
Figure 4.35 : Bode plot of coating $PC_{68}R_{50}EB$-162 on aluminium electrode in 0.1 M H_2SO_4 with increasing exposure time

Figure 4.36-4.38 show Tafel plots of $P_{50}R_{50}EB$-162, $PC_{68}R_{50}EB$-162, $PC_{50}R_{50}EB$-118 and CF resin coated aluminium electrodes in 0.1 M H_2SO_4 at varying exposure time. Ecorr, Icorr, β_a, β_c and CR values obtained from these graphs are listed in Table 4.11-4.13.
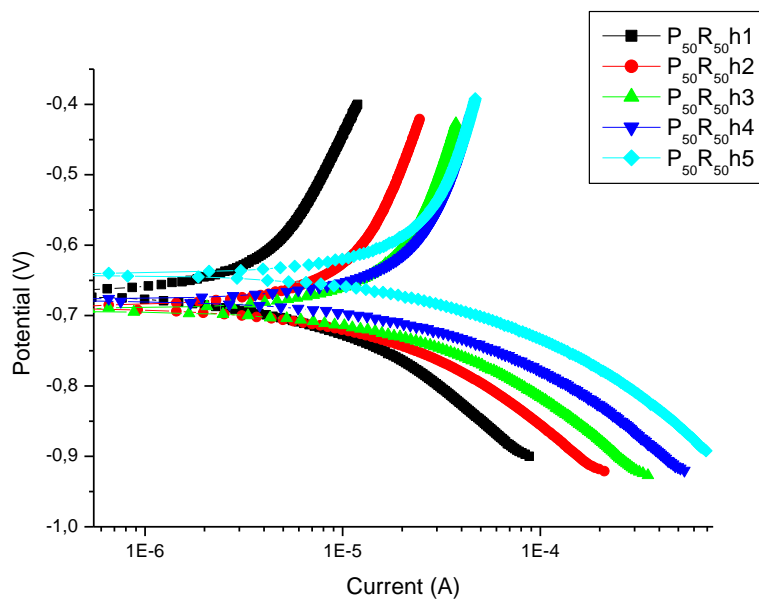
Figure 4.36 : Polarization curve of coating $P_{50}R_{50}EB$-162 on aluminium electrode in 0.1 M H_2SO_4 with increasing exposure time
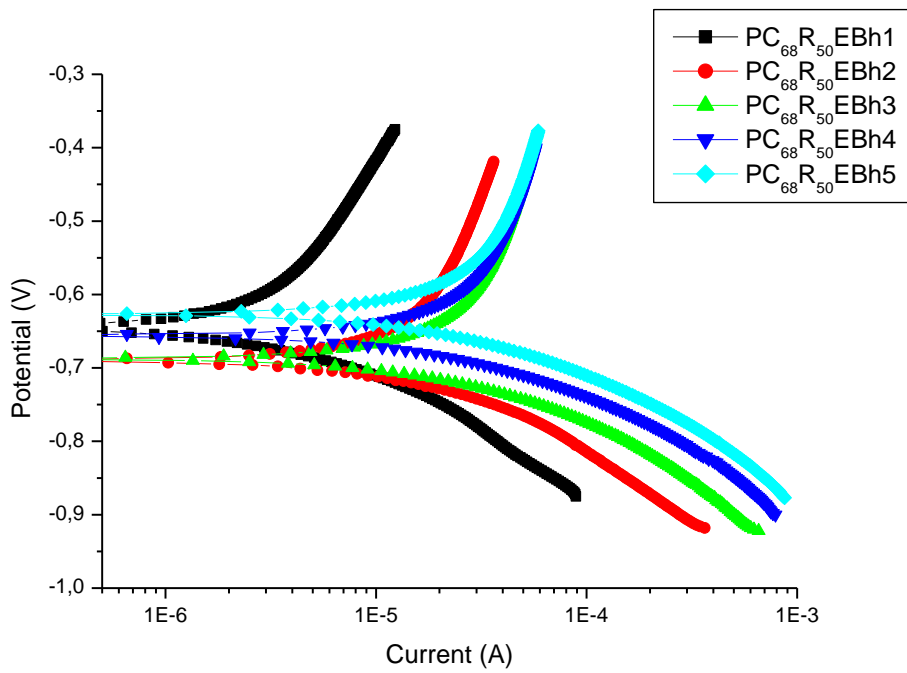
Figure 4.37 : Polarization curve of coating $PC_{68}R_{50}EB$-162 on aluminium electrode in 0.1 M H_2SO_4 with increasing exposure time
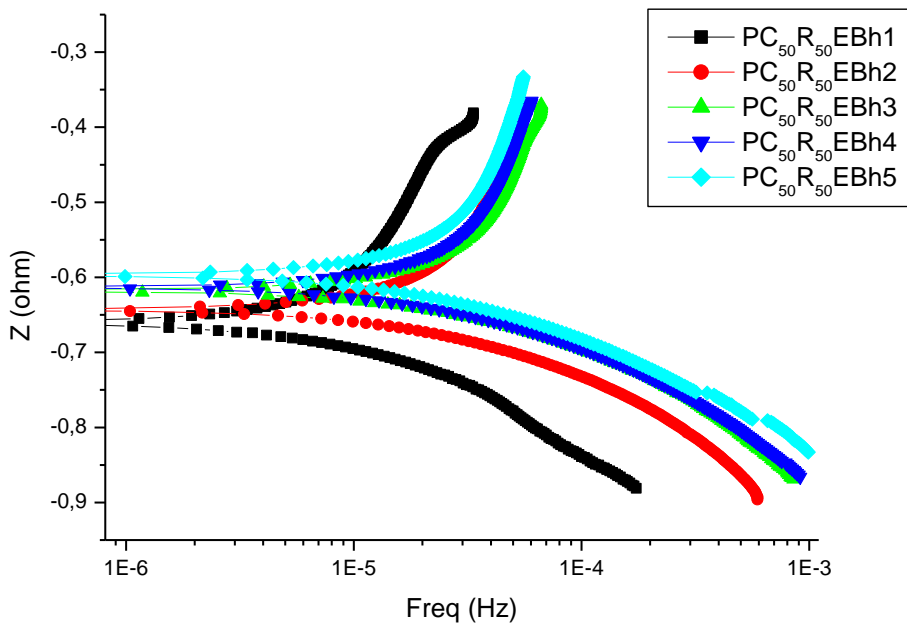
Figure 4.38 : Polarization curve of coating $PC_{50}R_{50}EB$-118 on aluminium electrode in 0.1 M H_2SO_4 with increasing exposure time

Table 4.11 : Polarization parameters for the coating $P_{50}R_{50}EB$-162 on aluminium in 0.1 M H_2SO_4 with increasing exposure time

|	Ecorr (mV)	I_{corr} ($\mu A.cm^{-2}$)	CR (mpy)	βa (mV)	βc (mV)	R_p ($\Omega.cm^2$)
BARE / h1	-663	34.8	15.0	512	111	1206
$P_{50}R_{50}EB$-162 / h1	-668	9.1	3.9	714	120	36697
$P_{50}R_{50}EB$-162 / h2	-689	17.9	7.7	433	109	3921
$P_{50}R_{50}EB$-162 / h3	-692	18.0	7.7	203	82	1910
$P_{50}R_{50}EB$-162 / h4	-678	35.6	15.3	404	116	1136
$P_{50}R_{50}EB$-162 / h5	-642	37.4	16.1	393	110	1106

Table 4.12 : Polarization parameters for the coating $PC_{68}R_{50}EB$-162 on aluminium in 0.1 M H_2SO_4 with increasing exposure time

	Ecorr (mV)	I_{corr} ($\mu A.cm^{-2}$)	CR (mpy)	βa (mV)	βc (mV)	R_p ($\Omega.cm^2$)
BARE	-663	34.8	15.0	512	111	1206
$PC_{68}R_{50}EB$-162 / h1	-645	4.1	1.8	217	83	92497
$PC_{68}R_{50}EB$-162 / h2	-690	31.4	13.5	657	119	4273
$PC_{68}R_{50}EB$-162 / h3	-687	46.3	19.9	556	116	1247
$PC_{68}R_{50}EB$-162 / h4	-656	17.0	14.5	245	93	890
$PC_{68}R_{50}EB$-162 / h5	-627	57.5	57.5	625	130	880

Table 4.13 : Polarization parameters for the coating $PC_{50}R_{50}EB$-118 on aluminium in 0.1 M H_2SO_4 with increasing exposure time

	Ecorr (mV)	I_{corr} ($\mu A.cm^{-2}$)	CR (mpy)	βa (mV)	βc (mV)	R_p ($\Omega.cm^2$)
BARE	-663	34.8	15.0	512	111	1206
$PC_{50}R_{50}EB$-118 / h1	-660	21.5	9.3	753	134	34184
$PC_{50}R_{50}EB$-118 / h2	-643	46.3	19.9	560	120	1709
$PC_{50}R_{50}EB$-118 / h3	-618	45.0	19.3	314	104	955
$PC_{50}R_{50}EB$-118 / h4	-614	49.7	49.7	437	117	855
$PC_{50}R_{50}EB$-118 / h5	-597	49.3	21.1	535	122	804

Table 4.14 : Values of the elements of equivalent circuit required for fitting the EIS of aluminium in 0.1 M H_2SO_4 solution in absence and presence of varying coating types with increasing exposure time

Aluminium Electrode - 0.1 M H2SO4	Rs ($\Omega.cm^2$)	CPEdl. Yo.10^5 ($\Omega^{-1}.s^n.cm^{-2}$)	n_{dl}	R1 ($\Omega.cm^2$)	C1 ($\mu F.cm^{-2}$)	R2 ($\Omega.cm^2$)	C2 ($\mu F.cm^{-2}$)	R3 ($\Omega.cm^2$)	W.Yo 10^5 ($\Omega^{-1}.s^5$)	Cel ($\mu F.cm^{-2}$)	CPEel. Yo.10^5 ($\Omega^{-1}.s^n.cm^{-2}$)	nel	Rel ($\Omega.cm^2$)
BARE	4.88	2.89	0.950	1222									
CF-R	11.32	19.67	0.540	36.03	3.40	0.05	0.00	0.01	5.113	13.65			20576
$P_{50}R_{50}$EB-162 / h1	15.45	28.41	0.690	916.42	1.77	3906	1.03	34877	38.6	0.01			29.76
$PC_{68}R_{50}$EB-162 / h1	0.00	7.08	0.350	0.00	0.001	290	0.02	1.62	0.078		0.36	0.94	84956
$PC_{50}R_{50}$EB-118 / h1	1.61	0.42	0.530	0.001	0.002	52.08	8.73	34249	0.065		3.00	0.40	0.87
$P_{50}R_{50}$EB-162 / h5	14.79	114.38	0.420	32.35	7.16	194	2647.70	0.34	2596E+4	0.24			898.32
$PC_{68}R_{50}$EB-162 / h5	12.83	19.75	0.660	15.06	6.72	37.10	15.72	94.11	5.44E+14	29.64			703.28
$PC_{50}R_{50}$EB-118 / h5	13.84	45.16	0.580	20.81	6.92	143.8	0.00003	0.00	216E+8	28.63			617.32

4.4 Measurements in Sea Water

In this part of the study corrosion phenomena of carbon steel was examined by polarization and EIS measurements in %3.5 (w/w) seawater.

Figure 4.39 shows the Rp values of bare and coated electrodes ($P_{50}R_{50}$-032, $PC_{68}R_{50}EB$-162 and $PC_{50}R_{50}EB$-118). All of the coatings have much larger loop than the bare electrode which means the coating is effective for corrosion protection.
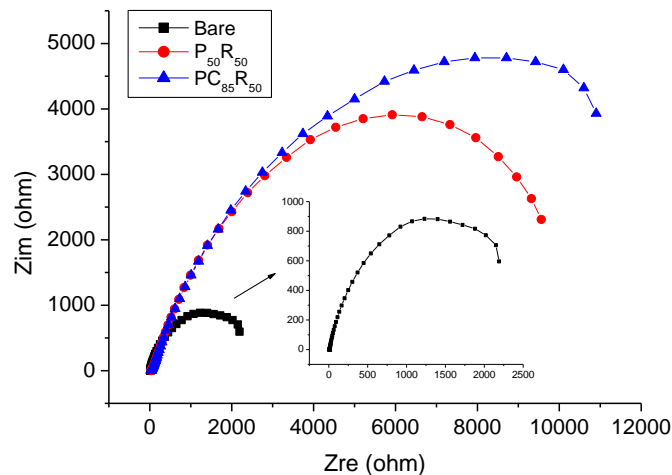
Figure 4.39 : Nyquist plot of bare carbon steel and 0.32 % concentration coatings of PANI and PANI/CeO$_2$ in seawater

Figure 4.40 shows the Tafel plot of bare, $P_{50}R_{50}$-032 and $PC_{85}R_{50}$-032 coated electrodes after 1 hour of exposure to sea water. There is a shift to a more positive corrosion potential which shows that the coatings inhibit the anodic reaction by acting as a barrier layer between electrode surface and corrosion environment [27].
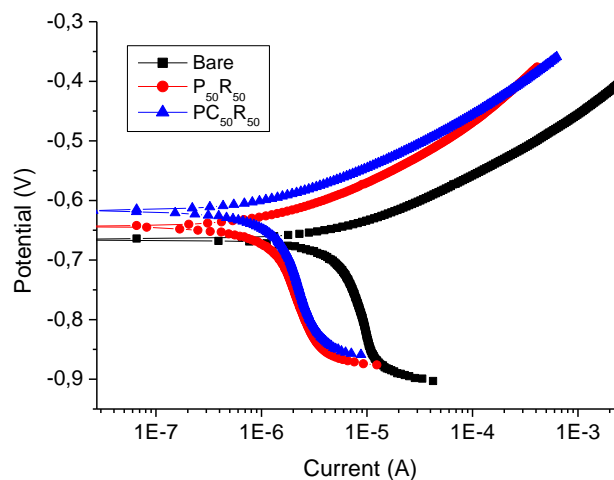
Figure 4.40 : Polarization curves of bare and 0.32 % concentration coatings of PANI and PANI/CeO$_2$ in 3.5 % seawater

Figure 4.41 shows the impedance measurement results of bare, $P_{50}R_{50}$-032, $PC_{85}R_{50}$-032, $P_{50}R_{50}EB$-162 and $PC_{50}R_{50}EB$-118 coatings on carbon steel in 3.5 % seawater. Results indicate that the coatings including emeraldine base form of PANI and PANI/CeO$_2$ ($PC_{68}R_{50}EB$-162 and $PC_{50}R_{50}EB$-118) have much better corrosion protection efficiency. Although polymer concentration used for $PC_{50}R_{50}EB$-118 coating is lower than $P_{50}R_{50}EB$-162 coating, it has a bigger loop than $P_{50}R_{50}EB$-162. This result shows that inclusion of CeO$_2$ nanocomposite to the PANI structure provides a more protective coating. This might be due to better durability of CeO$_2$ nanocomposite.
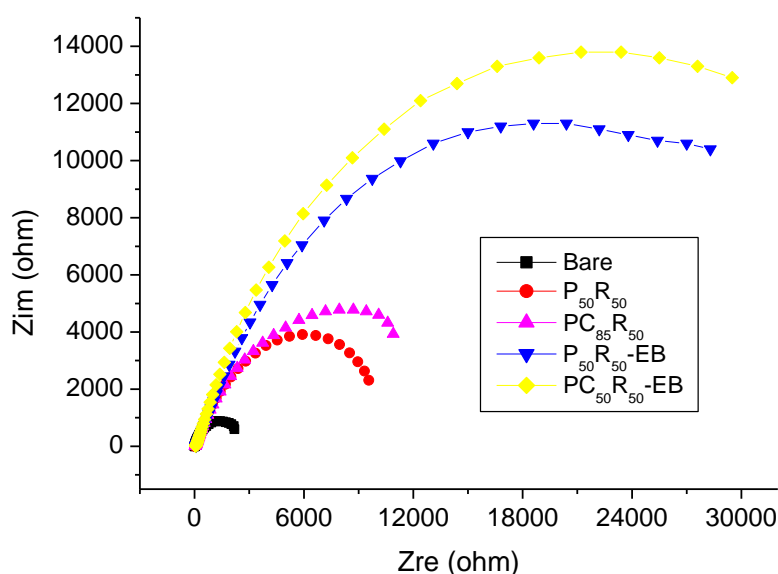
Figure 4.41 : Nyquist plot of bare, $P_{50}R_{50}$-032, $PC_{85}R_{50}$-032, $P_{50}R_{50}EB$-162, $PC_{68}R_{50}EB$-162 and $PC_{50}R_{50}EB$-118 coatings on carbon steel in 3.5 % seawater.

Figure 4.42 depicts the equivalent circuits to model electrochemical behavior belonging to $P_{50}R_{50}$-032, $PC_{85}R_{50}$-032, $P_{50}R_{50}EB$-162 and $PC_{50}R_{50}EB$-118 coated carbon steel in 3.5 % seawater. The electrochemical circuit model is represented by the conventional equivalent circuit consists of a series of a resistor and capacitor. Rs(Q (Rp W)) where Rs is the uncompensated ohmic resistance between the working electrode and the reference electrode, Rp is the polarization resistance and Cdl is the differential double layer capacitance which represents the total capacitance at the metal/electrolyte interface and Zw is the Warburg impedance which represents the diffusion processes within the pores in case of coated metal/solution interface [1, 27].

This is also complying with the circuit models belonging to previously studied coatings in H_2SO_4.

It is observed that a reasonable accuracy of the fitting was obtained. Chi-square is in the order of 10^{-3} and 10^{-4} for all the experimental data.
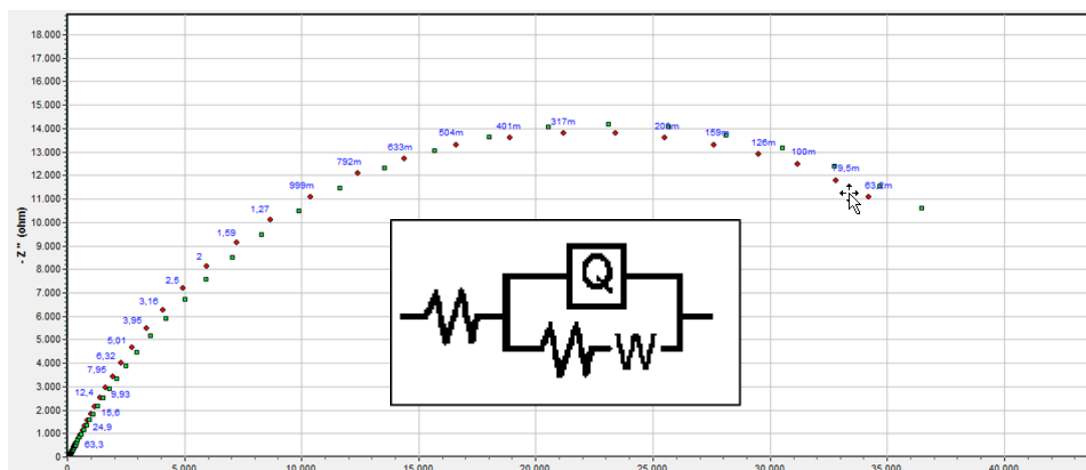
Figure 4.42: Values of the elements of equivalent circuit required for fitting the EIS of $P_{50}R_{50}$-032, $PC_{85}R_{50}$-032, $P_{50}R_{50}EB$-162 and $PC_{50}R_{50}EB$-118 coatings on carbon steel electrode in sea water

From Table 4.15, it is clear that emeraldine base form of PANI provides a better corrosion resistance in sea water. Addition of CeO_2 causes a slight increase in Rp value.

Table 4.15 : Values of the elements of equivalent circuit required for fitting the EIS of carbon steel in 3.5 % seawater in bare electrode and varying coating types

Circuit Model	Carbon Steel Electrode - 3.5% sea water	Rs ($\Omega.cm^2$)	Rp ($\Omega.cm^2$)	CPEdl. $Yo.10^5$ ($\Omega^{-1}.s^n.cm^{-2}$)	n_{dl}	W.Yo ($\Omega^{-1}.s^5$)	IE%
R(QR)	BARE	5.12	1187.88	30.44	0.793	0.005115	
R(Q(RW))	$P_{50}R_{50}$-032	18.29	7118.23	10.99	0.658	58650000	83
R(Q(RW))	$PC_{85}R_{50}$-032	16.67	9425.63	7.67	0.642	2771000	24
R(Q(RW))	$P_{50}R_{50}EB$-162	36.27	20982.70	2.81	0.650	0.004462	55
R(Q(RW))	$PC_{50}R_{50}EB$-118	30.30	23325.28	3.15	0.699	349.1	10

Figure 4.43 shows the bode plots of bare, $P_{50}R_{50}$-032, $PC_{85}R_{50}$-032, $P_{50}R_{50}EB$-162 and $PC_{50}R_{50}EB$-118 coatings on carbon steel in 3.5 % seawater. Results indicate that

the coatings including emeraldine base form of PANI and PANI/CeO$_2$ (PC$_{68}$R$_{50}$EB-162 and PC$_{50}$R$_{50}$EB-118) have much better corrosion protection efficiency.
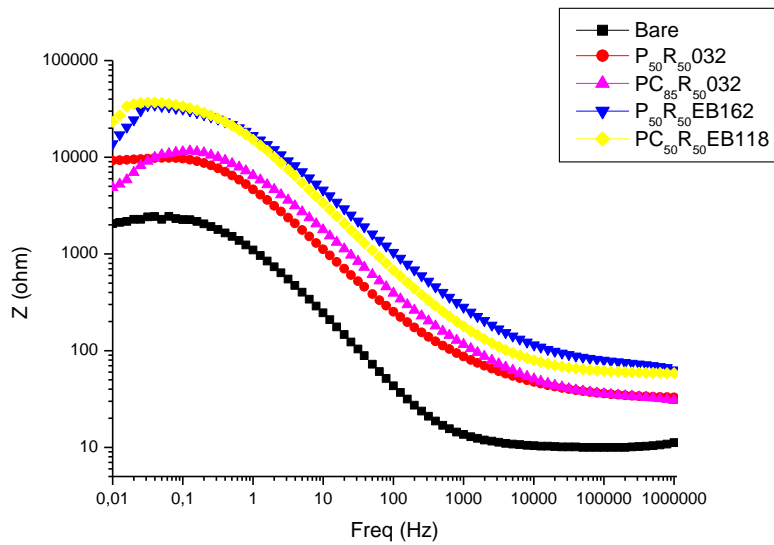
Figure 4.43 : Bode plot of bare, P$_{50}$R$_{50}$-032, PC$_{85}$R$_{50}$-032, P$_{50}$R$_{50}$EB-162 and PC$_{50}$R$_{50}$EB-118 coatings on carbon steel in 3.5 % seawater.

Figure 4.44 shows the polarization curves of bare, P$_{50}$R$_{50}$-032, PC$_{85}$R$_{50}$-032, P$_{50}$R$_{50}$EB-162 and PC$_{50}$R$_{50}$EB-118 coated carbon steel in 3.5 % seawater. The corrosion current of the 1.18% emeraldine base form coating of PANI/CeO$_2$ (PC$_{50}$R$_{50}$EB-118) has almost the same curves as 1.62% emeraldine base form of pure PANI coating (P$_{50}$R$_{50}$EB-162). Ecorr, Icorr, βa, βc, CR, IEIcorr and IERp values obtained from these graphs are listed in Table 4.16.
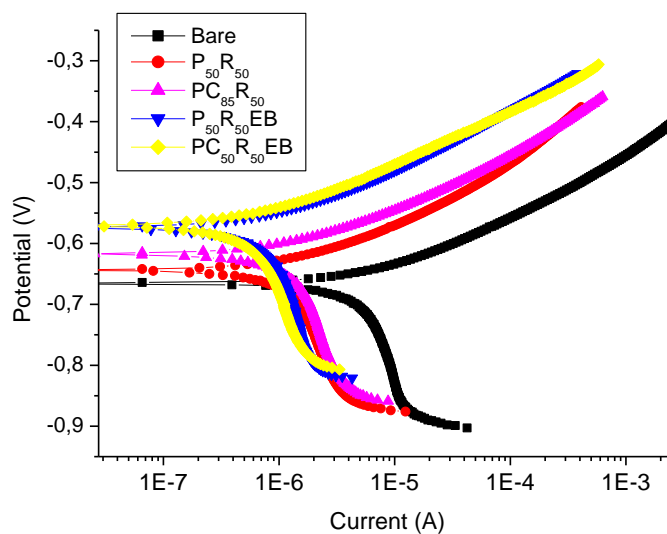
Figure 4.44 : Polarization curves of bare, P$_{50}$R$_{50}$-032, PC$_{85}$R$_{50}$-032, P$_{50}$R$_{50}$EB-162 and PC$_{50}$R$_{50}$EB-118 coated carbon steel in 3.5 % seawater

Table 4.16 : Polarization parameters of coatings on carbon steel in 3.5 % seawater

	Ecorr (mV)	Icorr ($\mu A.cm^{-2}$)	CR (mpy)	βa (mV)	βc (mV)	Rp ($\Omega.cm^2$)	IEIcorr (%)	IERp (%)
BARE	-666	2,65	1,22	34	70	1217		
$P_{50}R_{50}$-032	-644	2,51	1,15	75	383	5831	5	79
$PC_{85}R_{50}$-032	-617	2,21	1,01	70	293	8144	17	85
$P_{50}R_{50}EB$-162	-574	2,01	0,92	89	1693	19505	24	94
$PC_{50}R_{50}EB$-118	-571	1,72	0,79	89	1xe15	22823	35	95

Aluminium metal could not be measured in seawater since the coated aluminium electrodes give a very high corrosion resistance in seawater and the obtained value were out of the range of instrument each trial. As a result, the measurements of aluminium electrodes in seawater could not be conducted. This can be further investigated by reducing the film thicknesses of the coatings.

4.5 SEM (Scanning Electron Microscopy) Measurements

Morphology of commercially purchased CeO_2 nanoparticles, synthesized PANI, PANI/CeO_2 nanocomposite samples were investigated by SEM measurements.

CeO_2 nanoparticle contrubition in the synthesized PANI/CeO_2 nanocomposite structure can clearly be seen in the Figure 4.45-4.47.
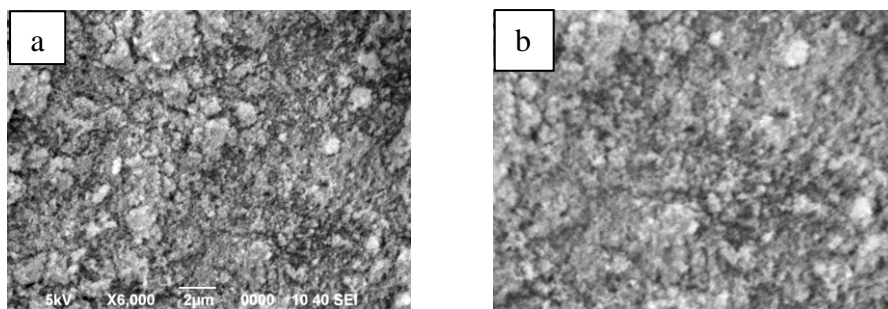
Figure 4.45 : SEM images of CeO_2 nanoparticles with a magnification of a) x6000 b) x10000
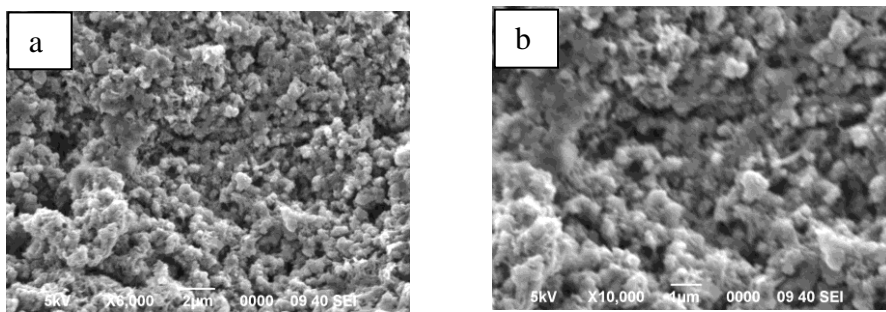
Figure 4.46 : SEM images of PANI/CeO$_2$ nanocomposite with a magnification of a) x6000 b) x10000
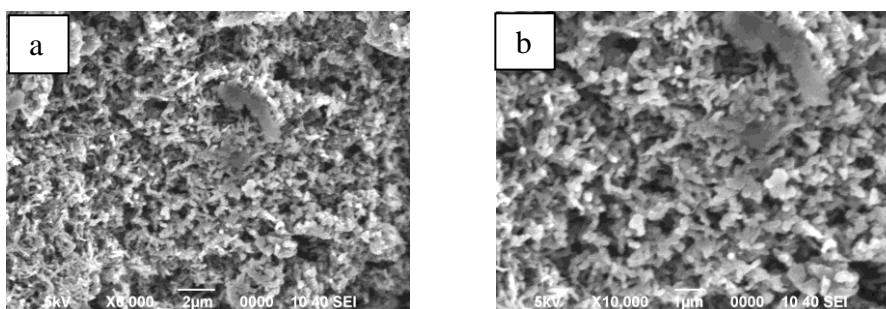
Figure 4.47 : SEM images of pure PANI with a magnification of a) x6000 b) x10000

Morphology of pure PANI and PANI/CeO$_2$ coatings on carbon steel electrodes can be seen in Figure 4.48 and Figure 4.49. Pure PANI coatings have a rough and curved structure whereas PANI/CeO$_2$ nanocomposite coating has a uniform, smooth structure. This morphology improvement can be attributed to one of the reasons of better corrosion protection property of PANI/CeO$_2$ nanocomposite coating compared to pure PANI coatings.
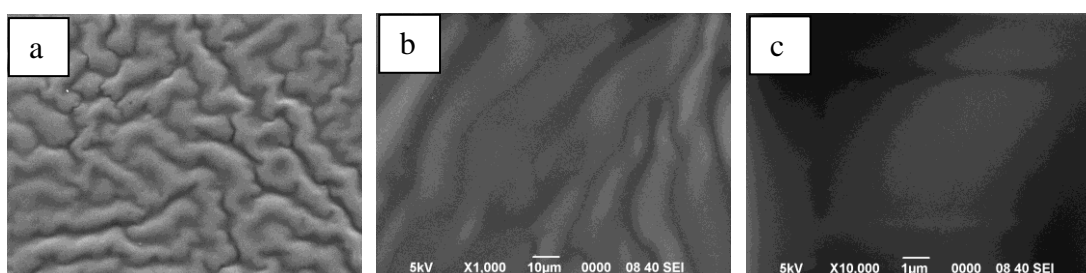
Figure 4.48 : SEM images of pure PANI coating with a magnification of a) x300 b) x1000 c) x10000
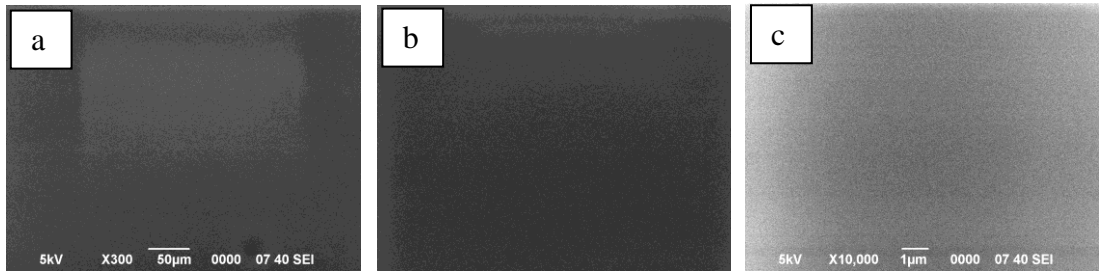
Figure 4.49 : SEM images of the coating including PANI/CeO$_2$ nanocomposite with a magnification of a) x300 b) x1000 c) x10000

After exposure to 0.1 M H$_2$SO$_4$ solution for 1 hour, both of the coatings defects started due to corrosive effect of the electrolyte.

The dots in the figures (Figure 4.50-4.51) may be indicating the presence of SO$_4^{-2}$ anions that act as a dopant ions and cause surface cracking.
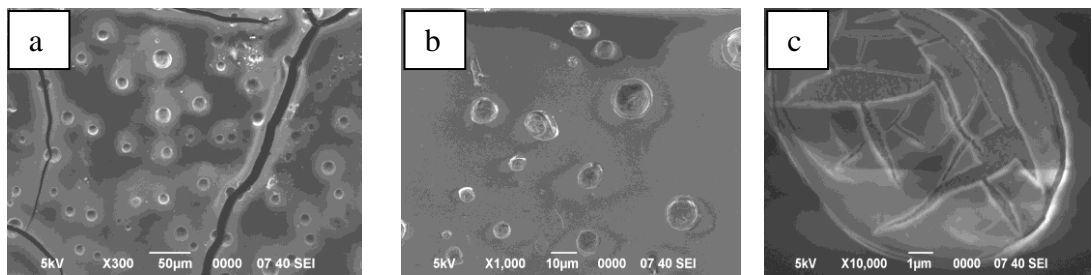
Figure 4.50 : SEM images of the coating including PANI/CeO$_2$ nanocomposite after 1 hour exposure to 0.1 M H$_2$SO$_4$ with a magnification of a) x300 b) x1000 c) x10000
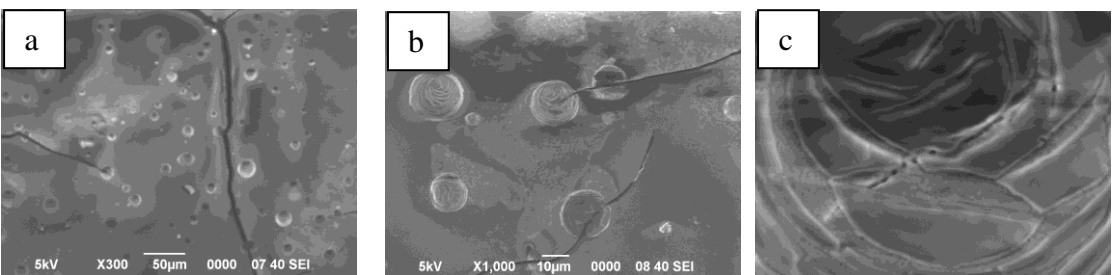
Figure 4.51 : SEM images of the coating including pure PANI coating after 1 hour exposure to 0.1 M H$_2$SO$_4$ with a magnification of a) x300 b) x1000 c) x10000

5. CONCLUSIONS

In this study, the corrosion behaviour of pure PANI and PANI/CeO$_2$ nanocomposite coatings on carbon steel and aluminium metals in corrosive environment was investigated by steady-state current-voltage curves and impedance spectroscopy measurements.

Synthesized PANI and PANI/CeO$_2$ nanocomposite polymers were characterised by FTIR, solid state conductivity, UV-Visible Spectroscopy and SEM analysis and it is confirmed by the analysis results that the polymer and nanocomposite were sucsessfully synhesized. It is also evident from the SEM images that the coatings of PANI/CeO$_2$ nanocomposite has a more uniform coating whereas pure PANI coatings have a rough and curved structure, which can effect the corrosion protection efficiency of PANI/CeO$_2$ nanocomposite in a positive way.

Coatings including different ratios of both PANI and PANI/CeO$_2$ polymers were investigated for their corrosion protection properties. In addition to emeraldine salt forms of the polymers, emeraldine base forms of both species were used in order to have more concentrated polymer solutions due to better solubility which increased PANI content of coatings.

The initial measurements were conducted in 0.1 M H$_2$SO$_4$ both for carbon steel and aluminium electrodes after 1 hour immersion to corrosive media. It is evident that both coatings inhibit corrosion of bare electrodes. The increase in polymer concentration effects the corrosion protection efficiency of the coating positively. PANI/CeO$_2$ polymers coatings showed slightly better corrosion protection efficiency over pure PANI coatings both for carbon steel and aluminium electrodes, which shows the advantage of CeO$_2$ nanoparticle contribution in the coating. It is evident from the polarization curves that the coatings retard both anodic and cathodic reactions. In other words, they reduce the anodic dissolution and also retard the hydrogen evolution reaction. The PANI/CeO$_2$ nanocomposite coating with 1,62 %

showed best corrosion protection performance on carbon steel and aluminium electrodes in 0.1 M H_2SO_4.

The corrosion protection efficiencies of the coatings including emeraldine base form of polymers were also measured with increasing exposure time. It was observed that the coating degradetion increased and consequently corrosion currents and corrosion rates increased as the exposure time to corrosive media increased. The differnace in corrosion protection property of the coatings became close to each other by increasing exposure time, which may be due to the effect of corrosion product formation on the electrode sureface.

EIS measurements were also supported by equivalent circuit models and it is observed that a reasonable accuracy of the fitting was obtained. Chi-square is the order of 10^{-3} and 10^{-4} for all the experimental data. Rp values obtained by equivalent circuits and experiments are in agreement with each other.

In order to see the protection performance of coatings in different corroion media, measurements in 3.5 % seawater for carbon steel electrodes were also carried out. Results suggest that the same concentration of PANI / CeO2 nanocomposites have better corrosion protection efficiency compared to pure PANI coatings even in emeraldine salt form which has lower concentration. The best performance was obtained by the coating $PC_{50}R_{50}EB-118$ in 3.5 % seawater.

It can be concluded that corrosion protection properties of coatings on carbon steel and aluminium metals can be improved by $PANI/CeO_2$ nanocomposite.

REFERENCES

[1] **Lu, W-K., Basak, S. and Elsenbaumer R.L.,** 1997: Corrosion inhibition of Metals by conductive polymers, in *Handbook of Conducting Polymers*, Second Edition, Chapter **31**, P. 881-918, M. Dekker, New York, USA.

[2] **Yano, J., Nakatani, K., Harima, Y. and Kitani, A.,** 2007: Bilayer polymer coating containing a polyaniline for corrosion protection of iron*, Materials Letters*, Volume **61**, Issue 7, P. 1500–1503.

[3] **Kumar, E., Selvarajan, P. and Muthuraj, D.,** 2012: Preparation and characterization of polyaniline/cerium dioxide (CeO_2) nanocomposite via in situ polymerization, *Journal of Materials Science,* Volume **47**, Issue 20, P. 7148-7156.

[4] **Nemes, P.I., Lekka, M., Fedrizzi, L. And Muresan, L.M.,** 2014: Influence of the electrodeposition current regime on the corrosion resistance of Zn–CeO2 nanocomposite coatings, *Surface and Coatings Technology,* Vol **252**, P.102–107.

[5] **Zarras, P. and Stenger-Smith, J.D.,** 2014: Corrosion processes and strategies for prevention: an introduction, , in *Handbook of Smart Coatings for Materials Protection,* Part **1**, P.3-28, Woodhead Publishing, United Kingdom.

[6] **Armelin, E., Oliver, R., Liesa, F., Iribarren, J.I., Estrany, F. And Alem´an, C.,** 2007: Marine paint fomulations: Conducting polymers as anticorrosive additives, *Progress in Organic Coatings*, V. **59**, P.46–52.

[7] **Riaza, U., Nwaohab, C. and Ashrafa, S.M.,** 2014: Recent advances in corrosion protective composite coatings based onconducting polymers and natural resource derived polymers, *Progress in Organic Coatings*, Volume **77**, Issue 4, P. 743–756.

[8] **Roberge, P. R.,** 1999: Aqueous corrosion, in *Handbook of Corrosion Engineering,* Chapter **1**, p.14, McGraw Hill, New York, USA.

[9] **Hihara, L.H.,** 2014: Electrochemical Aspects of Corrosion-Control Coatings, in *Intelligent Coatings for Corrosion Control,* Chapter **1**, p.1-15, Butterworth-Heinemann, United Kingdom.

[10] **Fenker, M., Balzer, M. And Kappl, H.,** 2014: Corrosion protection with hard coatings on steel: Past approaches and current research efforts, *Surface & Coatings Technology,* V. 257, P. 182–205.

[11] **Tan, Y., Huang, Y. And Mansfeld, F.,** 2014: Testing and analysis techniques in rare earth inhibitor research, in *Rare Earth-Based Corrosion Inhibitors*, Chapter 2, P. 38-83, Woodhead Publishing, United Kingdom.

[12] **Princeton Applied Research**, 1997: Electrochemistry and Corrosion: Overview and Techniques, *Application Note CORR-4*, EG&G Princeton Applied Research Corp., USA.

[13] **Sezer E.,** 2014: Korozyon ve Önlenmesi, *3. Ulusal Uygulamalı Elektrokimya Lisansüstü Yaz Okulu ve Çalıştayı*, 3-7 Haziran 2014 Balıkesir-Ayvalık.

[14] **Princeton Applied Research,** 1980: Basics of Corrosion Measurements, *Application Note CORR-1*, EG&G Princeton Applied Research Corp., USA.

[15] **Metrohm Autolab B.V.,** 2011: Measurement of Polarization Resistance, *Autolab Application Note COR03*, Corrosion Part 3, P.1-2.

[16] **Url 1**< http://www.gamry.com/application-notes/basics-of-electrochemical-corrosion-measurements/ >, accessed at 02.05.2015.

[17] **Kuznetsov, V., Maljusch, A., Souto, M.R., Bandarenka, A.S. and Schuhmann, W.,** 2014: Characterisation of localised corrosion processes using scanning electrochemical impedance microscopy, *Electrochemistry Communications*, 44, p. 38-41.

[18] **Grundmeier, G., Schmidt, W. and Stratmann, M.,** 2000: Corrosion protection by organic coatings: electrochemical mechanism and novel methods of investigation, *Electrochimica Acta*, Vol. **45**, P. 2515–2533.

[19] **Speight, J.G.,** 2014: Corrosion Monitoring and Control, in *Oil and Gas Corrosion Prevention*, Chapter 6, P.109-149, Gulf Professional Publishing, Houston, Texas, USA.

[20] **Hua, R.-G., Zhanga, S., Bua, J.-F., Lina, C.-J. and Song, G.-L.,** 2012: Recent progress in corrosion protection of magnesium alloys by organic coatings, *Progress in Organic Coatings,* **73**, P. 129-141.

[21] **Abu-Thabit, N.Y. and Makhlouf, A.S.H.,** 2014: Recent advances in polyaniline (PANI)-based organic coatings for corrosion protection, in *Handbook of Smart Coatings for Materials Protection*, **Part 17**, P. 459–486, Woodhead Publishing, United Kingdom.

[22] **Sapurina, I.Yu. and Shishov, M.A.,** 2012: Oxidative Polymerization of Aniline: Molecular Synthesis of Polyaniline and the Formation of Supramolecular Structures, *New Polymers for Special Applications*, Chapter 9, P. 251-312, InTech.

[23] **Zhanga, Y., Shaoa, Y., Zhanga, T., Menga, G. and Wang, F.,** 2013: High corrosion protection of a polyaniline/organophilic montmorillonite coating for magnesium alloys, *Progress in Organic Coatings*, 76, P. 804-811.

[24] **Fedel, M., Ahniyaz, A., Ecco, L.G. and Deflorian, F.,** 2014: Electrochemical investigation of the inhibition effect of CeO_2 nanoparticles on the corrosion of mild steel, *Electrochimica Acta*, 131, P. 71-78.

[25] **Kester, D. R., Duedall I. W., Connors D. N. and Pytkowıcz, R. M.,** 1967: Preparation of Artificial Sea Water, Department of Oceanography, Oregon State University, Corvallis 97331, Vol. 12, Issue 1, p. 178.

[26] **Url 2**< http://www.sigmaaldrich.com/catalog/product/aldrich/428329? lang=ee&region=TR >, accessed at 02.05.2015.

[27] **Oncul, A., Coban, K., Sezer, E.,** 2011: Inhibition of the corrosion of stainless steel by poly-N-vinylimidazole and N-vinylimidazole, *Progress In Organic Coatings,* Volume: **71**, Issue: 2, P. 167-172.

[28] **Jütner, K.,** 1990, *1501 Electrochim. Acta,* **10**.

[29] **Kalaivasan, N. And Shafi, S.S.,** 2012: Enhancement of corrosion protection effect in mechanochemically synthesized Polyaniline/MMT clay nanocomposites, *Arabian Journal of Chemistry,* Available online 4 August 2012.

[30] **Osken, I., Sezer, E., Ertas, E. and Ozturk, T.,** 2014: Electrochemical impedance spectroscopy study of poly[3,5-dithiophene-2-yldithieno[3,2-b;2',3'-d]thiophene] P(Th$_2$DTT), Journal of Electroanalytical Chemistry, **726**, 36–43.

CURRICULUM VITAE

PERSONAL INFORMATION

Name, Surname	**HANDE YOLSAL ACAR**
Address	Akkoza Sitesi Açelya Blokları
	G1 Blok D:51 Bahçeşehir / Istanbul
Telephone	GSM +90 555 783 5225
E-mail	handeyol@yahoo.com
Date and Place of Birth	08 February 1984, Istanbul

EDUCATION

2010-   **Istanbul Technical University, Polymer Science and Tech.**

2002-2006   **Istanbul Technical University,** Chemical Engineering

1995-2002   **Bayrampasa Anatolian High School**

WORK EXPERIENCE

04/2009 –   **İNTERLAB Laboratuar Ürünleri San. ve Tic. A.Ş.,**
01/2012 –   **Procurement Responsible**
04/2009 – 01/2012   **Retail Sales Responsible**

04/2007 – 10/2008   **PROSİM Kimya San. ve Tic. Ltd. Sti,** İstanbul
               Sales Responsible

07/2006 – 08/2006   **AGH University of Science and Technology,** Poland
               Internship – Faculty of Materials Science and Ceramics

08/2005 – 09/2005   **DYO Boya Fabrikaları San. ve Tic. AŞ,** Kocaeli
               Internship – Production Department

08/2004 - 09/2004   **SANOVEL İlaç San. ve Tic. A.Ş,** Istanbul
               Internship – Quality Control Department